Effect of Amino-2-Pyridine Inhibitor on the Rehabilitation of Chloride Contaminated Reinforced Concrete with Bidirectional Electro-migration Method

A Dissertation Report Submitted in Partial Fulfilment of the Requirement

For the Award of Degree of

MASTER OF ENGINEERING

IN

STRUCTURAL ENGINEERING

Submitted by-

TARUN SINGH RAJPUT

802124023

Under the supervision of

Dr. Shweta Goyal

Professor, CED

Dr. Arpit Goyal

Assistant Professor, CED

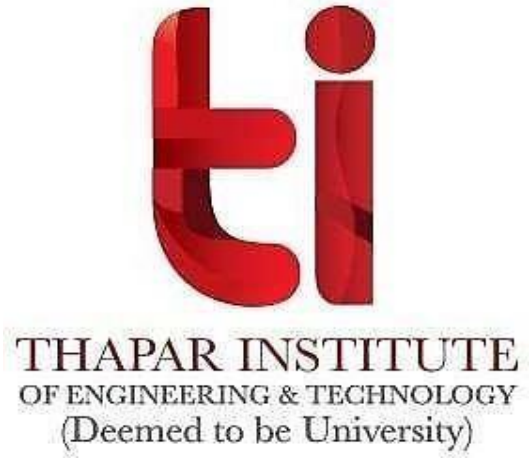

Department Of Civil Engineering

Thapar Institute of Engineering and Technology

(Deemed To Be University)

Patiala-147004 (Punjab)

(July 2023)

`DECLARATION

I hereby declare that the work which is presented in this seminar report entitled **"Effect of Amino-2-Pyridine Inhibitor on the Rehabilitation of Chloride Contaminated Reinforced Concrete with Bidirectional Electro-migration Method"** as per the requirement for the award of Master of Engineering in Structures, submitted in the Department of Civil Engineering, Thapar Institute of Engineering & Technology (Deemed to be University), Patiala, is a review carried out by me under the guidance of Dr. Shweta Goyal, Professor, Department of Civil Engineering, Thapar Institute of Engineering & Technology, Patiala. and Dr. Arpit Goyal, Assistant Professor, Department of Civil Engineering, Thapar Institute of Engineering & Technology, Patiala.

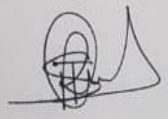

DATE: 16/09/2023

Tarun Singh Rajput

802124023

Certificate

This is to certify that the above declaration made by the student concerned is correct according to the best of my knowledge and belief.

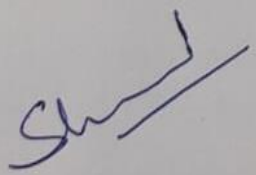

Dr. Shweta Goyal

Professor, CED

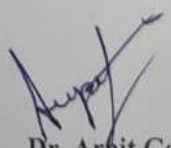

Dr. Arpit Goyal

Assistant Professor, CED

Thapar Institute of Engineering & Technology, Patiala.

ACKNOWLEDGEMENT

I wish to express my deep gratitude to **Dr. Shweta Goyal, Professor,** Departmentof Civil Engineering, Thapar Institute of Engineering and Technology (Deemed to be University), and **Dr. Arpit Goyal, Assistant Professor,** Department of Civil Engineering, Thapar Institute of Engineering and Technology (Deemed to be University), Patiala, for providing guidance, support, and patience in listening to my ideas and suggesting me with new ways for implementation and for the motivation and inspiration that encouraged me throughout my work. I would also like to thank all my colleagues for providing me with all the help and facilities required for completing this seminar report.

I want to mention a heartful thanks to **Mr. Ashish Tiwari and Ms. Purnima Dogra** for guiding me at different stages and very humbly explain me things.

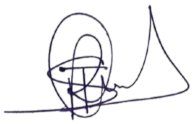

Tarun Singh Rajput

802124023

TABLE OF CONTENT

LIST OF FIGURES

LIST OF TABLES

LIST OF SYMBOLS AND ABBREVIATIONS

2AP	2 Aminopyridine
Cl-	Chloride ions
Fe	Iron
OH-	Hydroxide ions
CIA	Corrosion Inhibitor Admixtures
ABA	4-Aminobenzoic acid
2AP	2-Aminopyridine
SA	Salicyaldehyde
TEP	Triethylphosphate
TETA	Tri-ethylene tetra-amine
I_{corr}	Corrosion Current Density
E_{corr}	Corrosion potential
ICCP	Impressed current cathodic protection
HCP	Hybrid cathodic protection
GCP	Galvanic cathodic protection
LPR	Linear polarisation resistance
Rp	Polarization resistance
Rt	Total resistance
EIS	Electrochemical impedance spectra
RC	Reinforced-concrete
ECR	Electrochemical chloride removal
CP	Cathodic Protection
NaCl	Sodium Chloride

ABSTRACT

The corrosion of reinforcement presents a significant durability challenge, leading to a reduced design life of reinforced concrete structures. With the growing demand for longer service lives of infrastructure (typically 100–120 years) and the high costs involved in construction and maintenance, the repair and rehabilitation of concrete structures have become of utmost importance. To address this issue, a novel method known as Bidirectional Electro-Migration Rehabilitation (BIEM) technology has been developed to enhance the durability of existing reinforced concrete structures. The BIEM process involves applying an electric field between embedded steel cathodes and external anodes to inject a corrosion inhibitor from external electrolytes into the concrete while simultaneously extracting chloride ions from the concrete cover zone. As observed from the literature review in most of the research studies TETA was used as inhibitor so in this thesis the effectiveness of 2AP was studied, effect of Amino-2-Pyridine Inhibitor on the Rehabilitation of Chloride Contaminated Reinforced Concrete with Bidirectional Electro-migration method. The effectiveness of the BIEM repair technique was investigated on different aspects as current density, duration of treatment, initial chloride content and variation of inhibitor in the electrolyte.

In experimental studies, specimens were treated using the BIEM method, and then drilled to analyse the concentration profiles of corrosion inhibitor and chloride within the concrete. Along with it Icorr, Ecorr, HCP and LPR of the specimens was also monitored and investigated along with chloride and inhibitor profiles. The optimum results was found in the case of 15 of test duration, 1 A current density at 0.3 M inhibitor concentration. The maximum migration of inhibitor was observed 9.16 mM and maximum extraction of chloride ions was 47%. Overall, the BIEM technology shows promise in improving the durability and extending the service life of existing reinforced concrete structures, making it a potential solution for addressing the challenges of concrete corrosion and enhancing the sustainability of infrastructure.

CHAPTER 1. INTRODUCTION

1.1 CORROSION

Corrosion is a natural phenomenon wherein a pure metal undergoes a transformation into a more chemically stable state, typically as an oxide, hydroxide, or sulphide compound. It occurs through a gradual process of material breakdown, often involving chemical or electrochemical reactions with its surrounding environment. Corrosion represents the progressive degradation of metals due to the effects of air, moisture, or chemical agents (such as acids) acting upon their surfaces. One of the most prevalent examples of metal corrosion is the rusting of iron, which manifests as the formation of brown, flaky substances when iron objects are exposed to moist air. This natural conversion of refined metals into more solid compounds like oxides, hydroxides, or sulphides leads to the deterioration of the material. Consequently, corrosion poses a significant threat to both natural and historical structures, as well as increases the risk of catastrophic equipment failures.

Corrosion is the process that leads to the deterioration or degradation of a material when it is exposed to various environmental conditions. In the context of concrete, corrosion involves an electrochemical mechanism where both electrical currents and chemical reactions take place. In reinforced concrete structures, the steel reinforcement remains in a passive state and is shielded by a thin oxide layer, which forms due to the alkaline nature of concrete. This protective oxide layer helps prevent further corrosion of the steel (Qureshi et al., 2017).

The purpose of reinforcing concrete with steel is to enhance the structural element's strength in tension since concrete is inherently weak in that regard. However, structures can experience failures due to the corrosion of steel, which has become a significant and pervasive problem worldwide. The associated repair costs now amount to billions of dollars annually. Additionally, there are numerous intangible losses, including the energy required to manufacture replacements for corroded objects. The corrosion of steel in reinforced concrete diminishes its durability and can ultimately lead to structural failure (Qureshi et al., 2019).

1.2 The Global Impact of Corrosion

The consequences of corrosion encompass various aspects, including material and energy wastage, economic losses, and environmental impact (Hansson 2016:10-13; Javaherdashti 2000). According to Javaherdashti's (2000) research, on a global scale, approximately one ton of steel transforms into rust every 90 seconds. Astonishingly, nearly 50% of the total steel production worldwide is utilized solely for replacing corroded steel (Javaherdashti 2000). The impact of corrosion is often quantified in terms of economic losses, which can be both direct and indirect. To put it into perspective, the energy required to produce one ton of steel is equivalent to the energy consumption of an average family over a month. The global economic cost attributed to corrosion-related losses is estimated to be 3.4% of the world's Gross Domestic Product (GDP), amounting to a staggering 2.5 trillion USD (Hansson 2016; Hays 2010; Koch et al. 2016:3). To provide further insight, the breakdown of global corrosion costs categorized by region and sector for various countries is presented in Table 1.1. Additionally, Table 1.2 highlights the corrosion costs specifically associated with the construction industry in India (Koch et al. 2016).

Table 1.1 Global cost of corrosion (CoC) by region by sector (Koch et al. 2016: A-19)

Economic Regions	**Agriculture (USD Billion)**	**Industry (USD Billion)**	**Services (USD Billion)**	**Total CoC (USD Billion)**	**Total GDP (USD Billion)**	**CoC % GDP**
United States	2.0	303.2	146.0	451.3	16,720	2.7
India	**17.7**	**20.3**	**32.3**	**70.3**	**1,670**	**4.2**
European Region	3.5	401	297	701.5	18,331	3.8
Arab World	13.3	34.2	92.6	140.1	2,789	5.0
China	56.2	192.5	146.2	394.9	9,330	4.2
Russia	5.4	37.2	41.9	84.5	2,113	4.0
Japan	0.6	45.9	5.1	51.6	5,002	1.0
Four Asian Tigers + Macau	1.5	29.9	27.3	58.6	2,302	2.5
Rest of the world	52.4	382.5	117.6	552.5	16,057	3.4
Global	**152.7**	**1446.7**	**906.0**	**2505.4**	**74,314**	**3.4**

Table 1.2 Cost of corrosion in construction sectors for India (Koch et al. 2016: A-11; Lambert 2014:229)

Sector	India (2011-12 Study)
Construction	6,112 (8,015)
New Construction	4,935 (6,472)
Repair and Maintenance	1,176 (1,543)

The corrosion of steel reinforcement in concrete can have severe consequences, often leading to unexpected failures in infrastructure such as highways, electrical towers, buildings, parking structures, and bridges. These failures not only incur substantial repair costs but also pose a significant risk to public safety (Davis 2000). Recent studies have shed light on the direct costs associated with corrosion, estimating it to be around $276 billion in the United States alone (Popov 2015). In the Indian context, although no formal corrosion auditing has been conducted, it was reported at CORCON–2015 (International Conference on Corrosion held in Chennai, India) that corrosion leads to an annual loss of approximately 5 lakh crore rupees (approximately $76 billion) in India, considering the impact on energy, resources, and lives (Service 2015). Infrastructure corrosion alone accounts for a loss of 2 lakh crore rupees (approximately $31 billion) (India 2015).

Additionally, in 2002, the annual cost of infrastructure corrosion in the United States was estimated to be $63.6 billion (Hansson 2016:13). Indirect costs, such as those stemming from traffic delays, were found to be more than ten times higher than the direct costs. These indirect costs also include factors like product loss, shutdowns, efficiency reduction, product contamination, and the need for excessive design requirements for metal, food, structures, and equipment (Popov 2015). Consequently, corrosion poses a significant concern that demands attention, especially in the case of aging reinforced concrete structures (Ahmad 2003, Apostolopoulos and Papadakis 2008).

1.3 CORROSION MECHANISM IN CONCRETE

Corrosion in concrete is induced by the generation of electrochemical potentials in the following ways:

- When two different metals are present in concrete, such as steel rebars, and aluminium conduit pipes, or when significant variations exist in surface characteristics of the steel, the formation of composition cells can occur.
- Concentration cells may be formed near reinforcing steel because of the differences in the concentration of dissolved ions, such as alkalis and chlorides.

The following reactions as represented in Figure 1.1 (Equation 1.1 and Equation 1.2) occur at the anode and cathode:

Anode: $Fe \rightarrow Fe^{2+} + 2e^-$ (metallic iron) (Equation 1.1)

Cathode: $\frac{1}{2}O_2 + H_2O + 2e^- \rightarrow 2OH^-$ (Equation 1.2)

Certain parameters play a crucial role in initiating the process of corrosion. Oxygen and humidity (electrolyte) are two essential factors without which corrosion cannot occur. The rate of corrosion is relatively slow when the availability of water or oxygen is limited. However, the presence of humidity, moisture, and oxygen acts as catalysts, promoting the occurrence of corrosion by generating more hydroxide ions (OH-) and leading to the formation of rust, specifically the Fe(OH)- component. The following reactions (Equations 1.3-1.5) represent the formation of rust subsequent to the dissolution of iron at the anodic sites in the reinforcement.

$Fe^{2+} + 2OH^- \rightarrow Fe(OH)_2$ (ferrous hydroxide) (Equation 1.3)

$4Fe(OH)_2 + 2H_2O + O_2 \rightarrow 4Fe(OH)_3$ (ferric hydroxide) (Equation 1.4)

$2Fe(OH)_3 \rightarrow 2H_2O + Fe_2O_3 \cdot H_2O$ (rust) (Equation 1.5)

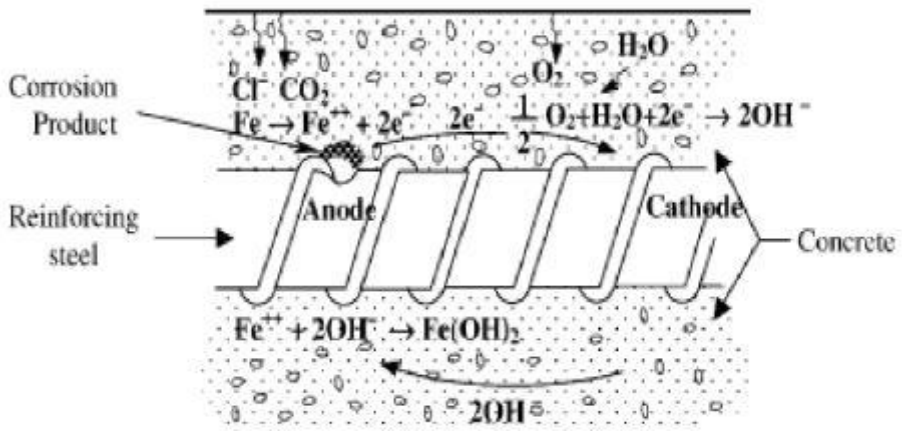

Figure 1.1: Electrochemical process of corrosion of steel in concrete (Qureshi et al 2017)

1.4 CHLORIDE-INDUCED CORROSION

Chloride attack is one of the main reasons behind the corrosion of steel in reinforced concrete. The major source of chloride ions (Cl^-) is de-icing salts or seawater. Cement, water, aggregate, and sometimes admixtures can also facilitate chloride in concrete. Chlorides penetrates into the concrete through the pore network and micro-cracks, forming the oxide film over the reinforcing steel and hence, accelerating the reaction of corrosion and concrete deterioration. The passivity of steel is broken when a sufficient quantity of chlorides is present in the pore solution. The passivity of steel also depends upon the OH^- concentration of the pore solution. Fan et al 2020 shows that the passivity is broken when the ratio of Cl^- concentration to OH^- concentration exceeds 1. The mechanism of reinforcement corrosion in concrete due to chloride attack is basically an electrochemical process by which the passivating layer of steel is lost by means of the formation of micro cells on the surface of steel by chloride ions. The moisture present in the pores of concrete acts as an electrolyte and the area adjacent to the concentration of chloride ions becomes a cathode, thus starting the electrochemical process.

$$Fe + 2H2O + 1/2O2 + 2Cl^- \rightarrow Fe2^+ + 2Cl^- + 2OH^- \quad \text{(Equation 1.6)}$$

Chlorides are present in concrete in two forms, namely bound chloride and free chloride. Among bound chloride, chemically bound chlorides are utilized in the hydration product of cement and physically bound chlorides are absorbed on the surface of the gel pores. This is important as only the free chlorides are relevant to the corrosion of reinforcement. Qureshi et al. 2017, defined the chloride threshold level as the chloride ion concentration of steel bars in concrete provided that there are no damages at the rebar concrete interface as shown in Table 1.3

Table 1.3 Corrosion risk classification at different chloride levels (Qureshi et al 2017).

S.No.	Risk of Corrosion	Chloride Content (% wt. of cement)
1	Negligible	0.4
2	Possible	0.4-1.0
3	Probable	1.0-2.0
4	Certain	>2.0

1.5 BINDING OF CHLORIDE IONS

The primary mechanism of chloride ion binding in cement is through its reaction with C3A, resulting in the formation of calcium chloro-aluminate. Similarly, C4AF reacts with chloride ions to produce calcium chloro-ferrite. Research indicates that a greater number of chloride ions are bound when the cement has a higher C3A content and when the cement content in the mixture is higher. Additionally, the presence of slag cement or concrete with ground granulated blast furnace slag (GGBS) enhances the binding of chloride ions.It is crucial to note that even in the absence of chloride ions, corrosion can still occur in cement or concrete with a pH value below 11.5. Other factors can contribute to the corrosion process in such environments.

Tale 1.4 Volume variations of rust products (Qureshi et al 2017).

Corrosion product	Colour	Volume in cm^3
Fe	Earthy	1.3
FeO	Black	1.9
Fe_3O_4	Black	2.1
$Fe(OH)_2$	White	3.8
$Fe(OH)_3$	Brown	4.2
$Fe(OH)_3.3H_2O$	Yellow	6.4
Fe_2O_3	Red	2.5

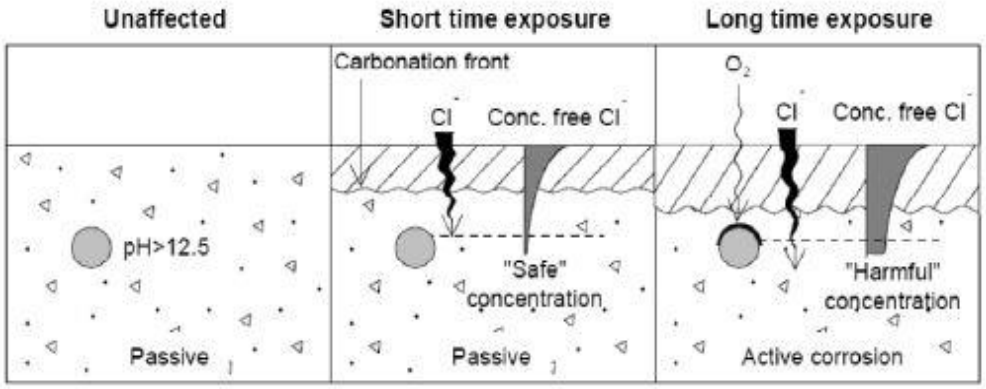

Figure 1.2 Corrosion by chloride ions and carbonation (Qureshi et al 2017).

1.6 CORROSION CONTROL MEASURES

Corrosion control is usually handled in design codes in the form of minimum concrete cover, minimum grade of concrete, maximum allowable crack width, etc., when exposure

conditions are particularly harsh, there is a need to apply special measures beyond the minimum provided in the design codes. These include both passive and active measures. The passive measures refer to the improvement of durability of concrete that includes the use of high-quality concretes produced by the incorporation of various chemical admixtures (e.g. plasticizers, superplasticizers, shrinkage reducing admixture corrosion inhibitors) and mineral admixtures. Active corrosion system, on the other hand, directly reduces the corrosion rate, which include cathodic protection, galvanization etc.

Repairs to corrosion-damaged concrete structures are broadly categorised into two classes*: Conventional repair methods and Electro-chemical methods.* Conventional repair methods involve the removal of delaminated/spalled concrete and replacement with new alkaline concrete and also patching, coatings, sealers, membranes and barriers, encasement and overlays, impregnation and the use of corrosion inhibitors. These are generally temporary techniques for corrosion prevention and can lead to acceleration of corrosion in nearby repaired areas. After serious damage has occurred, they are generally costly and less effective than electrochemical methods.

Some of the commonly used corrosion control measures are summarized as follows:

- Good quality concrete with low water/cement ratio
- Use of superplasticizers
- Provision of adequate concrete cover
- Use of pozzolans
- Use of corrosion inhibitor
- Use of other re-enforcing materials (like FRP, Galvanised steel etc.)
- Use of Electrochemical processes

1.6.1 CORROSION CONTROL BY INHIBITORS

Corrosion inhibitor is either liquid or powder chemical additive that reduce the rate of metal wastage on mixing to a corrosive aqueous condition. In ideal condition, corrosion inhibitor prevents corrosion in reinforced steel without adversely affecting properties of concrete. Inhibitors are uniformly distributed throughout the concrete matrix hence protecting the entire steel surface.

Corrosion inhibitor may include materials which mitigate reinforcement corrosion by one of the following mechanisms:

(i) Oxidation by passivation of the surface;

(ii) Formation of barrier layers;

(iii) Influencing the environment in contact with the metal.

Following are the requirements for effective corrosion inhibitor:

- The solubility should be such that rapid saturation of the corroding surface occurs without being readily leached out.
- The molecules should possess strong electron acceptor or donor properties or both.
- Induce polarization of the respective electrodes at relatively low current values.
- Be compatible with the intended system so that adverse side effects are not produced.
- The solubility should be such that rapid saturation of the corroding surface occurs without being readily leached out.
- The molecules should possess strong electron acceptor or donor properties or both.
- Induce polarization of the respective electrodes at relatively low current values.
- Be compatible with the intended system so that adverse side effects are not produced.

Inhibitors can be used by adding in concrete or applying externally on existing structures, the former type comes under the category of *Corrosion Inhibitor Admixtures (CIA)*, and can be classified as,

- **Anodic Inhibitors**

  Anodic inhibitors form a protective oxide film on the surface of the metal, promoting a large anodic shift of the corrosion potential which forces the metallic surface into the passivation region. The film initiates at the anode although it may eventually cover the entire metal surface. They are also sometimes referred to as passivators. An anodic inhibitor hinders the anodic process.

- **Cathodic Inhibitors**

  Cathodic inhibitors are generally less effective than the anodic inhibitors. Cathodic inhibitors function by: a) or selectively precipitating on cathodic areas to limit the diffusion of reducing species to the surface. The cathodic inhibitors reduce the corrosion rate indirectly by reducing the cathodic process in which they itself slow the cathodic reaction or they precipitate selectively on those areas which are cathodic to reduce the diffusion of reducing species to the surface.

- **Mixed Organic Inhibitors**

  Mixed inhibitors is a combination of both anodic and cathodic processes, as there is danger of pitting while using anodic inhibitors. Therefore, it became common practice to use mixed inhibitors instead of using both anodic and cathodic inhibitors at a time in concrete. (Fontana MG)

1.6.2 *CORROSION CONTROL BY ELECTRO-CHEMICAL PROCESSES*

With the increasing demand for longer service life and the significant costs associated with constructing and maintaining infrastructure, the repair of concrete structures has gained immense importance. The techniques employed for concrete repair and protection are based on chemical, electrochemical, or physical principles. Since corrosion is an electrochemical process, its key components are the cathode, the anode, and the electrolyte (in the form of concrete pore water). The absence of any of these three components can impede the corrosion process.

Electrochemical techniques, such as cathodic protection, cathodic prevention, electrochemical realkalization, and electrochemical chloride removal, have proven to be effective methods for preventing and mitigating corrosion. These techniques involve the suppression of chemical reactions and the flow of current resulting from corrosion through the application of an external direct current (DC) supply, often with the assistance of a temporary or permanent anode. The direct current is directed from the artificial anode to the reinforcing steel that requires protection. The current flows through the pore water of the concrete, carrying ions to the reinforcement. One advantage of such techniques is that only damaged or deteriorated concrete needs to be removed and repaired, minimizing the extent of repair work necessary.

1.7 BI-DIRECTIONAL ELECTRO-MIGRATION REHABILITATION (BIEM)

A novel method called BIEM (Bi-directional electro-migration) has been proposed as a promising approach to repair chloride-contaminated concrete, addressing limitations of traditional corrosion inhibitors and electrochemical techniques. This method involves the application of an electrical field between the embedded steel (cathode) and an external anode, which is immersed in the electrolyte and contacts the surface of the concrete specimen.

Under the influence of the electrical field, the cationic species of the corrosion inhibitor migrate into the concrete cover towards the cathode, while the chloride ions present in the concrete migrate outwards towards the anode. This migration process facilitates the formation of a protective film around the embedded steel bars, with the corrosion inhibitor effectively isolating corrosive substances like chloride and oxygen once its concentration reaches an adequate level. Furthermore, the generation of hydroxyl ions at the cathode due to the electrical field enhances the alkalinity of the pore solutions near the embedded steel bars. This alkalinity enhancement promotes the re-passivation of the steel, favoring its protection against corrosion. A schematic representation of the biem technique can be observed in figure 1.3.

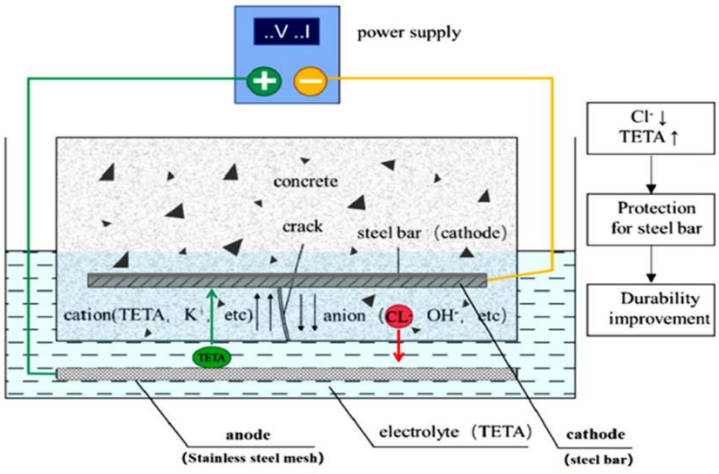

Figure 1.3 Schematic of the application of the BIEM technique

Corrosion poses a significant challenge to the longevity and durability of structures worldwide. It often leads to premature degradation of materials, reducing their lifespan. Over time, various techniques have been developed for the repair and prevention of

corrosion. These include the use of corrosion inhibitors, electrochemical processes, and, more recently, a combination of both methods. In this study, our focus will be on exploring the effectiveness of this combined approach in combating corrosion. By leveraging the benefits of both corrosion inhibitors and electrochemical processes, we aim to develop a more comprehensive and efficient strategy to address the corrosion-related issues in structures. Triethylenetetramine (TETA) has been extensively employed as an inhibitor in the Bidirectional Electro-migration (BIEM) process hence in the migration efficiency of a new organic inhibitor aminopyridine has been studied under the influence of an electric field to repair chloride damaged concrete in this research.

1.8 Research Gaps

- The most commonly used inhibitor for BIEM is triethylenetetramine (TETA) however organic inhibitors such as 2AP, Syrene etc. Need to be further experimented.
- Limited study on BIEM has been conducted till now.
- Lack of research on different parameters of BIEM.

1.9 Aim and Objectives

The aim of this study is to analyse the efficiency of Amino-2-Pyridine Inhibitor on the Rehabilitation of Chloride Contaminated Reinforced Concrete with Bidirectional Electro-migration Method. The objectives of the study are:

1. To investigate the combined effect of 2AP as inhibitor and the electro-chemical chloride extraction process on chloride-contaminated concrete, aiming to understand their synergistic or complementary actions in improving the corrosion resistance of concrete.
2. To analyse the effectiveness of the proposed technique by monitoring change in steel/concrete potential, corrosion rate, chloride and inhibitor migration.
3. To explore the effects of different parameters including applied current density, initial chloride content, inhibitor content and treatment duration on the effectiveness of the protection system.

4. To expose the treated specimens to wet and dry cycles and monitor the achieved protection

1.10 Outline of the thesis

Chapter 1: Introduction

This chapter introduces the research work, highlighting its significance in the field. It outlines the aims and objectives of the investigation, clarifying the purpose of the study. The chapter provides an overview of the entire thesis, giving readers an idea of what to expect in the subsequent chapters.

Chapter 2: Literature Review

This chapter delves into a comprehensive review of existing literature relevant to the research topic. It presents a thorough understanding of the current state of research and identifies gaps or areas for further exploration.

Chapter 3: Materials and Preparation

In this chapter, the materials used in the research work are described in detail. The methods of preparation for these materials are outlined, ensuring reproducibility and understanding of the experimental setup.

Chapter 4: Methodology

This chapter explains the chosen methodology for conducting the research work. It includes detailed information on the experimental procedures, data collection methods, and any analytical techniques employed.

Chapter 5: Results and Discussion

Here, the findings of the experimental investigation are summarized and presented. The results are thoroughly discussed, interpreted, and compared with the existing literature or theoretical expectations.

Chapter 6: Summary, Conclusion, and Future Recommendations

This chapter provides a comprehensive summary of the entire research work. It presents the conclusions drawn from the study, based on the results and analysis. Additionally, the chapter offers recommendations for future research directions or improvements to the methodology.

Chapter 7: References

This chapter lists all the references cited throughout the thesis.

CHAPTER 2. LITERATURE REVIEW

2.1 Effects of inhibitors on reinforcement of concrete in structures

Martinez et al. (2022) colourful thin oxide films were fabricated through galvanostatic anodization on Ti-6Al-4V alloy using three different aqueous solutions containing corrosion inorganic inhibitors (Na2MoO4, NaH2PO4, and NH4VO3). The researchers investigated the effect of these inhibitor anions on the corrosion behavior of the alloy in Ringer solution. The results demonstrated that regardless of the solution used, the anodized samples exhibited compact and amorphous oxide films without any pores or cracks. Among the different solutions, the sample anodized in Na2MoO4 solution showed the lowest corrosion current density (0.11 μA/cm2) and effectively protected the alloy even after 168 hours of immersion in Ringer solution. Notably, no cracks or corrosion products were detected, indicating the excellent performance of this oxide film. To evaluate the corrosion performance of both bare and anodized Ti-6Al-4V alloy in Ringer solution, various electrochemical techniques, including Tafel polarization, were employed. Tafel tests were conducted in Ringer solution after one hour of open circuit potential (OCP), starting from -0.20 to 0.20 V (SCE) versus OCP, with a potential scan rate of 0.001 V/s. The corrosion parameters were estimated using the Tafel extrapolation method. The corrosion current density (Jcorr) values were determined by extrapolating the anodic and cathodic branch lines to the corrosion potential (Φcorr) or by extrapolating the cathodic region of the curve to the Fcorr in cases of non-linear behavior in the anodic region.

Figure 2.1 depicts the Tafel polarization curves for both the bare and anodized Ti-6Al-4V electrodes in Ringer solution. The corresponding parameters extracted from these Tafel polarization curves are presented in Table 2.1. Notably, all the treated electrodes exhibited a noticeable shift in the corrosion potential (Φcorr) towards more positive values compared to the untreated alloy. Among the different treated electrodes, the most significant change in Φcorr was observed for Ti−6Al−4V0.50Mo (as shown in Fig. 2.2), displaying a substantial difference of 0.77 V when compared to the bare Ti−6Al−4V alloy (as depicted in Fig. 2.3). This shift in Φcorr indicates an improvement in the corrosion resistance of the Ti-6Al-4V alloy after anodization with Na2MoO4 solution.

Table 2.1 Corrosion parameters obtained from Tafel polarization curves (Martinez et al 2022)

Sample	Φcorr (vs SCE)/V	Jcorr/ (μA·cm−2)	βa/ (V·dec−1)	βc/(V·dec−1)
Ti−6Al−4V	−0.36	5.32	1.12	0.78
Ti−6Al−4V0.50Mo	0.41	0.11	∞	0.23
Ti−6Al−4V0.50P	0.31	1.33	∞	0.4
Ti−6Al−4V0.025V	−0.16	16.84	1.16	0.94

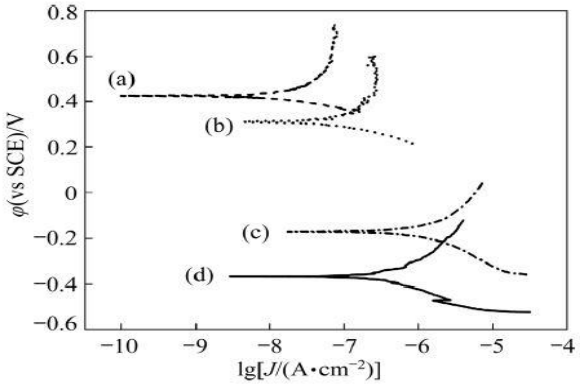

Figure 2.1 Tafel polarization curves obtained in Ringer solution for different samples: (a) Ti−6Al−4V0.50Mo; (b) Ti−6Al−4V0.50P; (c) Ti−6Al−4V0.025V; (d) Bare Ti−6Al−4V (Sweep rate: 0.001 V/s) (Martinez et al 2022)

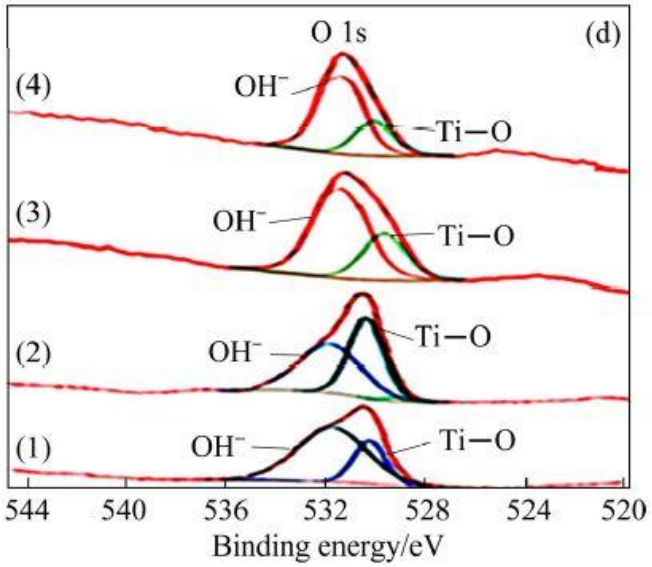

Figure 2.2 High resolution of XPS spectra of Ti 2p P 2p (Martinez et al 2022)

A noticeable decrease in the corrosion current density (Jcorr) was observed for Ti−6Al−4V0.50Mo and Ti−6Al−4V0.50P, with Ti−6Al−4V0.50Mo exhibiting the most favourable results among the treated electrodes. On the contrary, Ti−6Al−4V0.025V displayed the highest Jcorr, indicating that the oxide coating formed in this case did not contribute to the passivation of the alloy, unlike the other coatings. Comparing the obtained Jcorr values for the bare alloy with existing published data is challenging due to the dependence of the corrosion current density of Ti alloys on factors such as surface preparation and other variables. Nevertheless, the parameters obtained for the bare alloy are consistent with those reported in other research studies. Analysis of the cathodic slopes indicated that oxygen reduction takes place on the metal surface. As for the anodic slopes, both bare Ti−6Al−4V and Ti−6Al−4V0.50P exhibited similar values. However, for Ti−6Al−4V0.50Mo and Ti−6Al−4V0.50P, a non-linear behavior was observed due to the presence of a small active dissolution zone and the passivation achieved by the alloy in the anodic region. Consequently, in these specific cases, the calculation of the anodic slopes resulted in an infinite value.

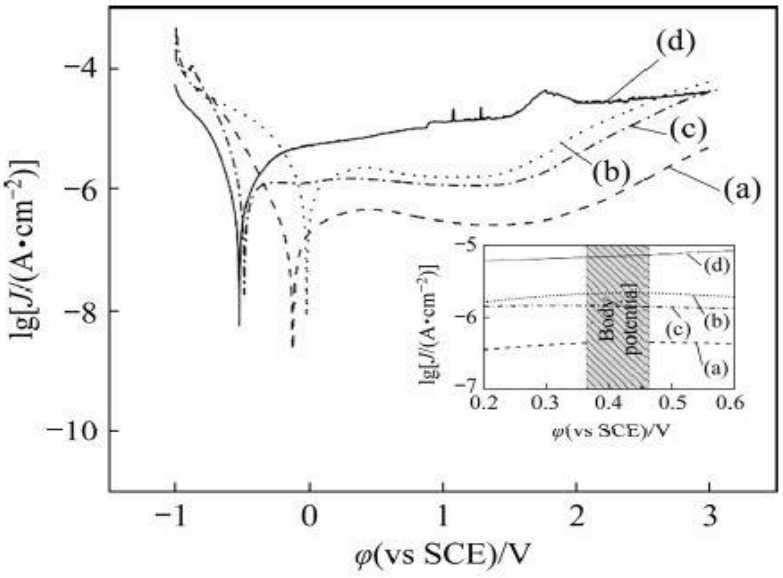

Figure 2.3 Polarization curves obtained in Ringer solution for different samples: (a) Ti−6Al−4V0.50Mo; (b) Ti−6Al−4V0.50P; (c) Ti−6Al−4V0.025V; (d) Bare Ti−6Al−4V alloy (Sweep rate: 0.001 V/s; Potential range:−1.0 to 3.0 V (vs SCE); Insert: magnified zone of polar (Martinez et al 2022)

The Tafel extrapolation method remains valid even if one of the branches of the polarization curves is under activation control. In such cases, the corrosion current density

(Jcorr) values were estimated by extrapolating the anodic Tafel lines to the corrosion potential (Φcorr), considering the behavior of the anodic branches. Fig. 2.8 illustrates the polarization curves for both the anodized and non-anodized samples. The anodic branch of the curves shows an active-passive transition for both the bare and treated samples. The obtained passivation current densities for Ti−6Al−4V0.50Mo, Ti−6Al−4V0.50P, and Ti−6Al−4V0.025V were found to be 99, 1565, and 1125 nA/cm2, respectively. After the passivation plateau, all current densities begin to increase, likely due to the occurrence of oxygen and chlorine evolution reactions at around 1.5 V (vs SCE). Despite the polarization being performed up to 3.0 V (vs SCE), no breakdown potential was detected. There is a shift in the corrosion potential to more noble values for Ti−6Al−4V0.50Mo and Ti−6Al−4V0.50P. Only in the case of Ti−6Al−4V0.50Mo, a decrease in the corrosion current density is observed. It is important to carefully analyze the potential range between 0.4 and 0.5 V (vs Ag/AgCl) for a comprehensive understanding of the corrosion behavior.

Liu et al. (2022) a series of organic corrosion inhibitors were investigated using density functional theory (DFT) to analyze their molecular geometry, electronic structure, and adsorption behavior. Among these inhibitors, 1H-benzotriazole was found to be an excellent corrosion inhibitor due to its considerable adsorption energy. The electronic structure analysis revealed that 1H-benzotriazole has the smallest HOMO-LUMO gap compared to other inhibitors in the study. Geometric optimization and electrostatic potential analysis indicated that the triazole ring in 1H-benzotriazole has three potential sites for adsorption on the Fe (111) surface. The strong adsorption behavior was attributed to the donor-acceptor bonding interaction between the Fe (111) surface and the 1H-benzotriazole molecule. The molecular geometries of all organic corrosion inhibitors were optimized using the M06-2X functional with 6-311G (d) basis sets, and the calculated geometric parameters fell within a rational range based on reported data elsewhere. The frontier molecular orbitals (FMOs) of the inhibitors were calculated and analyzed. The frontier molecular orbitals (FMOs) of the organic corrosion inhibitors were calculated and their energy levels were listed in Fig. 2.11. The calculated HOMO-LUMO gap values were found to increase in the following order: a (7.756 eV) < f (8.125 eV) < b (8.247 eV) < e (8.280 eV) < h (8.712 eV) < c (9.402 eV) < g (9.777 eV) < d (19.498 eV). The energy level of the highest occupied molecular orbital (HOMO) was found to

increase in the following order: b (-7.694 eV) < f (-7.831 eV) < c (-8.057 eV) < a (-8.131 eV) < h (-8.576 eV) < e (-9.096 eV) < d (-9.209 eV) < g (-9.227 eV). The HOMO-LUMO gap and HOMO energy levels were found to vary among the inhibitors. Notably, 1H-benzotriazole exhibited the smallest HOMO-LUMO gap, while another inhibitor, b, had the lowest HOMO energy level but the third smallest HOMO-LUMO gap. The analysis indicated that the differences in HOMO-LUMO gap mainly arose from significant changes in the LUMO energy level for all the inhibitors studied, with N,N-dimethylethanolamine (d) showing the largest HOMO-LUMO gap due to its very high energy level of LUMO among all the inhibitors.

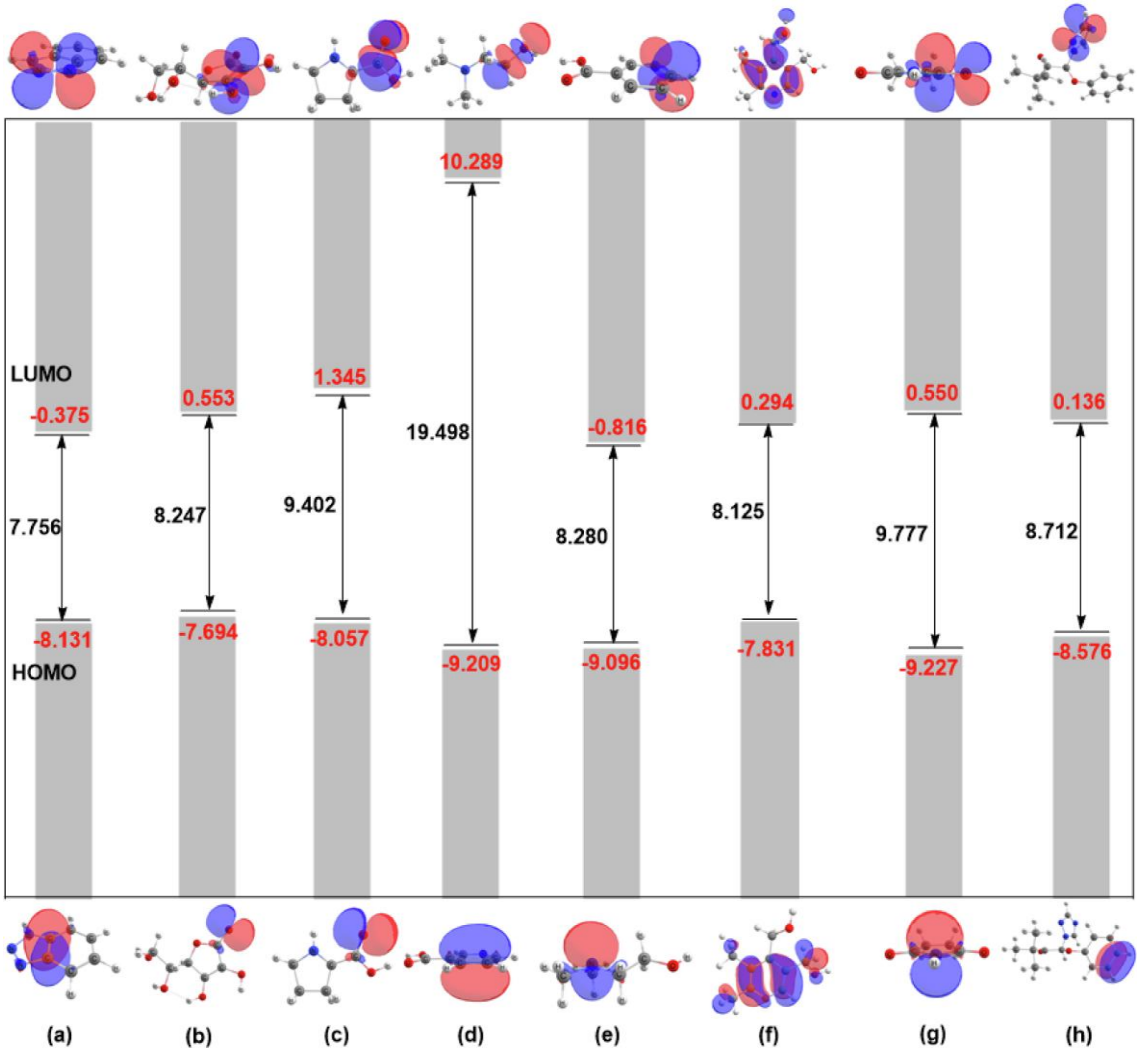

Figure 2.4 FMOs of the series of organic corrosion inhibitors studied here obtained by M06-2X/6 311G (d) calculations. (Liu et al 2022)

The DFT calculations have been utilized to investigate the molecular geometry, electronic structure, and adsorption behavior of a series of organic corrosion inhibitors. Among these inhibitors, 1H-benzotriazole demonstrates a significant adsorption energy on the Fe(111) surface. Additionally, electronic structure analysis reveals that 1H-benzotriazole possesses the smallest HOMO-LUMO gap when compared to the other corrosion inhibitors studied in this work. The EP (electrostatic potential) analysis further indicates that the hydroxy, carboxyl, amino, and triazole groups present in these organic corrosion inhibitors are all located in the basic region. According to Lewis' acid-base theory, these regions are considered potential active sites for adsorption on the Fe(111) surface. The findings from this study provide valuable insights and a clear understanding of the interaction between the Fe(111) surface and the series of corrosion inhibitors investigated. This knowledge is essential for further understanding and optimizing the effectiveness of these inhibitors in mitigating corrosion processes.

Tiwari et al. (2022) the effectiveness of three generic compounds, namely 4-Aminobenzoic acid (ABA), 2-Aminopyridine (2AP), and Salicyaldehyde (SA), as migratory inhibitors on hardened concrete surfaces was investigated to mitigate corrosion caused by a combination of chloride and carbonated environment. The researchers used two types of cement, Portland cement, and fly ash blended cement, to prepare concrete mixes for testing. Various electrochemical techniques such as Linear Polarization Resistance (LPR) and Electrochemical Impedance Spectroscopy (EIS) were employed, along with gravimetric analysis, to evaluate the corrosion performance of the treated samples. The percolation ability of the inhibitors was assessed using UV-visible spectroscopy. Additionally, the chloride profile and carbonation depth were analyzed after specific exposure durations to identify the dominant cause of corrosion and the effect of inhibitor application on these parameters.

The results indicated that steel in blended cement was more susceptible to corrosion compared to Portland cement. The study revealed that carbonation had a significant impact on the corrosion process during combined exposure, with chloride ions initiating the corrosion process in the first phase, leading to pitting corrosion. In the second phase, carbonation further aggravated the corrosion mechanism. The application of corrosion inhibitors (CoI) effectively reduced the corrosion rate. Among the inhibitors tested, ABA displayed the highest inhibition efficiency of 79.64% in Portland cement and 88.31% in

blended cement concrete, followed by 2AP and SA. The inhibition order correlated with the concentration of the inhibitors at the rebar level, indicating a direct relation between these two parameters. Optical examination of the exposed concrete surface and the extracted rebar's surface validated the inhibitory effect of the inhibitors. Notably, the application of inhibitors led to a reduction in crack width on the concrete surface. Interestingly, the vulnerability to corrosion of the blended cement concrete system was significantly reduced after the application of inhibitors, making it comparable to the corrosion resistance of Portland cement concrete. Overall, the study demonstrates the potential of migratory inhibitors to effectively curb corrosion in reinforced concrete structures exposed to chloride and carbonated environments.

The concentration of the generic compounds in Ordinary Portland Cement (OPC) and Portland Pozzolana Cement (PPC) based specimens was analyzed, and the results are presented in Fig. 2.5. The bar chart illustrates that all the inhibitors were capable of percolating and reaching the rebar level within 15 days, regardless of the type of cement used. Among the inhibitors, ABA showed the highest concentration, followed by AP and SA, in both concrete systems. This concentration order was consistent across both cement types. The high migration rate of ABA can be attributed to its high molecular weight, which facilitates its movement through the concrete. The percolation process in this study was induced solely by gravity, and the molecular weight of the inhibitors played a crucial role in their migration. In the case of AP, the existence of an amine group close to the nitrogen atom in the pyridine ring may have resulted in the formation of a chelating ring with Ca^{2+} ions present in the concrete. This chelating interaction may have slowed down the dispersion of AP, leading to a lower concentration of AP at the cover depth (as depicted in Fig. 2.5). For SA, its concentration at 15 mm was found to be the lowest among the three inhibitors. This can be attributed to the hydroxyl functional group of SA, which electrostatically interacts with Na^{+} ions present in the concrete, reducing its migration ability.

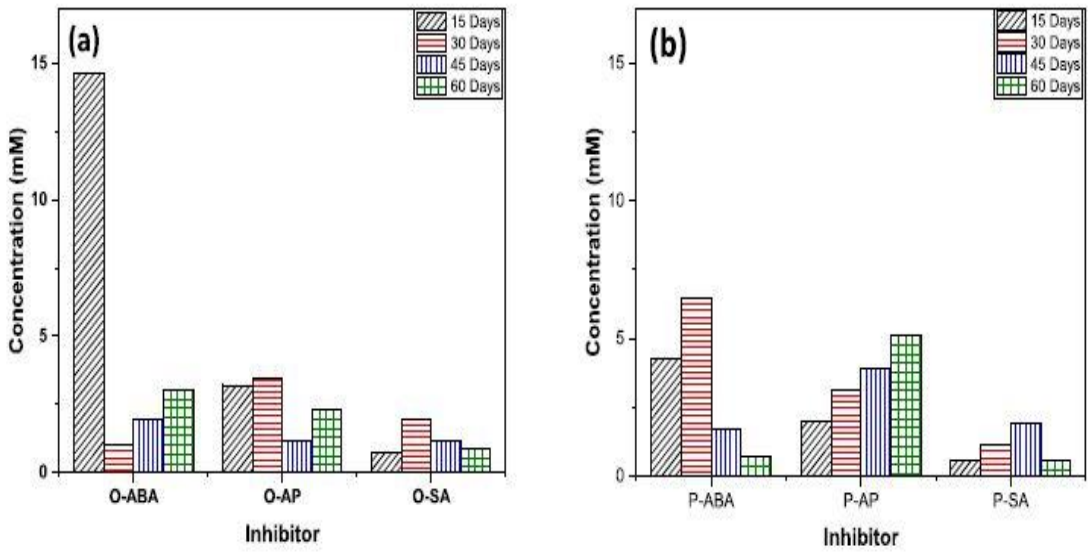

Figure 2.5 Concentration of compound at cover depth up to 60 days after application for (a) OPC-based concrete (b) PPC based concrete. (Tiwari et al 2022)

The interaction between the corrosion inhibitors and the concrete has been evidenced by the shift in UV spectra, indicating the occurrence of secondary pozzolanic reactions. As a result of these reactions, Portland Pozzolana Cement (PPC) concrete exhibits higher values of carbonation depth compared to Ordinary Portland Cement (OPC) concrete due to the presence of a lesser amount of portlandite. This observation is consistent with findings from other researchers. The effect of Corrosion Inhibitors (CoI) on carbonation depth was also studied at specific time intervals. In OPC specimens, the application of inhibitors did not lead to a reduction in CO2 ingress. However, in PPC specimens, a slight reduction in the carbonation front was observed for all the inhibitors. This improvement can be attributed to the formation of a layer on the hardened concrete surface, which acted as a barrier for CO2 diffusion. OPC concrete is more porous, allowing inhibitors to freely move within the concrete, thereby not leading to the formation of a surface layer. On the other hand, PPC concrete has a denser structure, causing the inhibitors to stay on the surface, thus reducing the carbonation depth. This phenomenon is supported by the slow percolation of inhibitors in PPC specimens during the concentration evaluation test. ABA demonstrated the highest percolation ability, followed by 2AP and SA, regardless of the concrete type (OPC or PPC). Furthermore, it was observed that chloride ions were responsible for initiating the corrosion process, and carbonation aggravated the corrosion

mechanism. The order of inhibition efficiency was found to be ABA > 2AP > SA, which is directly proportional to the amount and form of the compound reaching the rebar. ABA reached the rebar level in its pure form and at the highest concentration, whereas 2AP and SA reached with lower concentrations and in their modified forms. In terms of the concrete's compressive strength, the application of the generic compounds on both OPC and PPC concrete did not have any negative effects, indicating that the inhibitors did not compromise the mechanical properties of the concrete.

Tiwary et al. (2021) the corrosion inhibition effect of two generic compounds, Triethylphosphate (TEP) and Salicyaldehyde (SA), in simulated carbonated pore solution contaminated with chloride ions (Cl-) was investigated. The study involved electrochemical measurements using Potentiodynamic polarization curves. The results in the simulated pore solution demonstrated that both TEP and SA effectively reduced the corrosion rate, regardless of the tested concentration levels. For TEP, its efficiency increased from 65.36% to 83.18% with an increase in concentration from 0.05 M to 0.2 M. On the other hand, SA exhibited high inhibition efficiency even at a concentration as low as 0.05 M, reaching 96.4%. Surface analysis data confirmed that the corrosion product on specimens immersed in the contaminated environment contained FeOOH, Fe2O3, and Fe3O4. However, the presence of the phosphate group in TEP was able to reduce the formation of corrosion products.

The mechanism of inhibition for both compounds depended on the type of heteroatom present within their molecular structures. TEP retarded the corrosion of rebar by promoting the growth of the iron oxide film and healing defects in the protective film. On the other hand, SA formed an adsorptive black layer over the exposed surface through a chelation process. Among the two compounds, the inhibition efficiency of SA was particularly high, reaching 99%. The study was divided into two levels: a) investigating the corrosion inhibition mechanism of the compounds through tests on bare steel in simulated concrete pore solution, and b) studying the migration ability of the compounds through tests conducted on concrete specimens. Based on the obtained electrochemical data, it can be concluded that both TEP and SA are efficient in retarding the corrosion rate in a combined chloride and carbonated environment.

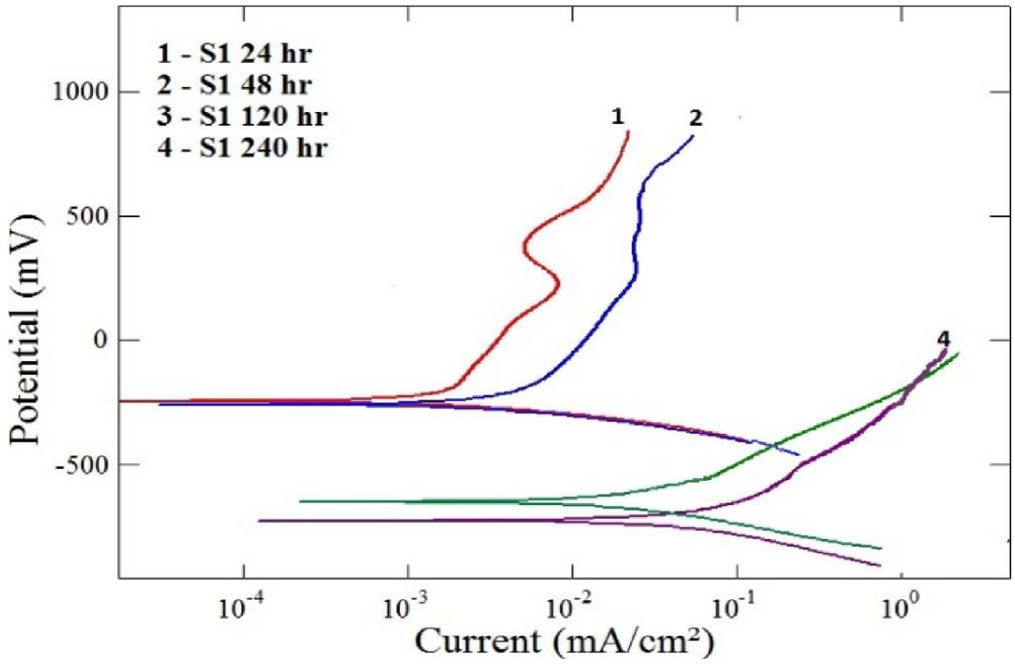

Figure 2.6 Polarization curve recorded on steel in carbonated chloride solution. (Tiwary et al 2021)

As the concentration of Triethylphosphate (TEP) increases from 0.05 M to 0.2 M, its inhibition efficiency also increases from 65.3% to 83%, showing a positive correlation between concentration and protection effectiveness. On the other hand, Salicyaldehyde (SA) exhibits very high inhibition efficiency even at low concentration levels. The corrosion protection mechanisms of both compounds are influenced by the heteroatoms present in their molecular structures. In the case of TEP, which contains oxygen (O) and phosphorus (P) as heteroatoms in its inorganic functionality, these elements enhance its protection mechanism by increasing its reactivity with ferrous ions on the exposed surface. Surface analysis further confirmed that TEP retards corrosion by promoting the growth of an iron oxide film, which is susceptible to damage in the presence of chloride ions (Cl-). For SA, the inhibition mechanism is governed by the presence of oxygen (O) as a heteroatom in the form of carbonyl and hydroxyl groups on its organic benzene ring. This provides SA with additional chelating capabilities, allowing it to adsorb effectively on the metal surface. The phenolic group of SA breaks down to phenoxide ions, further enhancing its chelating efficiency with ferrous ions, ultimately forming a visible protective layer on the surface of the rebar.

Zomorodian et al. (2021) in the investigation of corrosion inhibitors' performance in the critical chloride concentration (Ccrit), various electrochemical techniques such as open circuit potential and linear polarization were employed in synthetic pore solutions. Potentiodynamic polarization and electrochemical impedance spectroscopy were used to assess the corrosion activities and passivation mechanism of the inhibitors at Ccrit. The results revealed that the selection of appropriate corrosion inhibitors can effectively protect the reinforcing steel. Among the inhibitors studied, casein exhibited the highest corrosion inhibition efficiency, displaying a minimum current density of 9.19 × 10-8 µA/cm2 and an inhibitor efficiency of over 80%. Casein was found to provide passivity to the reinforcing steel in the presence of Ccrit in the pore solution, effectively preventing corrosion. Furthermore, the addition of inhibitors to the pore solution containing the critical concentration of chloride ions significantly influenced the open circuit potential (OCP) values, as depicted in Figure 2.7. This indicates that the inhibitors play a crucial role in controlling the corrosion process and maintaining the passivity of the reinforcing steel under critical chloride conditions.

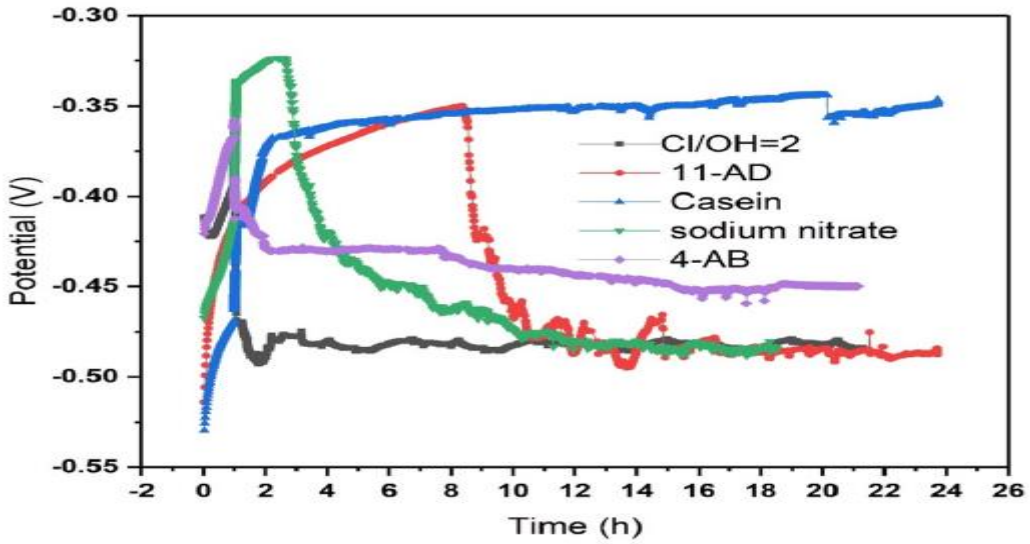

Figure 2.7 The OCP value of reinforcing steel in synthetic pore solution with different inhibitors at critical concentration of Cl/OH ratio. (Zomorodian et al 2021)

According to ASTM C876-09, active corrosion of embedded rebar in cement is identified when the Open Circuit Potential (OCP) value is more negative than 0.273 V. However, various environmental factors, such as the availability of oxygen (as described earlier in

reaction 3) or the presence of other additives, can influence the corrosion process and OCP values. In this research, the use of sodium nitrate as an inhibitor caused a shift in the potential of the reinforcing steel from 0.48 V to a more positive value. Nitrates are considered anodic inhibitors that form an insoluble protective film on the corroding steel's anodic spots, thereby blocking further anodic reactions and facilitating the re-passivation of the steel surface. However, the increase in OCP in the presence of sodium nitrate was limited to the first few hours, after which a breakdown in OCP was observed, and the potential shifted back towards the cathodic values close to the potential of corroding steel (0.48 V). This breakdown in potential can be attributed to the pH and availability of oxygen in the pore solution since nitrates can enhance the formation of a passive film in acidic solutions. Overall, the passive film formed in the presence of nitrates is nearly independent of the alkaline solution. When the inhibitor 11AD was applied, it promoted a limited and sustained shift to a positive potential for only 8 hours, after which it exhibited a breakdown toward the corroding potential. Similarly, when 4AB was used as an inhibitor, the OCP also broke down, but even after this collapse, the recorded OCP value was 0.42 V, which was still higher than the corroding potential of the reinforcing steel (0.48 V), as shown in Figure 2.8. This indicates that both 11AD and 4AB provided some degree of corrosion inhibition, but their protective effect was not as stable or effective as that of sodium nitrate.

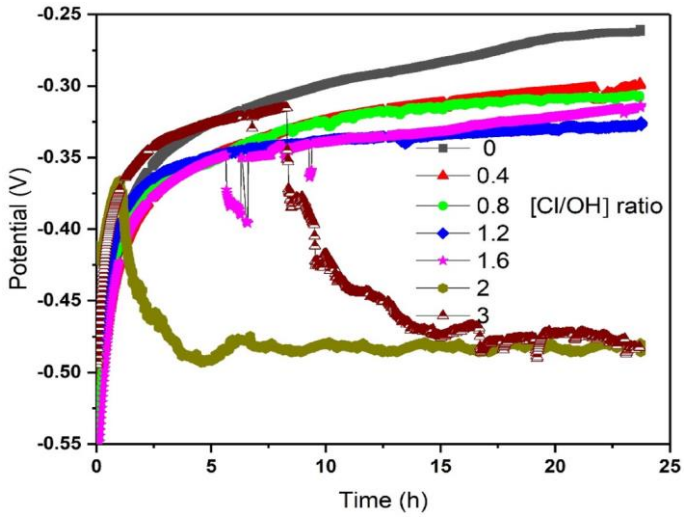

Figure 2.8 Variation of OCP value for reinforcing steel in synthetic pore solution at different ratios of [Cl]/ [OH] in absence of corrosion inhibitor. (Zomorodian et al 2021)

In contrast to the previous inhibitors, casein demonstrated a highly effective corrosion inhibition performance. When casein was applied as an inhibitor, it shifted the OCP of the corroding steel to more noble values, and there was no significant decrease or breakdown in OCP observed during immersion in the pore solution containing Ccirt. The enhanced passivity of the reinforcing steel, even at Ccirt, can be attributed to the absorption of casein into the surface of the steel. Casein contains several polar functional groups, such as carbonyl, amide, and amino groups, which may facilitate the formation of a complex of iron oxide and casein on the steel surface, subsequently altering the chemistry of the interface. As a result, the OCP value of the passivated reinforcing steel in the presence of casein was approximately 0.32 V, which is 0.280 V higher than the corroding OCP potential. The research concluded that the Open Circuit Potential (OCP) of the reinforcing steel shows a clear relationship with the chloride concentration of the synthetic pore solution. An increase in chloride concentration leads to a shift in potential to a more cathodic value. The first radical change in potential due to the increasing chloride concentration indicates the chloride threshold value, beyond which corrosion initiation occurs. Additionally, the OCP can be considered as a criterion for evaluating the efficiency of inhibitors in a pore solution containing Ccirt. More effective inhibitors tend to shift the OCP to nobler potentials. It was observed that de-passivation of the reinforcing steel occurred at [Cl-]/[OH-] = 2, most likely associated with a drop in polarisation resistance (Rp). However, casein as a green corrosion inhibitor provided sufficient corrosion protection to the reinforcing steel and can be used as a viable alternative to toxic corrosion inhibitors.

Carranza et al. (2021) investigated the corrosion inhibition properties of selected small organic compounds using various electrochemical measurements, such as potentio-dynamic polarization (PDP), linear polarization resistance (LPR), and electrochemical impedance spectroscopy (EIS). Additionally, density functional theory (DFT) calculations were performed to gain further insights into the inhibition mechanism. The experiments were conducted on mild steel (MS) in 1 M HCl, and the inhibition efficiency (IE %) of each inhibitor was determined. The results demonstrated that the presence of the inhibitors led to a decrease in corrosion current density (Icorr) values and an increase in polarization resistance (Rp). Moreover, it was observed that higher concentrations of inhibitors resulted in higher inhibition efficiency. The Tafel slopes and shifts in the

corrosion potential values indicated that the tested inhibitors were of mixed-type, forming a protective layer on the surface of the substrate.

Among the organic compounds tested, 4-ethylpyridine (EP) showed the highest Rp values and inhibition efficiency based on the PDP, LPR, and EIS analyses. The DFT calculations confirmed the chemisorption of the inhibitors on the MS surface and revealed negative adsorption energies, indicating the formation of a hydrophobic protective film against corrosion. The study established correlations between the quantum chemical values and electrochemical data. The research concluded that the presence of electronegative O, S, and N atoms, as well as aromatic rings in the inhibitors, promoted surface protection by preventing aggressive ionic species from binding onto MS. The inhibitors formed a protective layer on the Fe surface through chemisorption, with the aromatic rings interacting with the surface, and the alkyl chains oriented towards the solution, providing higher inhibition efficiency. While the findings suggest a promising alternative to inorganic compound inhibitors, the study has limitations, and further investigations, such as thermodynamic studies and surface microscopic spectroscopy, should be carried out to validate the Langmuir isotherm characteristics and film-forming ability of the chosen inhibitors. Overall, this research presents an environmentally friendly and accessible option for corrosion inhibition in acidic environments.

Harilal et al. (2020) indicated a substantial improvement in the corrosion resistance of steel in the CFNI (calcium ferrite and nanosilica) concrete compared to other concrete systems. The polarization resistance (Rp) in CFNI concrete was five times higher than in the control concrete, indicating superior corrosion resistance in CFNI. Additionally, the chloride ingress rate was significantly lower in CFNI specimens, and Field Emission Scanning Electron Microscopy (FESEM) images showed no micro cracks or pores at the corroded concrete steel interface in CFNI specimens. The apparent diffusion coefficient (Dcl) of the concrete system, determined using the bulk diffusion test and chloride profiling, was found to be one order of magnitude lower in CFNI concrete compared to other concrete specimens. This result indicates that CFNI concrete exhibits enhanced resistance against chloride attack, making it a promising ternary-blended concrete mix for achieving long corrosion-free service life in aggressive chloride environments.

The research involved fabricating four types of M45 grade concrete compositions with different mix designs as follows:

(i) CC – Conventional Concrete with M45 grade and 100% Ordinary Portland Cement (OPC). (ii) CF – Concrete with 60 wt% OPC and 40 wt% fly ash. (iii) CFN – Concrete with 58 wt% OPC, 40 wt% fly ash, and 2 wt% nano-phase modifiers (1 wt% nano-anatase TiO2 and 1 wt% nano-CaCO3). (iv) CFNI – Concrete with 56 wt% OPC, 40 wt% fly ash, nano-phase modifiers, and corrosion inhibitors (1 wt% nano-CaCO3, 1 wt% nano-TiO2, and 2 wt% NaNO2 inhibitor).

The total volume of cementitious materials in all the specimens was maintained at 450 kg/m3. The water-to-cement ratio for all the specimens was adjusted to achieve a constant target slump of 100 mm. The detailed mix designs used for casting the concrete specimens are provided in Table 2.2-2.3. The compositions vary based on the percentage of OPC, fly ash, and nano-phase modifiers used in each concrete mix. CFN and CFNI concretes also include specific corrosion inhibitors to enhance their corrosion resistance properties.

Table 2.2 Mixture proportion for the various concrete systems (Harilal et al 2020)

Concrete type	Cement (kg/m3)	Fly Ash (kg/m3)	F. Agg. (kg/m3)	C.Agg. (kg/m3)	TiO2 (kg/m3)
CC	450	–	797	1090	–
CF	270	180	744	1017	–
CFN	261	180	733	1010	4.5
CFNI	252	180	724	1003	4.5

Table 2.3 Mixture proportion for the various concrete systems (Harilal et al 2020)

Concrete type	CaCO3 (kg/m3)	Inhibitor (kg/m3)	Water (kg/m3)	Superplasticizer (kg/m3)	Water binder Ratio
CC	–	–	166.5	3.6	0.37
CF	–	–	171	4.5	0.38
CFN	4.5	–	162	5.4	0.36
CFNI	4.5	9.0	144	5.4	0.32

Fig. 2.9 presents the average depth of chloride ion penetration in different concrete compositions: CC (Conventional Concrete), CF (Concrete with Fly Ash), CFN (Concrete with Nano-Phase Modifiers), and CFNI (Concrete with Nano-Phase Modifiers and

Corrosion Inhibitors). The depths of chloride penetration were estimated after conducting the chloride migration test to evaluate the resistance of each concrete mix against chloride ingress. The results indicate that the depth of chloride penetration in CC concrete was 23 mm. When 40 wt% of fly ash was added in CF concrete, the chloride penetration depth reduced to 11 mm, representing a 50% reduction compared to the conventional concrete. The incorporation of nano-phase modifiers in CFN concrete led to a significant decrease in chloride penetration depth, reducing it to 8 mm. The presence of nano-anatase TiO2 and nano-CaCO3 acted as fillers, leading to a denser microstructure and thereby improving the concrete's resistance to chloride ion ingress. In CFNI concrete, which includes both nano-phase modifiers and corrosion inhibitors, the chloride penetration depth was further reduced to 6 mm. Although the addition of inhibitors increased the chloride resistance, it was not visibly prominent in the fractured concrete piece shown in Fig. 2.9.

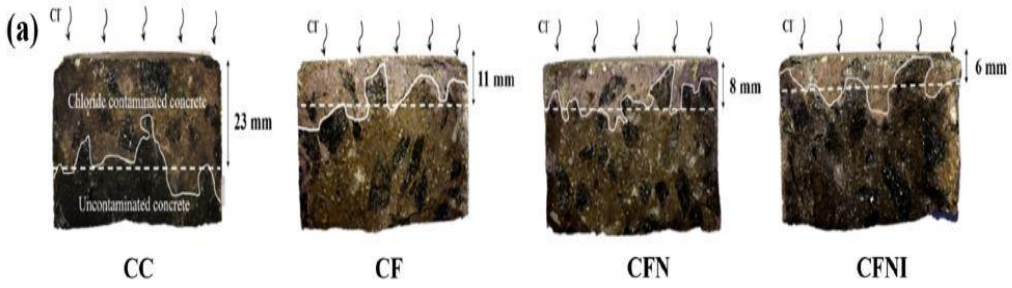

Figure 2.9 Average depth of chloride penetration measured using silver nitrate spraying for various concrete specimens (Harilal et al 2020)

The results of the chloride migration test, as shown in Fig. 2.9, provide a quantitative measure of the resistance of concrete specimens against chloride ingress. The parameter obtained from the test is the non-steady state migration coefficient, which represents the rate of chloride ingress when a potential is applied across the concrete. In the case of CC specimens (Conventional Concrete), the migration coefficient was found to be 3.43 x 10-12 m2/s. The addition of fly ash in CF specimens reduced the migration coefficient to approximately 0.96 x 10-12 m2/s, representing a 72% reduction compared to CC. Further, the incorporation of nanoparticles in CFN specimens decreased the migration coefficient to around 0.73 x 10-12 m2/s, resulting in a 78% reduction compared to CC.

However, upon the addition of the inhibitor in CFNI specimens, the migration coefficient increased to 1.16 x 10-12 m2/s. This increase in the migration coefficient suggests that the inhibitor might not have been effective in mitigating chloride ingress due to the application of the potential during the migration test. The charged ions of the inhibitor might have migrated in response to the applied potential, which may not occur in the natural environment, leading to an overestimated depth of chloride penetration in CFNI specimens. Despite the increase in the migration coefficient in CFNI specimens, the study concludes that the combination of fly ash, nanoparticles, and inhibitor in the newly developed M45 grade concrete composition (CFNI) enhances the corrosion resistance of reinforcements embedded in the concrete. The lower chloride concentrations on the surface of CFNI and CFN specimens indicate an improved chloride binding capacity. Additionally, the lower Dcl value for CFNI concrete signifies enhanced resistance against chloride attack, and the corrosion current density values of rebars embedded in CFNI and CFN specimens indicate higher resistance to corrosion activities compared to CC specimens. These findings highlight the potential of CFNI concrete as a durable and corrosion-resistant material for structures in aggressive chloride environments.

Nezhad et al. (2020) investigated the corrosion resistance of electrodeposited super hydrophobic Ni films in the presence of varying concentrations of Sodium Molybdate (0 M, 0.03 M, 0.06 M, and 0.1 M) as an inorganic corrosion inhibitor. The experiments were conducted in a 3.5 wt% NaCl solution at 25 °C for a duration of up to 120 hours. The super hydrophobic Ni film was prepared through a two-step electrodeposition process at 60 °C, which included an initial 8-minute electrodeposition at a constant current density of 20 mA, followed by a 1-minute electrodeposition at a constant current density of 50 mA/cm2. After the electrodeposition, a chemical modification step was performed in stearic acid solution. The resulting micro-nano structured Ni film had a mean thickness of 4 µm and exhibited surface features consisting of micro-nano cones with sizes ranging from 50 to 1000 nm. The researchers characterized the surface topography of the film using atomic force microscopy (AFM) and found that the root-mean-square of height was 14.4 nm, while the skewness was 0.21. The super hydrophobic film demonstrated passivation behavior and a pitting potential, indicating its potential to resist corrosion. Electrochemical impedance spectroscopy (EIS) was used to study the electrical properties of the Ni film. The EIS analysis identified the Ni film as a non-ideal capacitor, and an

equivalent circuit model with two parallel time-constants was fitted to the EIS data. After immersing the super hydrophobic Ni film in the electrolyte containing 0.1 M of sodium molybdate for 120 hours, the corrosion inhibitor efficiency was found to be approximately 80%. Additionally, the Ni film exhibited the best passivation behavior and the lowest corrosion current density under these conditions.

Fig. 2.10 presents a bar chart showing the corrosion inhibitor efficiency versus immersion times for different concentrations of sodium molybdate (0.03 M, 0.06 M, and 0.1 M). At the early stage of immersion (0.5 h), the calculated corrosion inhibitor efficiencies are negative, indicating that the presence of the corrosion inhibitor in the electrolyte reduces the corrosion resistance of the super hydrophobic Ni film. Particularly, when the concentration of the corrosion inhibitor is increased at 0.5 h immersion time, the corrosion efficiency of the inhibitor drops dramatically, resulting in reduced corrosion resistance of the Ni film. This can be attributed to an increase in the concentration of Na2MoO4 molecules in the electrolyte, which leads to the formation of a more defective stearic acid layer. Figure 2.11 shows that the contact angle of the super hydrophobic Ni film decreases with increasing immersion time in the presence of Na2MoO4. This trend supports the formation of a defective stearic acid film in the presence of the corrosion inhibitor, which could contribute to the initial reduction in corrosion resistance at early immersion times.

However, as the immersion time increases from 0.5 h to 120 h (Fig. 2.10), the efficiency of the corrosion inhibitor improves, indicating an enhanced corrosion resistance of the Ni film. This improvement in corrosion resistance can be attributed to the action of sodium molybdate as an anodic corrosion inhibitor. As the immersion time increases, sodium molybdate creates a protective oxide layer (passive film) on the surface of the Ni film, making it more resistant to corrosion attacks. Consequently, the samples immersed in the electrolyte with 0.06 M and 0.1 M of sodium molybdate exhibit the best corrosion behavior after 48 h and 120 h of immersion times, demonstrating the synergistic effect of super hydrophobicity and the corrosion inhibitor in enhancing the corrosion resistance of the Ni film.

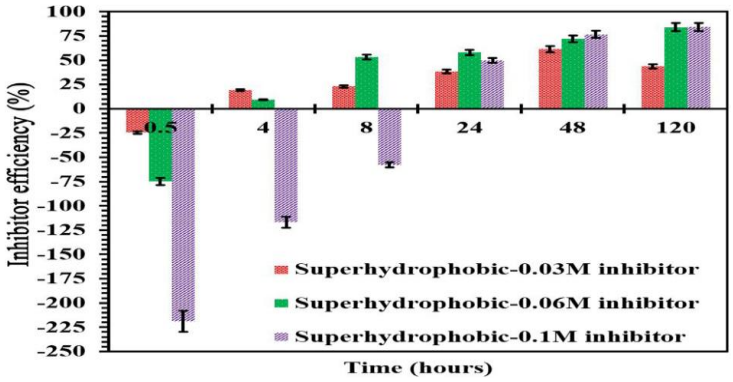

Figure 2.10 Corrosion inhibitor efficiency on super hydrophobic Ni film after 0.5, 4, 8, 24, 48, and 120 h of immersion times in the presence of 0.03 M, 0.06 M, and 0.1 M of Na2MoO4 (Nezhad et al 2020)

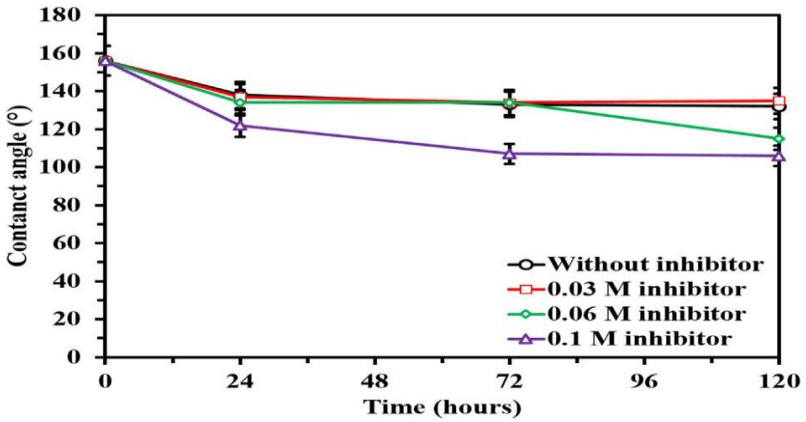

Figure 2.11 Measured water contact angle of the super hydrophobic Ni film after different immersion times in the presence of 0 M, 0.03 M, 0.06 M, and 0.1 M of Na2MoO4 (Nezhad et al 2020)

Wang et al. (2020) investigated the corrosion inhibition properties of MoO42- for AA6061 aluminum alloy in simulated concrete pore solutions. Electrochemical methods were used to assess the corrosion behavior of AA6061, and surface characterizations were performed to analyze the composition and morphology of oxide layers. The results revealed that at a low concentration of MoO42- (6 mM), corrosion inhibition was not effective. However, at higher concentrations of MoO42- (10-30 mM), corrosion inhibition was observed to be effective. The inhibition mechanism of MoO42- on AA6061 aluminum alloy was found to follow the Langmuir adsorption isotherm, which indicates that the inhibitor molecules form a monolayer on the metal surface. MoO42- was identified as an anodic inhibitor, meaning it acts by impeding the anodic corrosion process of the aluminum alloy. Among the different concentrations tested, 10 mM

MoO42- was found to exhibit the highest corrosion inhibition efficiency, providing the most effective protection against corrosion.

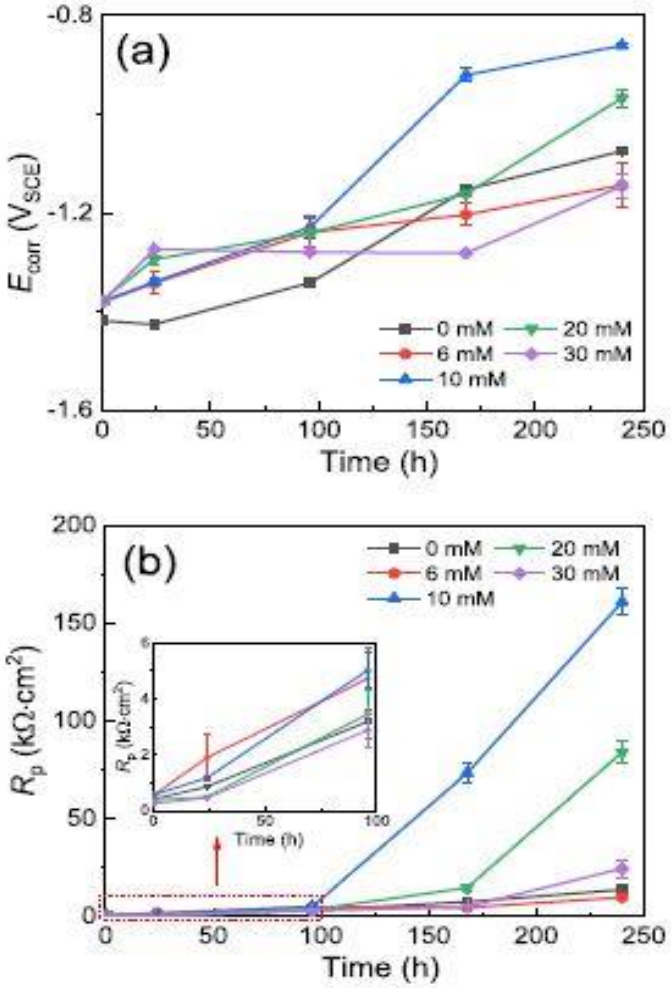

Figure 2.12 (a) Ecorr and (b) Rp of AA6061 immersed in simulated concrete pore solutions without and with MoO42- over 240 h. (Wang et al 2020)

The inhibition efficiency and the underlying mechanism of MoO42- in simulated concrete pore solutions are directly related to the concentration of MoO42-. At a moderate concentration of 10 mM, a uniform oxide layer consisting of Al-Ca-Mo(V)-O(H) complexes was formed on the surface of the aluminum alloy, resulting in the highest corrosion inhibition efficiency. On the other hand, at a higher concentration of 30 mM, an inhomogeneous oxide layer consisting of Al-Mg-Si-O(H) and Al-Ca-Mo(VI)-O(H) complexes was formed, which may have led to a decrease in the corrosion inhibition efficiency compared to the 10 mM concentration.

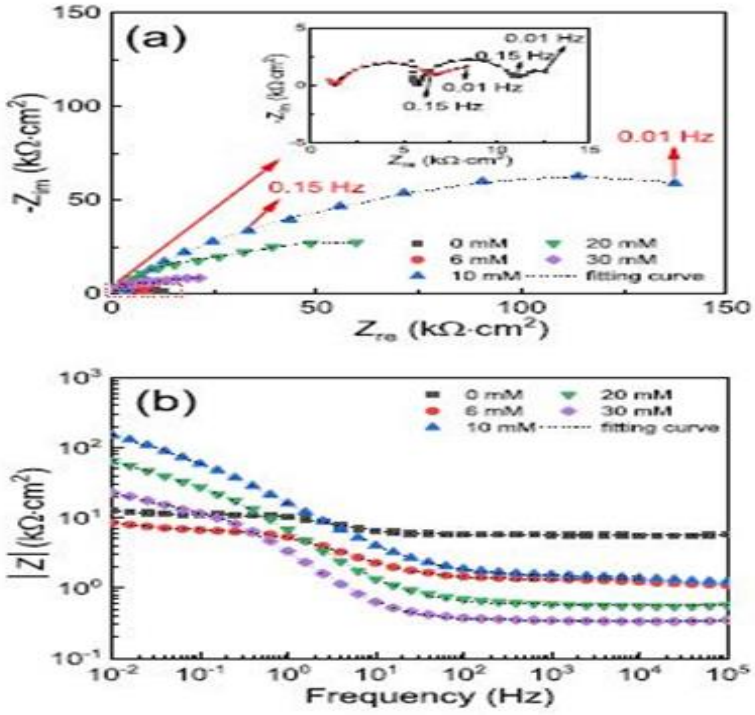

Figure 2.13 Measured and fitting EIS data of AA6061 in simulated concrete pore solutions with various concentrations of MoO42-after immersion for 240 h. (a) Nyquist plots; and (b) Bode modulus plots. (Wang et al 2020)

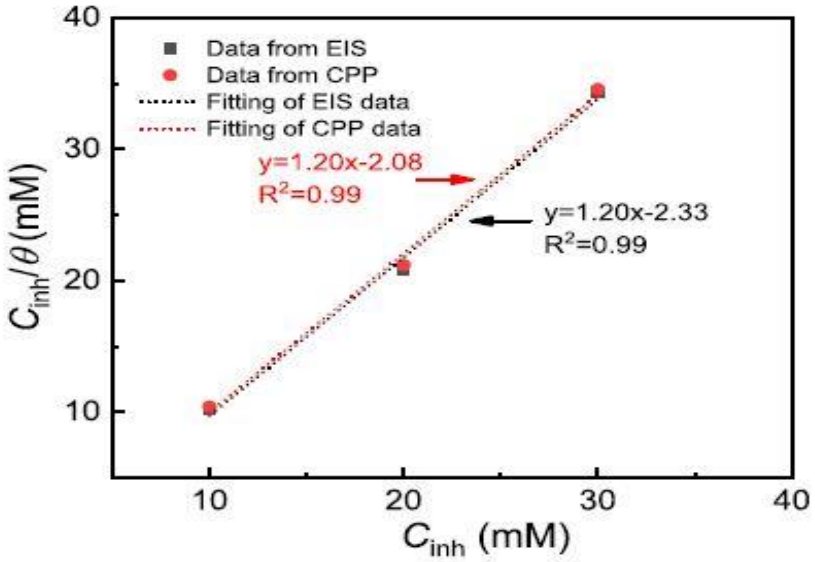

Figure 2.14 Adsorption isotherm plots of AA6061 calculated based on the EIS and CPP results in simulated concrete pore solutions with MoO42-. (Wang et al 2020)

According to the electrochemical results (Figs. 2.12 and 2.13), a low concentration of MoO_4^{2-} (6 mM) cannot inhibit the corrosion of AA6061 effectively, while higher

concentrations of MoO_4^{2-} (10–30 mM) contribute to good corrosion inhibition of AA6061. Moreover, the MoO_4^{2-} of concentrations ranging from 10 mM to 30 mM obey Langmuir adsorption isotherm, which is not the case for 6 mM MoO_4^{2-} , as verified in Fig. 2.8 and also has been reported in previous study.

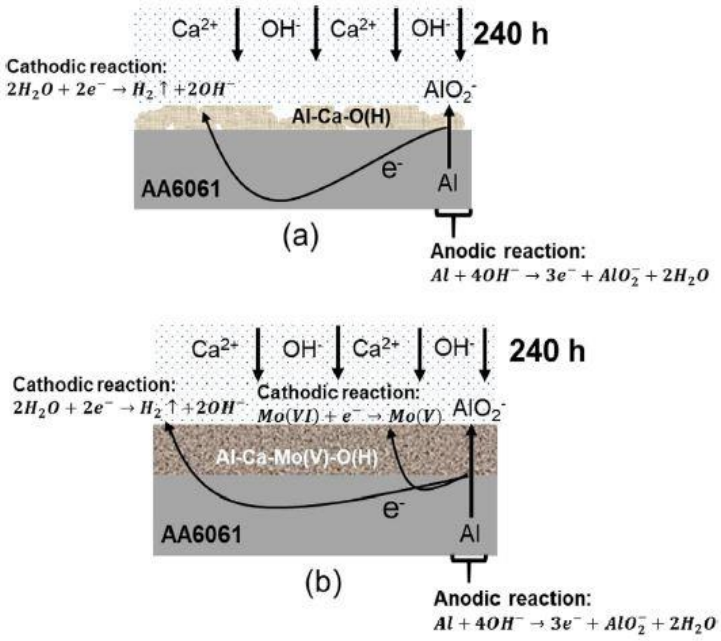

Figure 2.15 Schematic illustration of the inhibition mechanisms of MoO42-in simulated concrete pore solutions. (a) Without MoO42-; (b) moderate MoO42- concentration (10 mM) (Wang et al 2020)

Furthermore, the corrosion inhibition properties of MoO42- for AA6061 aluminum alloy in a simulated concrete pore solution. The results showed that at a moderate concentration of MoO42- (10 mM), the corrosion inhibition efficiency was the highest. This finding was different from previous studies that showed increasing inhibition efficiency with increasing MoO42- concentration in acid and mild alkaline conditions. Thus, the inhibition mechanism of MoO42- in the highly alkaline concrete environment was proposed to be different. Based on the results, a schematic illustration of the inhibition mechanisms of various concentrations of MoO42- for AA6061 in simulated concrete pore solutions was presented in Fig. 2.14. In the absence of MoO42-, a porous layer consisting of Al-Ca-O(H) formed on the surface of AA6061, resulting in very low corrosion resistance in the simulated concrete pore solution. However, after the addition of a moderate concentration of MoO42- (10 mM), a different mechanism was proposed. The presence of MoO42- caused rapid OH- consumption on the anodic sites, leading to a local

pH decrease and favoring the redox capacity of Mo(VI). This resulted in the accumulation of metastable Mo(V) species at these locations. The Mo(V) species could then react with the aluminate ions generated at the same locations via an oxidation reaction. Previous literature reported that the oxide layer formed in an alkaline solution with MoO42- may consist of Al2(MoO4)3 and Al2O3.

Table 2.4 Elemental composition of the surface of AA6061 after 24 h and 240 h of immersion in simulated concrete pore solutions without and with 10 mM MoO42- (Wang et al 2020)

MoO42- concentration	Immersion time	Element (wt. %)							
		Al	O	Ca	Mo	Mg	Si	Fe	Mn
0 mM	24 h	08.90	71.14	19.96	-	-	-	-	-
10 mM		5.91	69.07	17.88	6.09	0.87	0.17	-	-
0 mM	240 h	9.76	74.26	15.99	-	-	-	-	-
10 mM		5.41	76.10	16.77	1.33	-	0.39	-	-

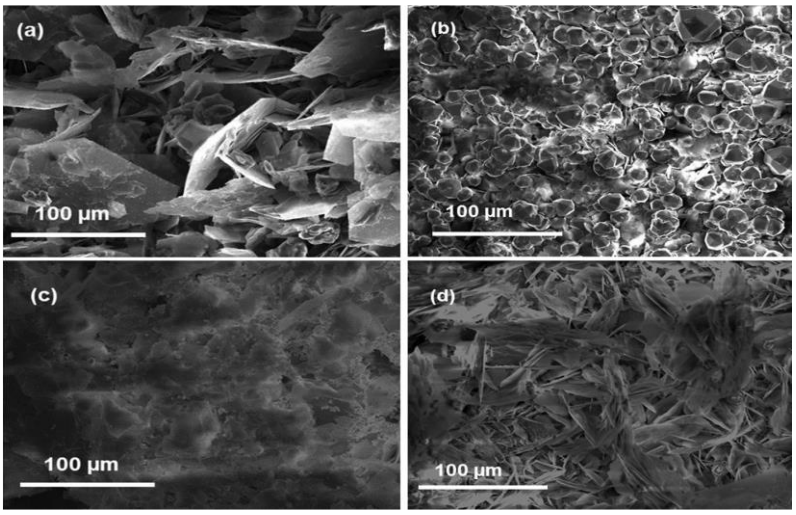

Figure 2.16 . SEM images of the oxide layer formed on the surface of AA6061 immersed in simulated concrete pore solutions. (a) without MoO4 2 for 24 h; (b) without MoO4 2-for240 h; (c) 10 mM MoO4 2 for 24 h; and (d) 10 mM MoO4 2for 240 h (Wang et al 2020)

Velten et al. (2018) suggested a specific zone known as the body potential was defined, which corresponds to the oxidation-reduction potential of the body fluid. Comparing anodized samples with the untreated alloy in this region, it was observed that the current density of the anodized samples is lower than that of the untreated alloy. To conduct a

more precise investigation, chrono-amperometry measurements were performed at an applied potential of 0.5 V (vs Ag/AgCl) for 1 hour in Ringer solution. The results show a comparison of the corrosion behavior of the samples (Fig. 2.17). The untreated alloy displayed the highest current density, concluding the experiment with a value of 15.34 μA/cm2. On the other hand, the anodized electrodes exhibited current densities below 4 μA/cm2, with Ti-6Al-4V-0.50Mo sample having the lowest value of 1.34 μA/cm2, indicating a superior corrosion resistance compared to the untreated Ti-6Al-4V alloy within the body potential range. This suggests that the anodization process has enhanced the corrosion resistance of the alloy in the relevant physiological conditions, making it a promising approach for biomedical applications.

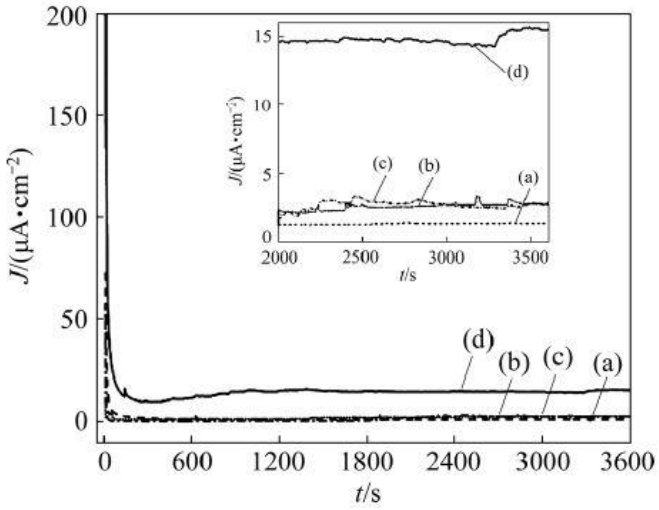

Figure 2.17 Ag/AgCl) during 1 h for different samples: (a) Ti−6Al−4V0.50Mo; (b) Ti−6Al− 4V0.50P; (c) Ti−6Al−4V0.025V; (d) Bare Ti−6Al−4V (Insert: magnified zone of chrono-amperometric (Velten et al 2018)

Whelan et al. (2016) suggested a novel sealing process for anodized aluminium has been developed, utilizing environmentally compliant corrosion inhibitors. The process involves sealing nanoporous oxide films formed by sulphuric acid anodizing on aerospace grade AA2024-T3 aluminium with a combination of corrosion inhibitors and surface hydration. The corrosion resistance of the sealed oxide film was evaluated using electrochemical impedance spectroscopy and accelerated corrosion testing in a neutral salt spray environment. The study investigated the synergistic anti-corrosion mechanism of the inhibitors within the oxide film on the corrosion-prone alloy. Various corrosion inhibitor solutions were used to prepare post-anodizing washes for the sulphuric acid-

anodized aluminium. By immersing the freshly anodized aluminium in inhibitor-rich solutions, the active agents were allowed to penetrate the pore structure of the anodic layer.

Certainly, known corrosion inhibitors were found to have a slightly negative effect on the corrosion resistance of the anodized aluminium, possibly due to their impact on surface hydration or the concentration used. However, nitrogen-rich compounds demonstrated a positive effect on the protection provided to the base metal, particularly in suppressing pits when exposed to chloride-rich environments. Among the inhibitors tested, 3,6-Di-2-pyridyl-1,2,4,5-tetrazine showed the best performance, enhancing barrier properties and pit suppression. Notably, these inhibitors had not been previously studied for bare or anodized aluminium, suggesting new possibilities for corrosion inhibition of aluminium and related alloys. The developed sealing process with environmentally compliant corrosion inhibitors presents significant potential for industrial applications, offering improved corrosion resistance and protection for anodized aluminium, particularly in challenging environments.

Yohai at el. (2015) the effectiveness of phosphates as inhibiting agents for steel bars embedded in mortars was investigated in this study. Three different mix designs were used: mix A as a reference without admixed chlorides, mix B contaminated with 1% chlorides by weight of cement, and mix C, which also incorporated 7% Na3PO4.12 H2O. After setting for 48 hours, the samples were cured for 7 days and immersed in water. Subsequently, three specimens of each group were immersed in aerated saline solutions with 0.5 mol L-1 NaCl for a period of 720 days. The study monitored the corrosion potential (Ecorr), the polarization resistance (Rp), and the electrochemical impedance spectra regularly throughout the immersion period. After 720 days, one set of mortars was anodically polarized, and another set was cathodically polarized. Raman spectra of corrosion products were recorded after polarization. Additional specimens were used to evaluate porosity and chloride profiles. The presence of phosphate ions as inhibitors showed no significant effect on Ecorr values, indicating mixed-type inhibition. Mix C remained passive until 180 days of exposure, with a polarization resistance (Rt) greater than 100 kV cm2. Beyond 180 days, Rt decreased over time, but the inhibition percentage remained consistently above 95% when evaluated by impedance spectra and above 70% when measured by linear polarization.

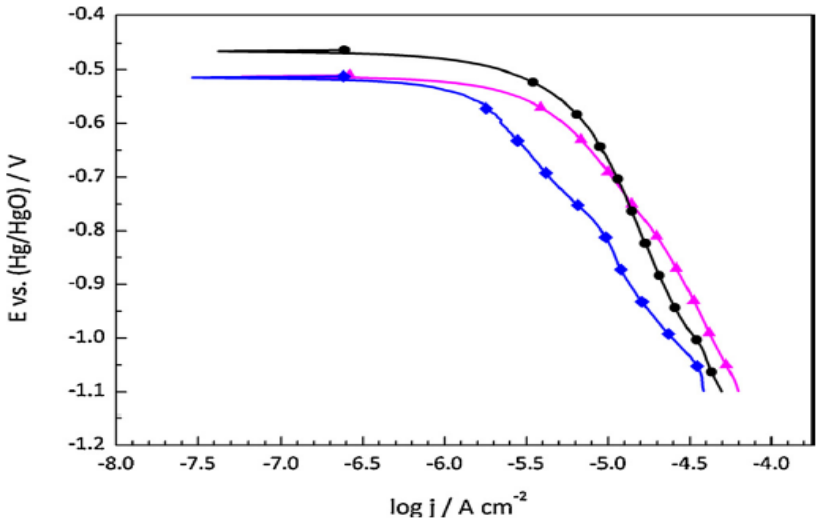

Figure 2.18 Cathodic polarization curves of rebar's after 720 days of immersion in NaCl 0.5 mol L_1.Mix A ( ); Mix B ( ) and Mix C ( ). Lines represent the experimental data and points are shown to distinguish the curves. (Yohai at el 2015)

Anodic and cathodic polarization curves, along with corrosion potential values, suggested that phosphates act as a mixed-type inhibitor, influencing both processes. The presence of phosphate ions led to the formation of a more compact and thin corrosion products layer, mainly composed of Fe3O4, which inhibited iron dissolution and delayed oxygen diffusion. Additionally, the presence of Ca3(PO4)2 blocking pores contributed to the delayed diffusion of detrimental species. The study also compared samples with and without chloride and with chloride and phosphates admixed. As expected, chloride ions proved highly aggressive and triggered rebar corrosion. However, even in chloride-contaminated mortars, the addition of phosphates was beneficial. In mix C, the polarization resistance remained higher than 100 kV cm2 during the initial 270 days of immersion, indicating that the steel remained passive. While this value decreased over the next 540 days, the inhibition efficiency remained consistently above 95% when measured by EIS and above 70% when measured by linear polarization. Overall, the results indicate that phosphate ions act as effective inhibitors for the corrosion of rebars in mortars, even in chloride-contaminated environments, and their presence has a positive impact on corrosion resistance.

2.2 Electro-chemical Processes for corrosion protection of steel in reinforced concrete

Brueckner et al. (2022) Cathodic protection is an effective corrosion management strategy employed for deteriorating reinforced concrete structures, and it can also serve as a preventive measure in situations where corrosion is anticipated during the service life due to environmental exposure conditions. Over time, advancements in technology have led to the development of various cathodic protection systems, categorized as impressed current cathodic protection (ICCP), hybrid cathodic protection (HCP), and galvanic cathodic protection (GCP). Among corrosion engineers, ICCP is generally regarded as the most powerful and robust solution for managing corrosion in structures with widespread deterioration. However, both HCP and GCP can also be viable options, even in aggressive environments, provided there is a plan for future maintenance intervention. Choosing the most suitable cathodic protection system involves considering various aspects, including technical applicability, environmental impact, sustainability, health, safety, and whole-life costs.

Table 2.5 Design Assumptions (Brueckner et al 2022)

CP System	**GCP**	**HCP**	**ICCP**
Design Life:			
Anode system	15-20 years	25-30 years	75+ years
Electrical equipment	-	-	25 years
Estimated Cost / Unit:			
Design and installation	£300/m2	£400-£555/m2	£480-540/m2
Anode removal	£150/m2	£150/m2	-
Electrical equipment and replacement/ installation	-	-	£3,500-£6,000 EA plus Traffic management
Monitoring	Required annually by ISO 12696 but often undertaken as part of General	Required annually by ISO 12696 but often undertaken as part of General (every 2 years) and	Required annually by ISO 12696; Initial first year monitoring (ISO 12696):£3,000-£6,000;

	(every 2 years) and Principal Inspections (every 6 years)	Principal Inspections (every 6 years);Initial first year monitoring (ISO 12696): £3,000-£6,000;Annual monitoring: £1,000-£2,000/year {£1,500-£5,000 [CPA (2019)]}	Annual monitoring: £1,500-£2,000/year {£1,500-£5,000 [CPA (2019)]}
Operation and Maintenance	Replacement of anodes / monitoring equipment at 15–20-year intervals or earlier depending on monitoring (costs see design / installation)	Replacement of anodes / monitoring equipment at 25+ year intervals or earlier depending on monitoring (costs see design / installation)	Replacement of electrical power supply and monitoring systems at 25+ year intervals; Potentially remote monitoring equipment: £500 to £1000 [CPA (2019)]; Electricity costs: approx. £30/year

While ICCP systems may have the longest design life and are ideal for long-term service life extensions, GCP systems are more suitable for one-time short-term repairs, and HCP systems are better suited for medium-term repairs. It is essential to weigh the benefits of each system, taking into account sustainability, environmental impact, health, safety, and whole-life costs, in addition to technical considerations. In recent years, there has been a significant push in the UK to prioritize sustainability, reduce environmental impact, and prioritize health, safety, and well-being, alongside construction and operational costs and technical applicability. Authorities now emphasize a weighted assessment that places greater importance on non-technical aspects when selecting a repair strategy involving cathodic protection systems. Under the Welsh Government National Application Annex to CS 462, sustainability, environment, health, safety, and wellbeing are given a higher weight of 60% compared to 40% for costs and technical applicability. Authorities are willing to invest more to achieve sustainability goals, reduce environmental impacts, and benefit the local economy and society throughout the specified service life, as long as the repair strategy meets the technical requirements. While ICCP systems are the most robust with the longest design life and are often the preferred choice for long-term service life

extensions, GCP and HCP systems can also be suitable depending on the repair duration and specific requirements of the structure. The selection of the most appropriate cathodic protection system involves a comprehensive evaluation of technical, environmental, sustainability, health, safety, and economic factors.

Table 2.6 Practical Considerations (Brueckner et al 2022)

CP System	**GCP**	**HCP**	**ICCP**
Network disruptions / installation time	Initial: Less than HCP and ICCP but depending on area to be protected; Maintenance: Reoccurrence of network disruptions during system replacement. More frequently than HCP system; Overall: Highest network disruption during whole-life cycle of a structure.	Initial: More than GCP but less than ICCP but depending on area to be protected.; Maintenance: Reoccurrence of network disruptions during system replacement; Overall: More network disruption during the whole-life cycle than ICCP but less than GCP due to slightly longer design life.	Initial: Longer than GCP and HCP but depending on area to be protected and the system used; Maintenance: Minimal disruption during replacement of power supply and monitoring systems; Overall: Less network disruption during whole-life cycle.

Cobbs et al. (2022) the use of galvanic anodes is becoming increasingly popular in the repair, rehabilitation, and maintenance of reinforced concrete structures affected by chloride-induced corrosion due to the added durability benefits they provide. With aging infrastructure, the impacts of climate change, and the push for reusing structures to reduce carbon emissions, there is a growing consensus among engineers that the demand for galvanic anodes will continue to rise. As a result, new manufacturers are likely to enter the market to meet this increasing demand. However, currently, there is no standardized approach for galvanic anodes used in concrete, which may lead to products that fail to function effectively as anodes, resulting in incomplete corrosion arrest and potential need for repeated intervention. This paper presents a developed methodology for assessing the functionality of anodes in a short-term test. Anodes were embedded in concrete, and their drive voltage, resistivity, and resultant current were measured when connected to an external cathode. This test setup was applied to various commercially available galvanic

anodes, and all anodes achieved a current output of 0.35 mA in this experimental setup. This testing approach offers a rapid screening method for new anodes entering the market.

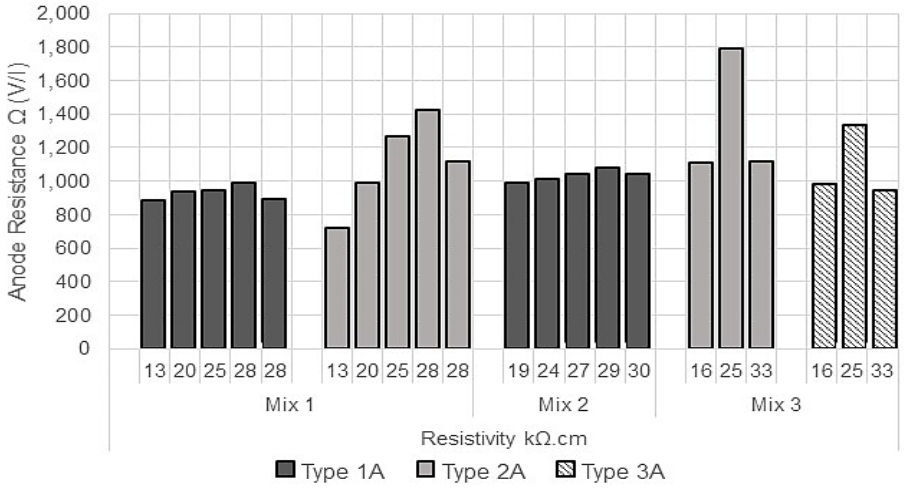

Figure 2.19 Anode Resistance (V/I) Type A anodes (Cobbs et al 2022)

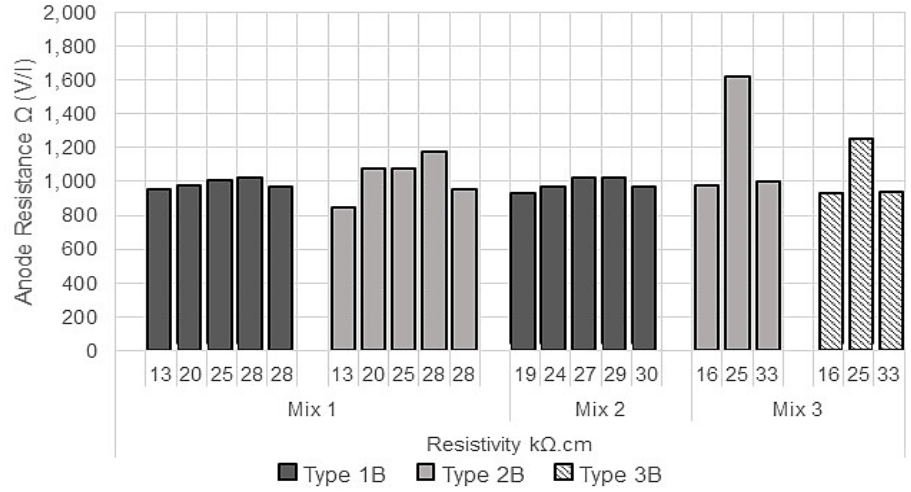

Figure 2.20 Anode Resistance (V/I) Type B anodes (Cobbs et al 2022)

The analyses revealed that the inherent behavior of different galvanic anodes varied with different manufacturers, and even among replicate anodes. Such variations in behavior could potentially influence the long-term performance of the anodes. The results also indicate that certain anodes and larger types (type B) may exhibit greater efficiency, and proprietary components used by individual manufacturers, such as encasement material, shape, and chemical composition, likely play a significant role in determining inherent

performance. However, the resistivity of the surrounding concrete also needs to be considered. The lack of standardization for galvanic anodes underscores the need for control over the quality and performance of products from different manufacturers. Establishing standardization would enable engineers to make informed decisions regarding appropriate values for utilization and efficiency factors. This research study compared a range of zinc galvanic anodes from different manufacturers used in the UK and successfully developed a testing method to assess their behavior. While the recorded results validate the test methodology, further research is required to draw conclusive insights into the performance of different anodes. Expanding the testing method with more data and time will help develop a standardized test that can be widely used in the industry to ensure the quality of sought-after galvanic anodes.

Goyal et al. (2022) focuses on the development and application of a specialist conductive coating anode system known as Concrete CAP for Impressed Current Cathodic Protection (ICCP). Laboratory investigations demonstrated that the developed anode system offers several advantages, including enhanced protection, long service life, higher durability, and easier application compared to existing coating anodes available in the market. This paper presents the real-world performance of the Concrete CAP when applied to a live structure on a crossbeam in a car park that supports the ring road in Coventry, United Kingdom. The crossbeam was severely corroded due to constant water seepage from the ring road.

Table 2.7 Results of polarization and depolarization for different anodes zones (Goyal et al 2022)

Zones	**Reference Electrode**	**Initial Potential (mV)**	**Instant OFF Potential-initial (mV)**	**24 hour decay (mV): 1 month**	**24 hour decay (mV): 3 months**	**24 hour decay (mV): 6 months**	**24 hour decay (mV): 1year**
1	Z1.1	-352.3	-964.6	123.8	97 (satisfied criterion1)	98 (satisfied criterion1)	101 (satisfied criterion1)
	Z1.2	-99.8	-310.1	143	102	100	117
2	Z2.1	-482.7	-802.9	237.9	243	136	207
	Z2.2	-165.9	-274.4	119.8	189	126	173
3	Z3.1	-369.2	-490.1	163.2	104	110	147
	Z3.2	-86.9	-334.5	250	197	189	153

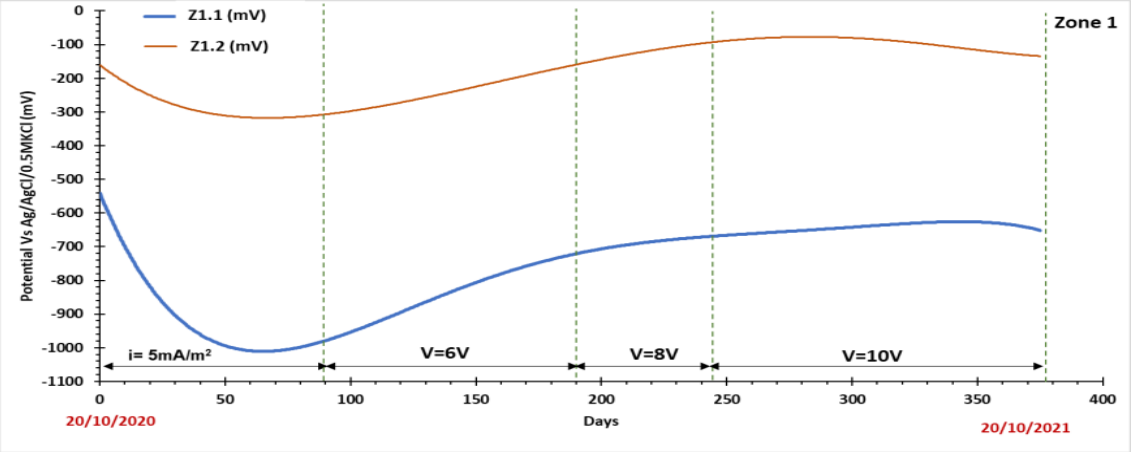

Figure 2.21 Polarization performance of the Concrete CAP anode system (Goyal et al 2022)

Steel corrosion in concrete is responsible for a substantial portion, approximately 70-90%, of structural failures. To effectively address this issue, impressed current cathodic protection (ICCP) has emerged as one of the most successful techniques for controlling steel corrosion in reinforced concrete structures. The Concrete CAP was applied as part of the ICCP system and has been continuously monitored for the past year. The field results are presented in this paper. It was found that the anode system meets the CP monitoring criterion according to BS EN ISO 12696:2016, even in the most adverse environmental conditions. The new anode system is performing satisfactorily, and it effectively protects the structure from further corrosion. The anode maintains the design current and shifts the potential of the steel to a more negative direction, even in the worst exposed condition of water damage. However, the polarization behavior of the anode system varies with changes in environmental conditions. Therefore, it is recommended to conduct subsequent monitoring to adjust the system requirements, especially during the early stages after energization. So far, the system has satisfied the depolarization requirements for the reported one-year period, as per BS EN ISO 12696:2016. The structure is still under continuous monitoring to ensure ongoing protection. The application of the Concrete CAP anode system has proven to be successful in protecting the corroded crossbeam in the car park from further deterioration. The promising results from this field study highlight the potential of this innovative anode system for future use in similar corrosion protection applications.

Goyal et al. (2020) Cathodic Protection (CP) is widely used to safeguard reinforced concrete structures exposed to aggressive environments from corrosion. However, the effectiveness of CP relies on several key parameters, including concrete resistivity, applied current density, and the arrangement of the anode and cathode. In this study, we conducted a numerical investigation to analyze the distribution of potential and protection current along different layers of reinforcement within concrete. A parametric study was carried out to assess the impact of applied current density and concrete resistivity on the protection achieved by different layers of reinforcement. The results showed that concrete with anodes applied to one surface could only protect the top two reinforcement layers with a current density of 40 mA/m2. In contrast, when anodes were placed on two adjacent concrete surfaces, all four layers of reinforcement were protected with a minimum current density of 10 mA/m2. Approximately 80-90% of the protection current reached the top layer of steel near the anode, while the bottom layers of reinforcement received minimal current, resulting in negligible protection. The level of protection significantly decreased with each reinforcement layer moving away from the anode. Additionally, the effectiveness of protection was highly dependent on concrete resistivity.

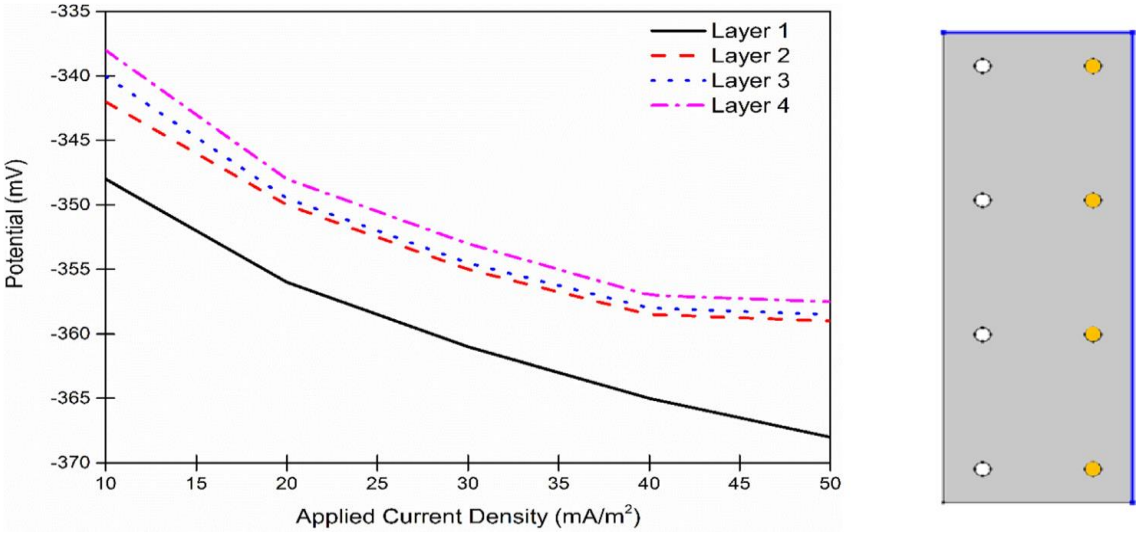

Figure 2.22 Potential at different layer of reinforcement immediately under the anode relative to anode current density. (Goyal et al 2020)

The reinforcement layer closest to the anode experienced the highest protection current, leading to a substantial potential shift compared to other reinforcement layers. However, this potential shift decreased significantly with increasing distance from the anode, necessitating a very high protection current density to meet the 100 mV decay criterion

for protection of the lower reinforcement layers. To protect the lower layers effectively, the anode needs to have a more uniform distribution, preferably applied on the sides of the beam. Separate modelling with anodes coated on two adjacent concrete surfaces supported this finding, as it demonstrated that even an anode current density of 10 mA/m2 could sufficiently protect all four layers of reinforcement from corrosion. The parametric study highlighted the significant influence of concrete resistivity and applied anode current density on potential and current distribution. Lower concrete resistivity resulted in a more uniform distribution of current compared to higher resistivity conditions. In practice, factors such as bar size, number of stirrups, and other geometrical arrangements will affect potential and current distribution. Numerical simulation provides a valuable tool for designing an effective and cost-efficient CP system that considers all relevant conditions, which can be challenging to estimate generally and may lead to under or overprotection with respect to the required protection current density. It can also aid in determining optimal anode placement. Further analysis and model development are necessary, considering time-dependent analysis and anode polarization behavior, to study the long-term effects of protection. Overall, this study enhances our understanding of CP system design and optimization for reinforced concrete structures, enabling more effective corrosion protection and prolonged durability.

Goyal et al. (2018) the commonly accepted criterion for Cathodic Protection (CP) in reinforced concrete, which involves a 100 mV decay, has been based on experimental investigations and may not always be accurate. An alternative approach involves monitoring the corrosion rate as a means to assess the adequacy of CP. This study explores the possibility of predicting the corrosion rate of steel in concrete by analyzing polarization data induced by known applied current density using the Butler Volmer equation. In this context, the value of the cathodic Tafel slope (ßc) is crucial; reducing ßc from 210 to 60 mV leads to a significant 92% decrease in the corrosion rate at a current density of 20 mA/m2. The effectiveness of this method is evaluated by applying Impressed Current Cathodic Protection (ICCP) to concrete specimens with a zinc-rich paint (ZRP) serving as an external anode for a short duration of time.

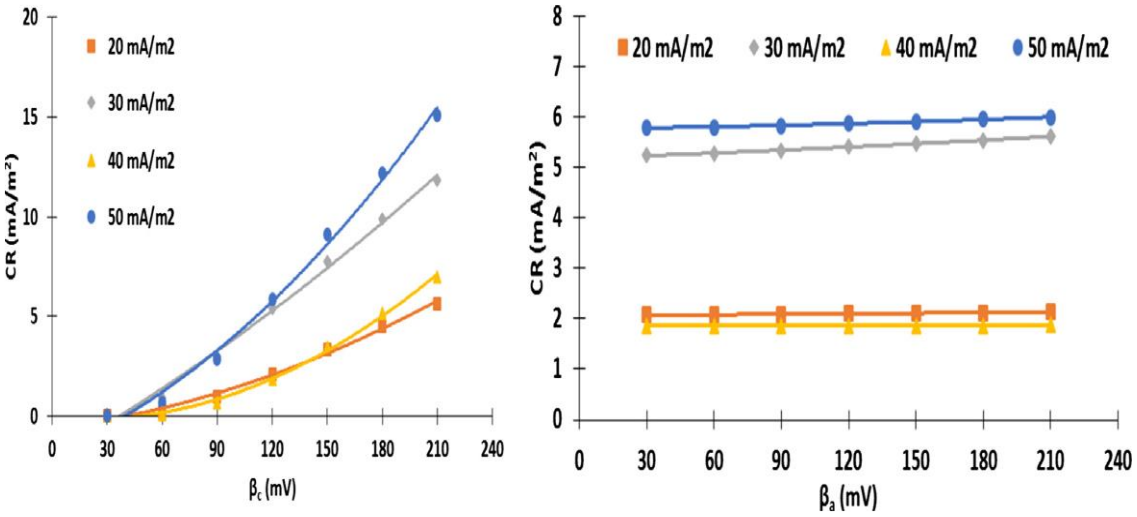

Figure 2.23 Effect of (a) Cathodic and (b) Anodic Tafel slope on corrosion rate estimation at different current densities. (Goyal et al 2018)

The results indicate that to achieve at least 100 mV of depolarization, the applied current density should be at least 7 times the corrosion rate for the ZRP anode. However, this consideration is limited to the short duration of the tests. For atmospherically exposed concrete polarized over a longer period, CP performance criteria could be achieved with lower current density. The estimation of the corrosion rate of steel in concrete using the Butler Volmer equation based on potential shift data obtained from polarization results appears to be successful. It was observed that the cathodic Tafel slope (ßc) significantly impacts corrosion rate estimation. Keeping ßc constant, as is done in the case of Linear Polarization Resistance (LPR) testing, leads to an underestimation of the corrosion rate. In conclusion, predicting corrosion rates from the Butler Volmer equation using potential shift data forms the basis for an improved cathodic protection performance criterion for atmospherically exposed reinforced concrete structures. It offers valuable insights into optimizing CP strategies and enhancing the durability of reinforced concrete in various environmental conditions.

2.3 Electro-chemical Chloride Extraction (ECE)

Fajardo et. al. 2004 Electrochemical Chloride Extraction (ECE) was investigated using cylindrical concrete specimens containing chlorides obtained from simulated seawater ("artificial" sea-water). The ECE treatment was conducted over two different periods: 21 days and 90 days, employing current densities of approximately 1A/m2 of the steel

surface. On average, around 60% to 50% of the initial chloride content in the concrete was removed during the treatment. After the ECE process, approximately 1% of the chloride, by mass of cement, still remained near the steel reinforcement.

Interestingly, anolyte refreshment after treatment did not show any significant impact on the efficiency of chloride removal. The quantities of chloride removed in the laboratory study correlated well with real-world observations during practical applications of ECE. During the ECE treatment, the negative polarity of the steel rebar led to the accumulation of Na+, K+, and Ca++ ions from the concrete pore solutions near the steel surface. Among these cations, K+ ions exhibited faster movement towards the steel rebar compared to the others studied in the research. The ECE treatment demonstrated a reduction in both chloride content and steel dissolution. However, the study did not guarantee complete re-passivation of the steel rebar, which is essential for preventing further corrosion.

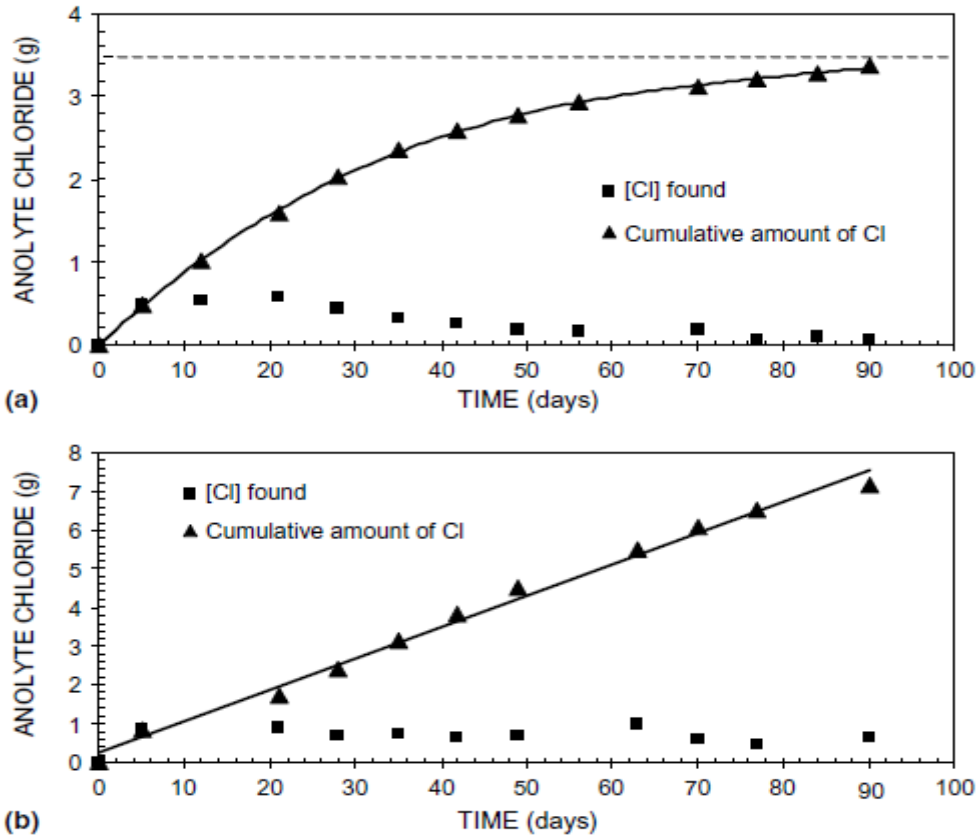

Figure 2. 24 Chloride content and cumulative amount in the anolyte (with interruption and renewal of anolyte):

(a) 20 mm cover depth and (b) 50 mm cover depth.

In Fig. 2.24, the variation in the quantity of chlorides present in the anolyte over time is presented for two different cover depths. For specimens with a cover depth of 20 mm, a substantial amount of chloride extraction was observed during the initial 21 days of the application of Electrochemical Chloride Extraction (ECE). However, after this period, the amount of chloride in the anolyte decreased, and the cumulative curve reached an asymptotic behavior for the duration analyzed. This indicates that extending the treatment time beyond 21 days did not significantly increase the extraction of chlorides. This behavior can be explained by the hypothesis that, after a certain time, other anions like OH-, SO4, for example, could bring the current back from the cathode towards the anode, allowing chlorides to remain in the concrete matrix.

On the other hand, for specimens with a cover depth of 50 mm, the amount of chloride in the anolyte varied linearly with respect to time. This behavior resembled the early days of the curve obtained for specimens with shallow cover depths. These results demonstrate that even a duration of 90 days was still insufficient to extract all the chloride from the concrete, especially for specimens with greater cover depths.

Overall, the findings suggest that the efficacy of the Electrochemical Chloride Extraction process depends on factors such as the cover depth of the concrete and the duration of the treatment. While considerable chloride extraction can occur during the initial days, extending the treatment duration does not always result in a proportional increase in chloride removal, and achieving complete chloride extraction may require longer treatment periods, especially for deeper cover depths

Elsener et. al. (2007) the initial laboratory findings report the continuous monitoring of free chloride content in concrete blocks during the process of electrochemical chloride removal (ECR). To achieve this, chloride-sensitive electrodes were embedded at different depths within the concrete specimens, allowing measurement of the free chloride concentration throughout the ECR treatment. The total chloride content was assessed before and after the electrochemical process. The data collected provided valuable insights into the removal of chloride ions and the relationship between bound and free chloride.

During the ECR treatment, free chloride is removed from the concrete. Consequently, bound chloride is dissolved to restore the equilibrium between bound and free chlorides. However, the release rate of bound chloride is slower compared to the rate of chloride removal, leading to reduced efficiency in the ECR process. To overcome this, the system is periodically paused (current off periods), allowing the re-establishment of equilibrium between bound and free chlorides. As a result, the process becomes efficient again during subsequent periods.

The laboratory results indicate that the current application of the ECR process is inefficient. It suggests that by optimizing the treatment procedure and current distribution, the amount of charge required for desalination can be significantly reduced. This optimization is also crucial in mitigating the risk of undesirable side-effects that currently limit the widespread use of ECR.

In summary, the study highlights the importance of monitoring free chloride content during the ECR process and proposes potential improvements to enhance treatment efficiency, reduce energy consumption, and address concerns related to side-effects, making ECR a more effective and sustainable solution for chloride removal in concrete structures.

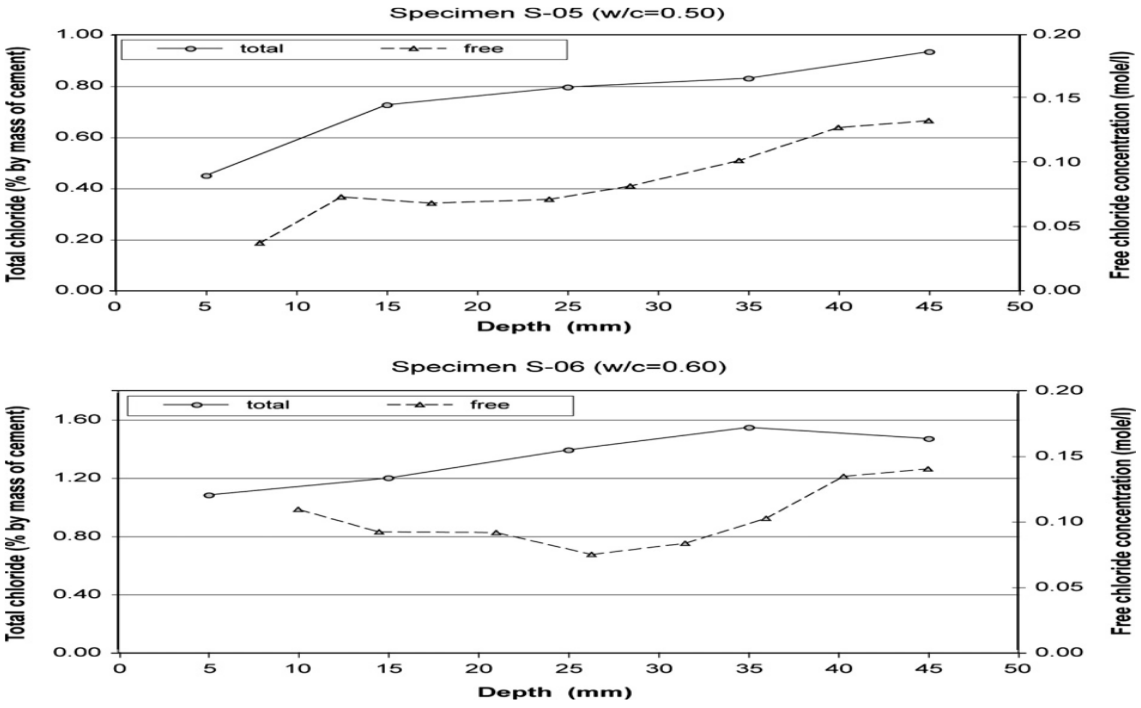

Figure 2. 25 Initial total and free chloride profiles in the specimens.

Figure 2.25 displays the total and free chloride concentration profiles in concrete specimens before the commencement of the electrochemical chloride removal (ECR) treatment. The total chloride content ranges from 0.45% to 0.95% by mass of cement in specimen S-05, while in specimen S-06, it varies from 1.10% to 1.45% by mass of cement. Both profiles exhibit similar patterns, showing an increasing concentration from the bottom side to the upper side of the specimens.

This concentration distribution can be attributed to the initial absorption of chloride-containing water by the concrete. The one-dimensional flow of water within the concrete moves the chloride ions from the lower side of the specimens towards the upper side, where the water eventually evaporates. As a result, the chloride ions accumulate at higher levels within the concrete specimens, leading to the observed concentration gradient.

The similarity in profiles between the two specimens indicates that the initial chloride distribution is consistent in this experimental setup. These concentration profiles serve as essential reference data for evaluating the efficiency of the ECR treatment and understanding the behavior of chloride ions within the concrete structures throughout the process.

Carmona et al. (2015) the durability of concrete structures is significantly compromised by the corrosion of steel reinforcement, primarily caused by the penetration of chlorides (Cl) into the concrete matrix. In response to this challenge, scientists have been actively developing electrochemical solutions since the late 20th century to prevent chloride ingress and mitigate its detrimental effects. Several patented methods have been established, and these approaches have demonstrated successful implementation in various infrastructure projects. Consequently, it is widely recognized that electrochemical chloride extraction (ECE) is an effective technique for prolonging the service life of reinforced concrete structures.

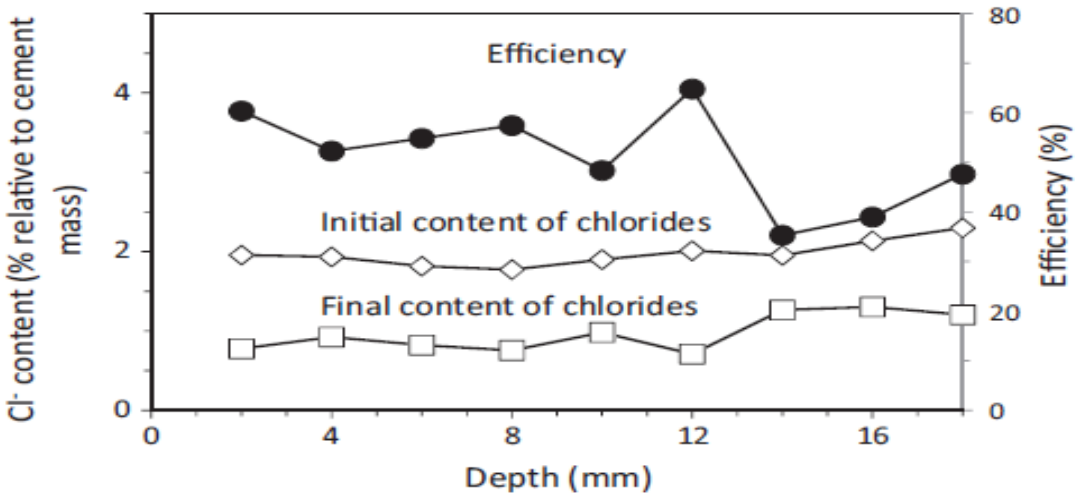

Figure 2. 26 Chloride concentration profiles before ECE (initial) and after ECE (final), and local efficiencies of the extraction process. ECE details: current density: 2 A/m2, charge density: 1.5 MC/m2, both related to exposed concrete surface.

The application of electrochemical chloride extraction (ECE) has demonstrated effective removal of a significant portion of chlorides with a low applied charge density. This approach also enhances the resistance of concrete to chloride penetration under certain external loads. By utilizing a graphite-cement paste anode system, it becomes possible to combine ECE and cathodic protection (CP) treatments by simply adjusting the current density in the power supply. Throughout the entire combined process, no damage was observed in the anode. This combination of ECE and CP has shown the capability to maintain or restore the desired protection conditions by appropriately setting the cathodic current density based on the chloride content present. Additionally, this combined treatment acts as a robust barrier against chloride penetration. However, further research is necessary to assess the reliability of these anodic systems under different conditions to ensure their practical applicability.

2.4 Bi-directional Electro-migration Rehabilitation Technique in Concrete Structures

Fan et al. (2020) Bidirectional electro-migration rehabilitation (BIEM) technology is an innovative approach aimed at enhancing the durability of existing reinforced concrete structures. The effectiveness of BIEM repairs is influenced by the duration of operation during different stages of concrete durability degradation. This study focuses on

evaluating the BIEM repair effects in three distinct durability deterioration stages: passivation, de-passivation, and corrosion. The evaluation of BIEM repair effects involved the analysis of various parameters, including polarization curve, chlorine removal efficiency, the amount of corrosion inhibition, and steel bar corrosion profile. Short-term effects demonstrated that BIEM efficiently removed chloride ions and altered the microenvironment around the steel bars, effectively preventing their corrosion. These effects were particularly pronounced in situations with low corrosion levels.

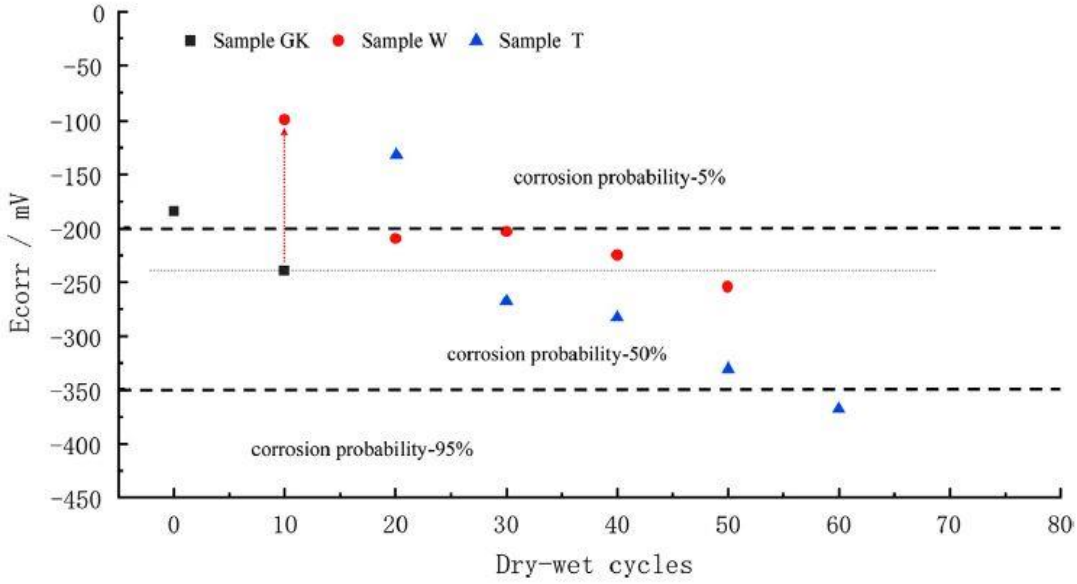

Figure 2.27 Corrosion potential variation during dry-wet cycles. (Fan et al 2020)

In the long term, BIEM treatment extended the passivation time for low-corrosion specimens to endure ten dry-wet cycles. However, once the initial corrosion exceeded a certain threshold, BIEM treatment could not prevent further corrosion. The corrosion ratio emerged as a crucial factor influencing the effectiveness of BIEM repair for a particular corrosion stage. Based on the results of long-term effects, repair strategies were discussed for both non-corrosion and corrosion stages of concrete. These findings contribute to understanding the potential and limitations of BIEM technology in rehabilitating concrete structures at different stages of durability degradation. The study sheds light on the benefits and limitations of BIEM as a repair technique for improving the durability and service life of reinforced concrete structures, providing valuable

insights for implementing appropriate repair strategies based on the specific corrosion stage of the concrete.

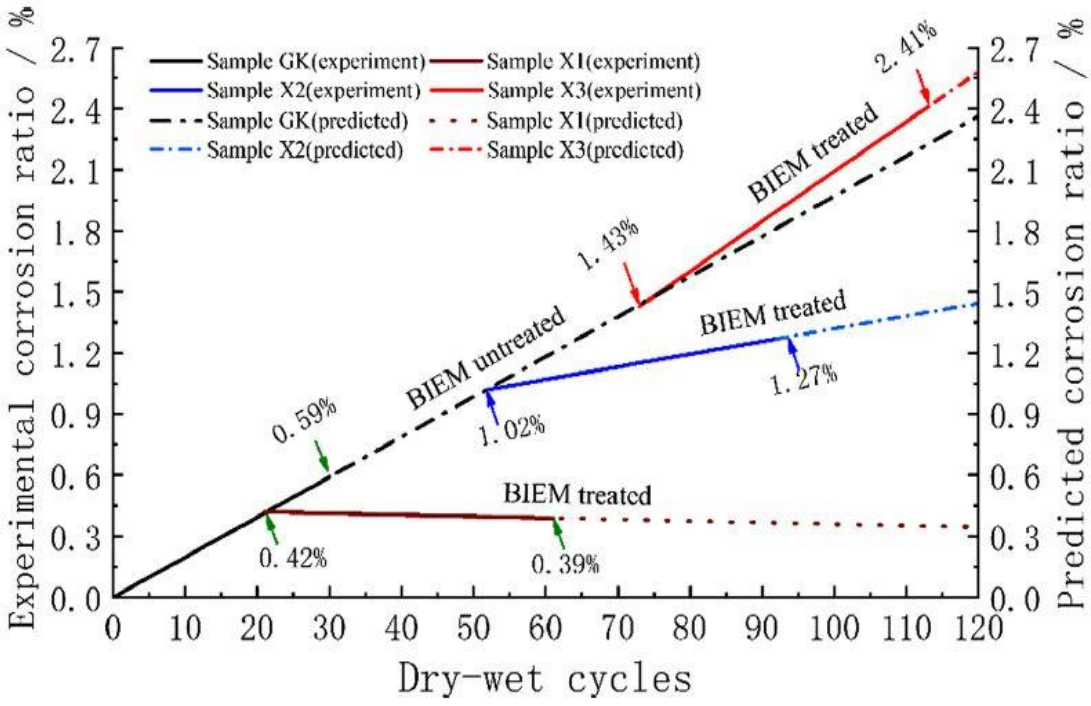

Figure 2.28 The repair results after BIEM treatment for corrosion samples. (Fan et al 2020)

The short-term and long-term effects of Bidirectional Electro-migration Rehabilitation (BIEM) treatment on reinforced concrete structures affected by chloride-induced corrosion. In the short term, BIEM treatment proved highly effective in removing chloride ions and altering the microenvironment around steel bars, thus preventing steel bar corrosion. Notably, this effect was most pronounced in cases of low corrosion levels. Our electrochemical parameter analysis further confirmed that BIEM treatment could prevent corrosion, but only when the degree of corrosion was initially low. Once the corrosion rate increased beyond a certain threshold (e.g., sample X3), BIEM treatment was no longer effective in slowing down or controlling the corrosion process. In the long term, we observed that the molar concentration ratio of the TETA inhibitor to chloride ions in each specimen initially declined rapidly. However, this rate of decline slowed with increasing dry-wet cycles during the process. For specimens with corrosion, the TETA inhibitor became exhausted due to increased ionic reactions, while rust expansion induced micro cracks in the concrete, accelerating ionic diffusion. Based on electrochemical

parameters, we found that BIEM treatment extended the passivation time by an additional 10 dry-wet cycles for specimens with low degrees of corrosion. However, as indicated in our short-term results, BIEM treatment could not prevent corrosion once the initial corrosion reached a certain threshold. An effective repair strategy based on these long-term effects for both non-corrosion and corrosion stages. BIEM treatment applied at the non-corrosion stage could reduce the corrosion rate and postpone the deterioration process. However, finding the right balance between life-cycle extension and financial considerations is crucial. The corrosion rate emerged as a critical factor influencing the repair effect for a given corrosion stage. Therefore, we recommend undertaking BIEM treatment as early as possible once steel corrosion is detected to achieve the best results.

Fan, Mao et al. (2020) focused on investigating the application of Bidirectional Electro-migration (BIEM) in cracked coastal concrete and how the relative position and width of a crack influence chloride removal and corrosion inhibition. Both numerical simulation and experimental research were conducted to ascertain the effects. The results revealed that, during the power-on state of BIEM, the current within the crack was higher compared to other positions, creating a current concentration effect. Utilizing the BIEM technique effectively restored the steel bar corrosion potential in cracked concrete to a high level. The width of a transverse crack did not significantly impact corrosion potential restoration, whereas a longitudinal crack demonstrated better corrosion potential restoration with increasing crack width.

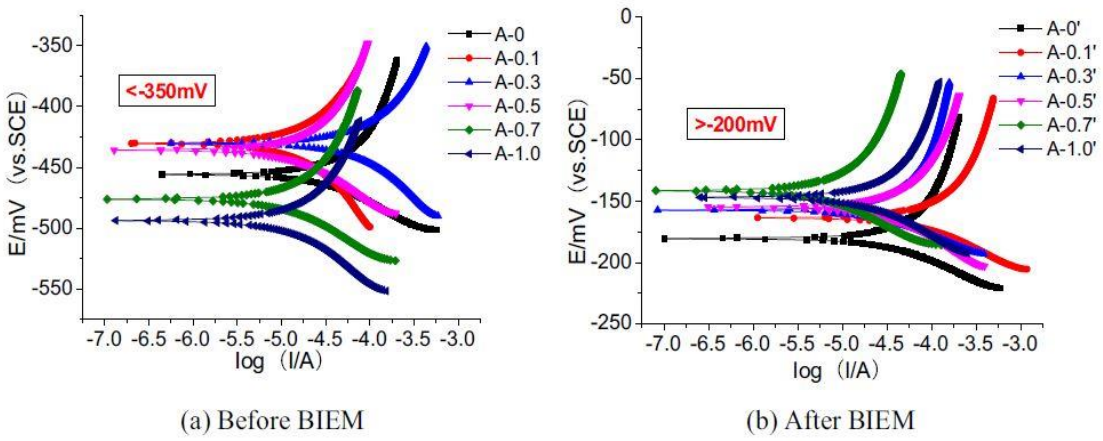

Figure 2.29 Low polarization Curves of Steel Bars Before and After BIEM (Fan, Mao et al 2020)

For cracks with a width less than 0.1 mm, BIEM demonstrated similar chloride removal and corrosion inhibition effects as in uncracked concrete. However, if the crack width exceeded 0.1 mm, the efficiency of removing chloride ions and migrating corrosion inhibitor increased with the crack width but decreased in positions far from the crack. The durability deterioration of coastal concrete structures was identified as a significant issue. The corrosion of steel bars due to chloride ion erosion resulted in protective cover cracking. Additionally, when concrete structures experienced cracking, their permeability coefficient and chloride ion diffusion coefficient significantly increased, accelerating structural deterioration and leading to early structural failure. BIEM shows promise as an effective approach to address chloride-induced corrosion in cracked coastal concrete, offering potential benefits in terms of corrosion potential restoration and chloride removal. However, careful consideration should be given to crack width and position to optimize the effectiveness of the BIEM technique in such concrete structures.

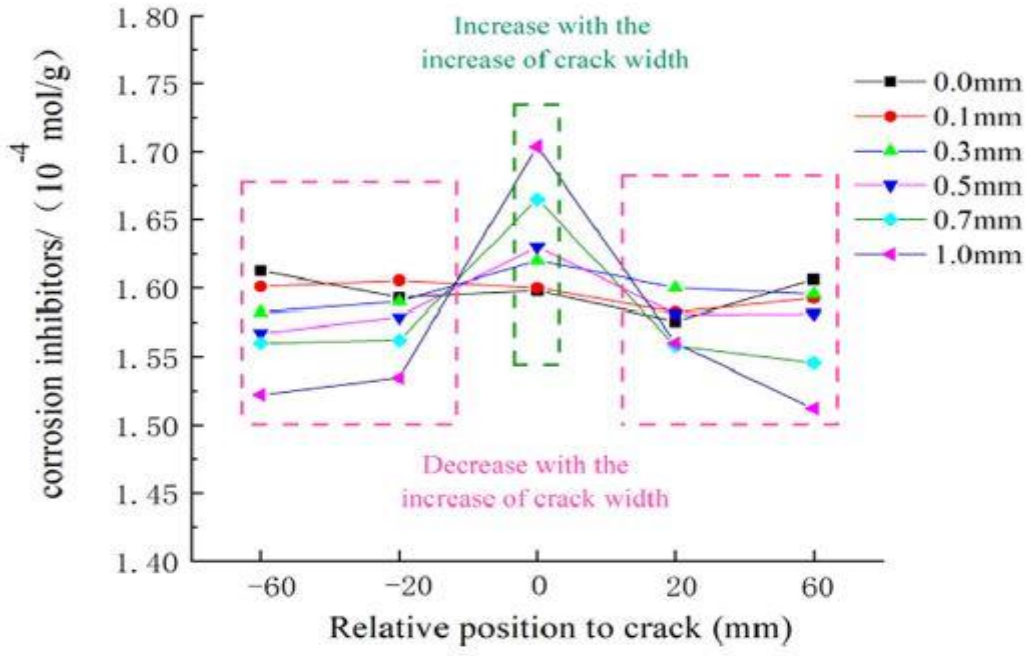

Figure 2.30 Comparison of Corrosion Inhibitor Concentration near Steel Bars. (Fan, Mao et al 2020)

The BIEM test results indicated that when the BIEM technique was employed to repair longitudinal cracks, the effectiveness of chloride removal and corrosion inhibition within the crack significantly improved with increasing crack width. However, the effectiveness

decreased in positions far from the crack, with a critical crack width observed at approximately 0.1 mm. Notably, after BIEM treatment, the steel bar corrosion potential could be restored to a high level, and the restoration effect on the corrosion potential improved with larger crack widths. For transversely cracked concrete specimens, the BIEM test and chloride ion migration test concluded that when the crack width exceeded 0.1 mm, the effect of chloride removal and corrosion inhibitor migration within the crack improved due to the concentration of current in the crack.

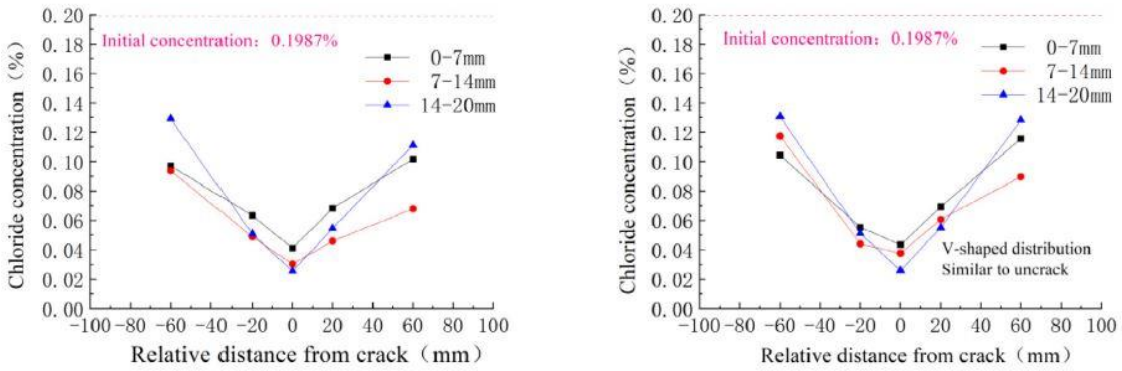

Figure 2.31 Chloride Ion Distribution after BIEM. (Fan, Mao et al 2020)

However, the effect became less prominent in positions distant from the crack. The current distribution near the crack displayed a "V-shaped" pattern, with wider cracks exhibiting a more pronounced trend. Although the corrosion potential of the steel bar could be restored to a high level after BIEM, the crack width had a less noticeable impact on increasing the steel bar corrosion potential. The findings highlight the influence of crack width on the effectiveness of BIEM in repairing cracks and mitigating chloride-induced corrosion. Larger crack widths showed better restoration effects but had diminishing impacts on increasing the steel bar corrosion potential. Understanding these relationships can aid in optimizing the BIEM technique's application to effectively rehabilitate cracked concrete structures and enhance their durability.

Pan et al. (2020) Concrete structures with steel bars are susceptible to severe corrosion when exposed to chloride salt-containing environments, which can significantly shorten the structure's service life. To address this issue, bidirectional electro-migration rehabilitation (BIEM) has emerged as a novel durability repair technology for reinforced

concrete (RC) structures experiencing chloride corrosion. BIEM involves applying an electric field to remove chloride ions from the concrete while simultaneously applying a rust inhibitor to the steel surface. Indoor experiments were conducted to analyze the migration of chloride ions and the corrosion inhibitor in RC structures in both atmospheric conditions and water-level-fluctuating areas. The efficiency of BIEM was enhanced by using an electroosmotic device. Notably, BIEM demonstrated exceptional effectiveness in wet-dry areas and when used in conjunction with the electroosmotic device. Within a 15 mm radius of the electroosmotic device, over 90% of the chloride ions on the steel surface were successfully removed, with a chloride ion migration rate ranging between 40% and 60%.Scanning electron microscopy (SEM) examination revealed that the surface of the steel bars appeared smooth after undergoing BIEM treatment, with no evident signs of pitting or corrosion products. Based on the prediction method of concrete service life, it was calculated that the concrete structure would enter the early warning zone after approximately 15 years, and the rust zone after around 30 years.The findings of this study suggest that BIEM, particularly in combination with the electro-osmotic device, can effectively mitigate chloride corrosion in concrete structures and prolong their service life. By utilizing this technology, early warning signs of corrosion can be detected, allowing for timely maintenance and potentially preventing costly structural damage in the long run.

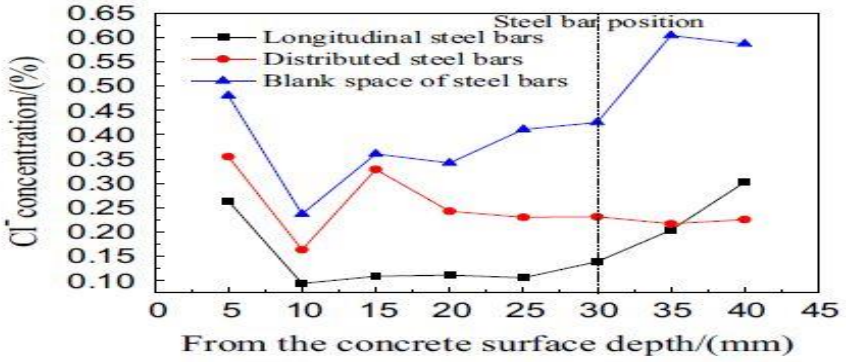

Figure 2.32 Chloride ion concentration in the BIEM area of Slab (Pan et al 2020)

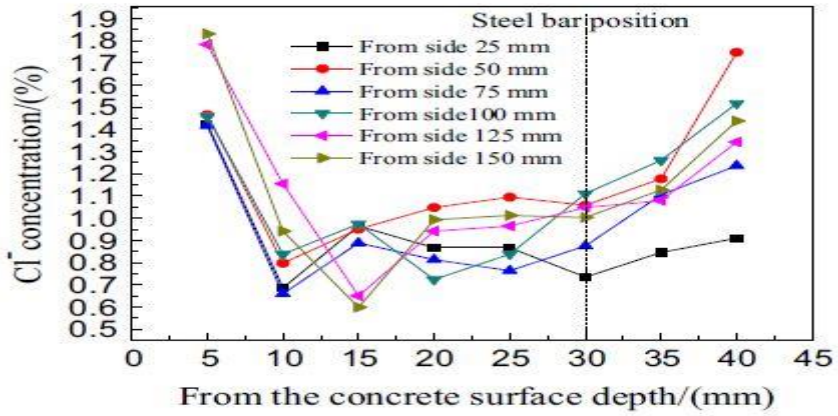

Figure 2.33 Chloride ion concentrations' area of influence for BIEM (Pan et al 2020)

In the BIEM device area, the effect was more pronounced in the part subjected to fluctuating water levels compared to the part exposed to the atmosphere. However, in the surrounding area, the BIEM device had a more notable effect in the part exposed to the atmosphere. Notably, in regions with changing water levels, BIEM demonstrated a significant impact on chloride ion discharge and the amount of rust inhibitor within the electroosmotic area. The efficiency of chlorine removal from the surface exceeded 90%. At locations approximately 15 cm from the infiltration device, the rate of chloride removal from the steel surface ranged between 40% and 60%, with the influence of the bidirectional infiltration device extending up to approximately 15 cm outside the electroosmotic area. For practical engineering applications, to enhance the efficiency of chlorine removal in areas affected by fluctuating water levels, it is recommended to reduce the arrangement distance between the electroosmotic devices or increase the power supply time. Post BIEM treatment, the chloride ion concentration in the concrete was significantly reduced, and the surfaces of the steel bars exhibited no evident pitting or corrosion products. The service life of the concrete engineering project was calculated using the prediction method for concrete. The results indicated that the concrete structure would enter the early warning zone after 15 years and the rust zone after 30 years. This suggests that BIEM treatment effectively extends the service life of the concrete structure by delaying the onset of corrosion-related deterioration.

Pan et al. (2019) Steel bars embedded in reinforced concrete are vulnerable to corrosion in high chloride environments. Bidirectional electro-migration rehabilitation (BIEM) is a novel method to enhance the durability of reinforced concrete by extracting chloride out

of concrete and introducing an inhibitor to the surface of the steel bar under the action of an electric field. During the migration process, a higher ionization capacity of the inhibitor with a symmetrical molecular structure was introduced.

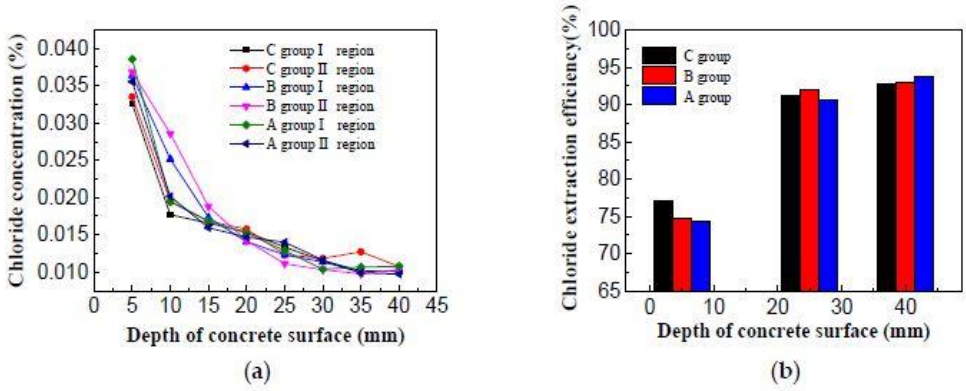

Figure 2.34 (a) Chloride concentration of concrete specimens; (b) Chloride extraction efficiency of concrete specimens (Pan et al 2019)

A new imidazoline inhibitor was, therefore, employed in this study due to its great ionization capacity. The effect of imidazoline and triethylenetetramine inhibitor on chloride migration, corrosion potential, and strength of concrete were explored. The research results showed that the effect of chloride extraction and electrochemical chloride extraction made no significant difference on the surface of the concrete, where chloride extraction efficiency was more than 70%, and the chloride extraction efficiency was more than 90% around the location of the steel. While a dry-wet cycle test, the potential of concrete increased by about 200 mV by mixing imidazoline inhibitor. The imidazoline inhibitor was found to be effective at facilitating chloride migration and ameliorating corrosion, meanwhile, it had a negligible impact on the concrete's strength.

The concentration of inhibitors in the concrete specimens was assessed after the bidirectional electro-migration rehabilitation (BIEM) process. Following a dry-wet cycle test, the concrete's potential increased by approximately 200 mV when the imidazoline inhibitor was used. Furthermore, the inhibitor content within the concrete specimens decreased across the thickness of the concrete protective layer. Interestingly, it was observed that the imidazoline inhibitor content in the concrete was higher than that of triethylenetetramine. This indicates that the electric migration ability of the imidazoline inhibitor was stronger than that of other compounds under the influence of an electric field during the BIEM process.

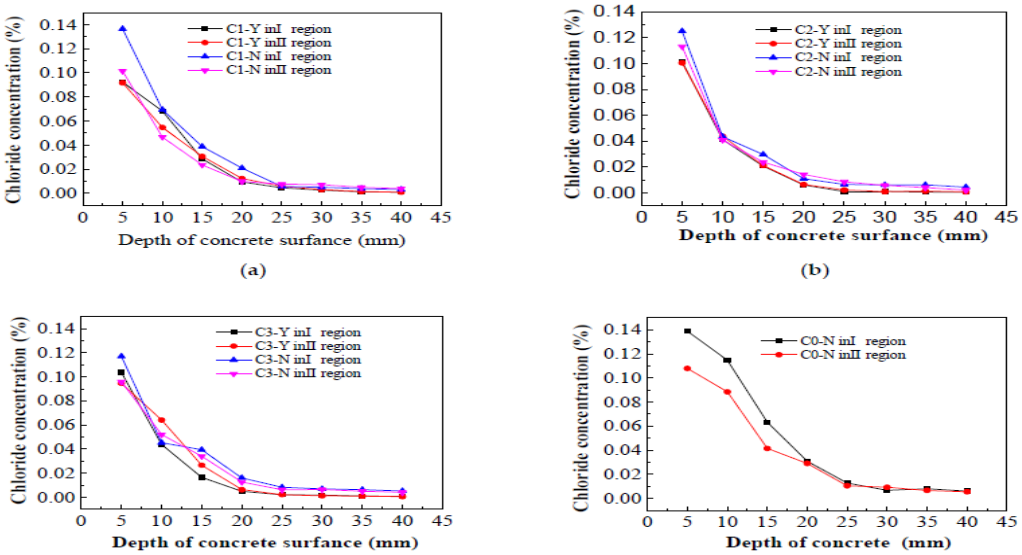

Figure 2.35 Chloride concentration. (a) 0.25% imidazoline inhibitor; (b) 0.5% imidazoline inhibitor; (Pan et al 2019)

The impact of electrochemical treatment using different inhibitors on chlorine salt erosion of reinforced concrete, focusing on corrosion potential and corrosion current. Imidazoline and triethylenetetramine inhibitors were examined, and it was observed that both inhibitors had a positive effect on increasing the corrosion potential to some extent. Specifically, the corrosion potential of imidazoline shifted positively in proportion to the amplitude ratio of triethylenetetramine. Moreover, both inhibitors were successful in reducing the corrosion current, with imidazoline displaying a more significant reduction compared to triethylenetetramine.

XU et al. (2016) focused on investigating the effectiveness of triethylenetetramine (TETA) as a corrosion inhibitor for steel in aqueous media. To introduce TETA into chloride-contaminated concrete specimens, a novel method called bidirectional electro-migration rehabilitation (BIEM) was employed. This process involved applying an electric field between embedded steel cathodes and external anodes to inject the corrosion inhibitor from external electrolytes into the concrete while simultaneously extracting chloride ions from the concrete cover zone. Control experiments were conducted using electrochemical chloride extraction (ECE) with saturated calcium hydroxide solution as the external electrolyte. As anticipated, the treatment led to a decrease in chloride content and an increase in alkalinity within the concrete. The concentration of the injected

inhibitor around the embedded steel bars was sufficient to provide effective corrosion protection.

The results of the study provide valuable insights for designing the BIEM process. The research emphasizes that surface-applied corrosion inhibitors often struggle to penetrate deep enough into the concrete to reach adequate concentrations for corrosion protection, especially when the concrete cover is thick or the compaction is high. As a result, exploring the use of electrical fields to accelerate the ingress of corrosion inhibitors in concrete becomes essential. The success of the electrochemical treatment relies heavily on selecting appropriate corrosion inhibitors. A suitable inhibitor for BIEM should offer sufficient corrosion protection even in the presence of chloride ions. Moreover, it should predominantly exist as cationic species in aqueous media under certain conditions. Amine- or alkanol amines-based corrosion inhibitors emerge as favorable choices considering these requirements.

The concentrations of Cl^-, OH^- and TETA are plotted with the variation in treatment time in Figures 2.33. Type 1 concrete with 3% sodium chloride was used and the current density was kept at 3 A/m^2. The residual Cl^- distributed relatively uniformly within a range of 20mm in front of the embedded steel bars, and increased gradually to the treated surface (Figure 2.19).

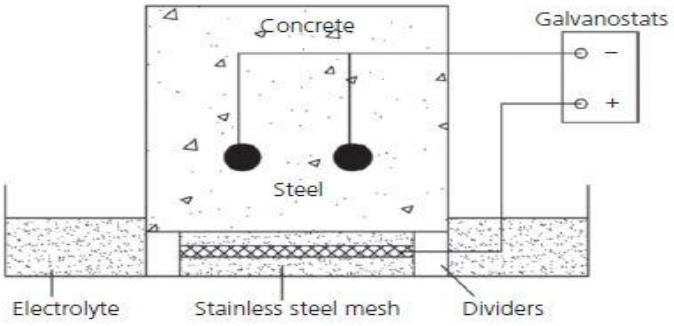

Figure 2.36 Schematic diagram of the experimental BIEM (Xu et al 2016)

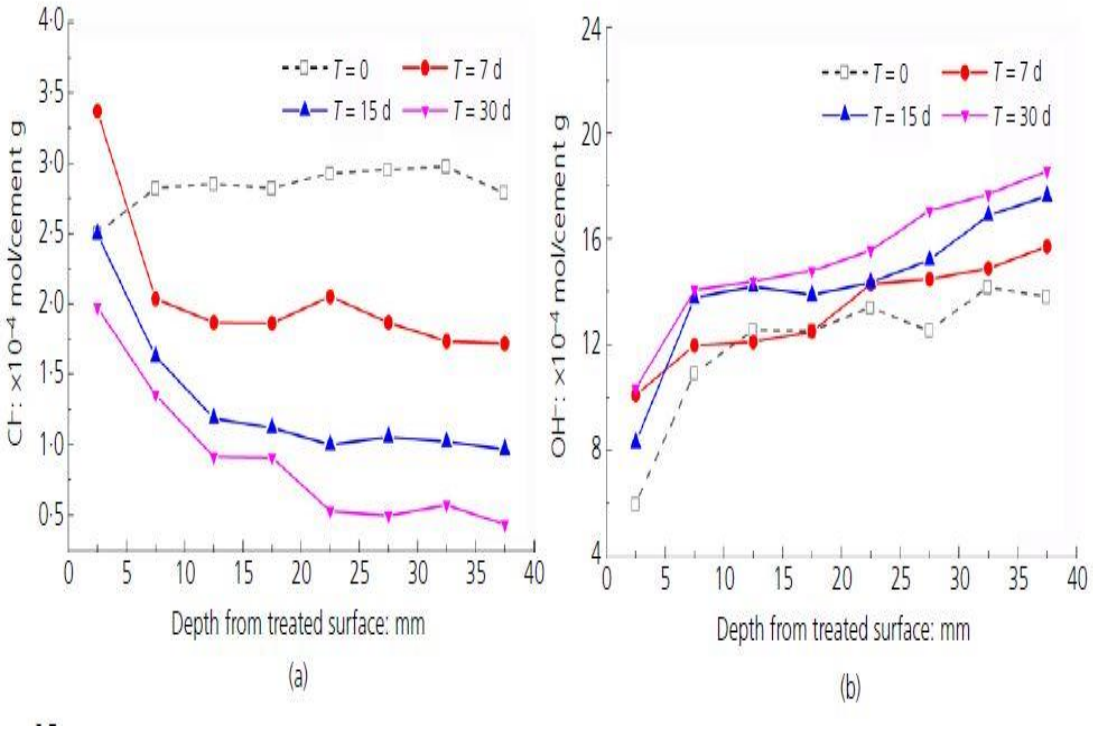

Figure 2.37 Concentration profiles/ratios in specimens after BIEM for different treatment durations: (a) concentration profiles of Cl−; (b) concentration profiles of OH−. (Xu et al 2016)

As the treatment duration increased, more Cl^- ions were extracted. In the layer close to the steel bars, 38% of Cl^- ions were removed after 7 d. When the treatment time increased to 15 d and 30 d, the percentage of Cl^- removed reached 65% and 85%, respectively. The concentration of Cl^- in the outermost layer exceeded the initial concentration by 35% after 7 d of treatment, because the Cl^- migrated to the anode under the influence of an applied electrical field. In that case, the difference in concentration of Cl^- between the inner part and the outer part of the specimen was enhanced, leading to the acceleration of counter-migration of Cl^- to the reinforcement after the treatment. The distribution tendency of OH^- in the concrete cover zone remained almost the same after BIEM, with a small decrease in the concentration difference (Figure 2.33). The alkalinity increased with the increase in treatment time. The increase in water-soluble OH^- around the steel was 14% after 7 d and 28% after 15 d. After 30 d, the increase reached 35%. This implies that, as the treatment duration lengthened, the increase in alkalinity slowed down.

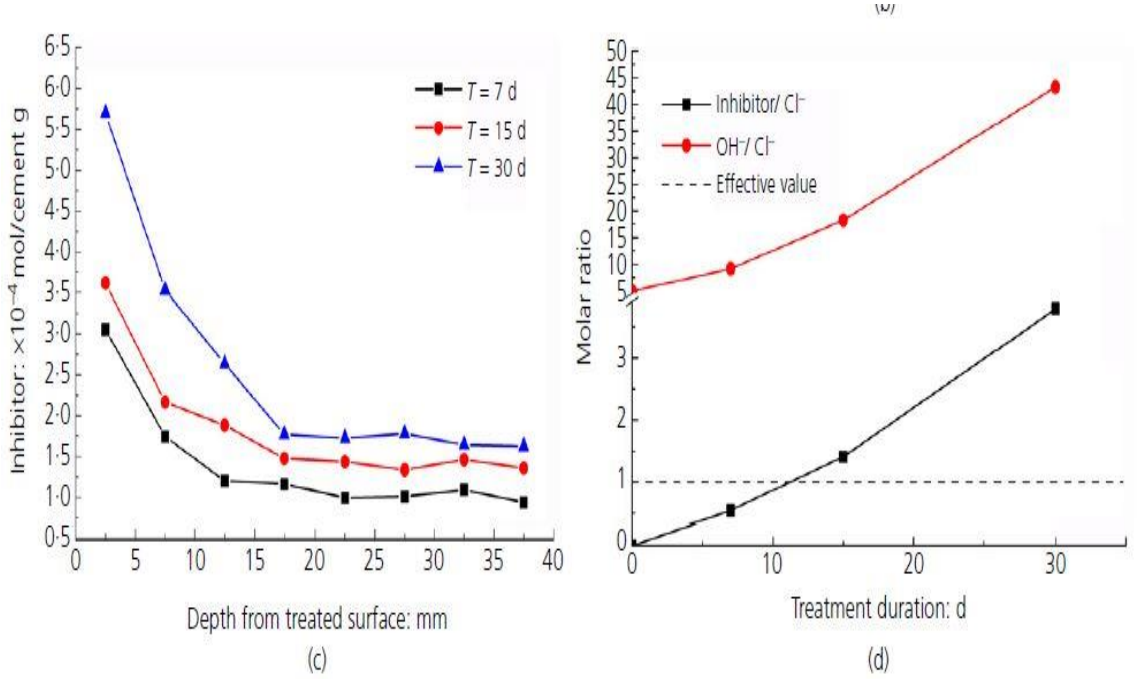

Figure 2.38 Concentration profiles/ratios in specimens after BIEM for different treatment durations (c) concentration profiles of m inhibitor; (d) ratios of proposed constituents close to the steel reinforcement. (Xu et al 2016)

The residual Cl^- concentration in the specimens decreased with the increase in current density. Obviously, the increase in current density could intensify the effectiveness of chloride extraction as the circuit charge increased. However, the residual Cl^- in the outermost layer was even higher than that in untreated specimens when the current density was less than 3 A/m^2, which means that the electric field applied was not enough to drive the Cl^- out completely, resulting in the accumulation of Cl^- in the outer layer of the specimens.

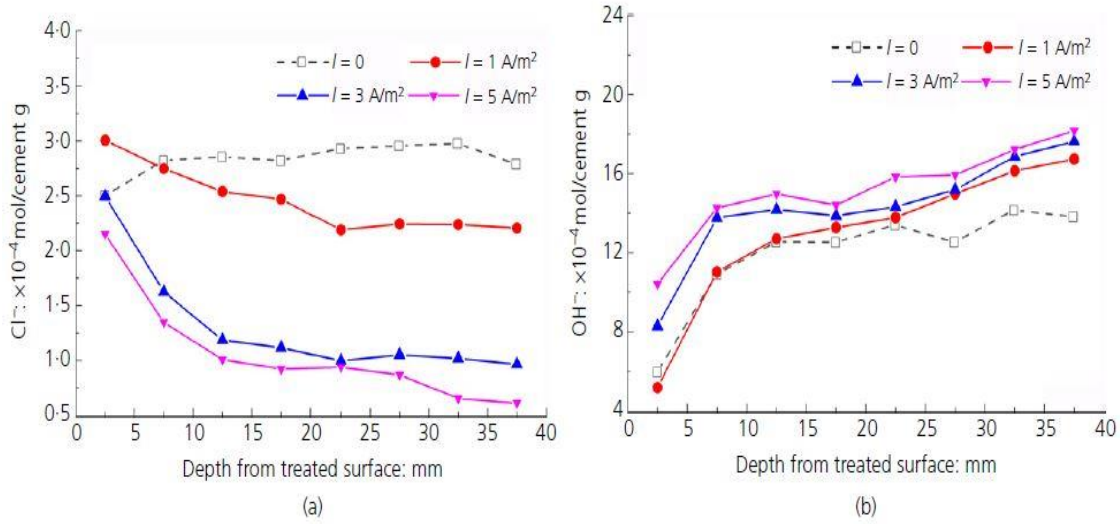

Figure 2.39 . Concentration profiles/ratios in specimens after BIEM for different current densities: (a) concentration profiles of Cl−; (b) concentration profiles of OH− (Xu et al 2016)

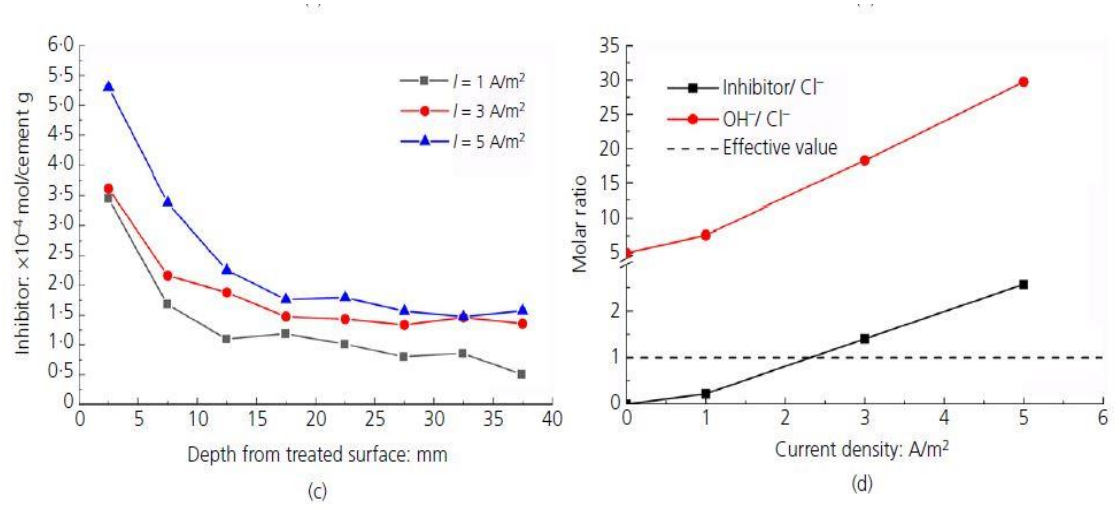

Figure 2.40 Concentration profiles/ratios in specimens after BIEM for different current densities: (c) concentration profiles of inhibitor; (d) ratios of proposed constituents close to the steel reinforcement (Xu et al 2016)

The present study defines the removal efficiency of Cl− as the ratio of the initial Cl− concentration to the residual Cl− concentration near the embedded steel. This efficiency was used to evaluate the chloride extraction effectiveness of the electrochemical process. Figure 5(a) illustrates that the Cl− removal efficiency increased from 21% to 65% and eventually reached 78% as the current density was varied from 1 A/m2 to 3 A/m2 and

then to 5 A/m2. It suggests that beyond a certain current density level, increasing the extraction effectiveness of Cl^- becomes more challenging. The electrochemical treatment of BIEM allowed for the effective injection of TETA, acting as a corrosion inhibitor, into both carbonated and noncarbonated concrete. This short-term treatment offered adequate inhibitor concentration around the embedded steel, providing corrosion protection. Moreover, the increased ratio of OH^- to Cl^- in the concrete cover favored the re-passivation of the reinforcement, resulting from the decrease in chloride ions and increase in hydroxyl ions.

In the BIEM process, the efficiencies of Cl^- extraction, OH^- enhancement, and TETA migration increased with higher current density and/or longer treatment time. However, excessively low or high current densities, as well as very short or long treatment durations, were found to be ineffective for rehabilitation purposes. The initial chloride content in the specimens emerged as a significant factor influencing Cl^- extraction through BIEM. Specimens with higher initial chloride content showed greater Cl^- removal. However, the initial chloride content had little impact on TETA migration. After BIEM treatment, the residual Cl^- concentration in the outer layer of the specimens remained higher than that in the inner layer. Both remedial techniques resulted in similar overall increases in alkalinity within the concrete cover zone. Nevertheless, for enhancing alkalinity near the steel bars, ECE (Electrochemical Chloride Extraction) proved to be a somewhat superior treatment compared to BIEM (Bidirectional Electrochemical Migration).

CHAPTER 3. MATERIALS AND ITS PREPARATION

3.1 Introduction

.This chapter focuses on the properties of various materials used in the present study. The study's primary objective is to evaluate the effectiveness of the BIEM technique for repairing corrosion in reinforced concrete structures. The chemical and physical properties of the materials utilized in the thesis are discussed in the chapter.

3.2 Constituents of Concrete

3.2.1 *Cement*

Ordinary Portland cement (OPC) was used as a binder to prepare specimens, confirms to IS: 8112-1989. In this study, OPC-43 grade cement was used to cast the specimens. Specifically, Shree brand OPC 43 cement, commonly available in the market, was utilized.

. The properties and characteristics of the cement such as setting time, workability, and strength development, were considered during the experimentation and evaluation process. The chemical compositions of the cement used as per the manufacturer are shown in Table 3.1

Table 3.1 Physical and Chemical properties of OPC 43 cement

Property	Value
Chemical Properties	
Silica (SiO_2)	21-25%
Alumina (Al_2O_3)	4-6%
Iron Oxide (Fe_2O_3)	2-3%
Calcium Oxide (CaO)	60-67%
Magnesium Oxide (MgO)	1-4%
Sulfur Trioxide (SO_3)	1-3%
Loss on Ignition (LOI)	1-3%

Physical Properties	
Fineness	225-280 m^2/kg
Setting Time	Initial: 30-90 minutes
	Final: 220-360 minutes
Soundness	Le Chatelier Expansion: <10mm
	Autoclave Expansion: <0.8%
Compressive Strength (at 28 days)	41-45 MPa
Bulk Density	1.13-1.19 g/cm^3
Specific Gravity	3.16
Heat of Hydration	Moderate

3.2.2 *Coarse Aggregates*

Nominal Sizes: The coarse aggregates used were crushed gravel with 10 mm and 20 mm nominal sizes. This means that the maximum particle sizes of the aggregates were 10 mm and 20 mm, respectively, as per IS 383:2016.

Specific Gravity:

- 10 mm Aggregates: The specific gravity of the 10 mm aggregates was reported as 2.69. Specific gravity is a measure of the density of a substance relative to the density of water. A specific gravity of 2.69 indicates that the density of the 10 mm aggregates is 2.69 times that of water.
- 20 mm Aggregates: The specific gravity of the 20 mm aggregates was reported as 2.71. This means that the density of the 20 mm aggregates is 2.71 times that of water as per IS 2386 (Part 3): 2016

Water Absorption:

- 10 mm Aggregates: The water absorption of the 10 mm aggregates was reported as 1.4%. Water absorption refers to the amount of water absorbed by the aggregate particles when immersed in water. Water absorption of 1.4% indicates that the 10 mm aggregates can absorb 1.4% of their weight in water.
- 20 mm Aggregates: The water absorption of the 20 mm aggregates was reported as 1.38%. Similarly, this means that the 20 mm aggregates can absorb 1.38% of their weight in water as per IS 2386 (Part 3): 2016.

The coarse aggregates specific gravity and water absorption properties are essential for concrete mix design and proportioning. These properties help determine the aggregates' relative density, volume, and water content, which in turn affect the overall characteristics of the concrete mixture, including its workability, strength, and durability.

3.2.3 *Fine Aggregates*

The fine aggregates used were river sand that conforms to Zone-II classification from Table 3.2. The Zone-II classification indicates that the sand falls within the acceptable range of particle size distribution specified in relevant standards, making it suitable for use in concrete.

Table 3.2 Gradation of Fine Aggregate

I.S. Sieve	Weight retained (gm)	Percentage weight Retained	Cumulative % of weight Retained	Cumulative % of weight Passing	Limit by IS 383 for Zone-II
4.75mm	13	1.3	1.3	98.7	90 to 100
2.36mm	10	1	2.3	97.7	75 to 100
1.18mm	385	38.5	40.8	59.2	55 to 90
600µm	169	16.9	57.7	42.3	35 to 59
300µm	267	26.7	84.4	15.6	8 to 30
150µm	120	12	96.4	3.6	0 to 10
Pan	36	3.6	-	-	
Total	1000	100	282.9		
Fineness Modulus		2.829		Hence, Zone II	

Specific Gravity:

- The specific gravity of the river sand was found to be 2.43. Specific gravity is a measure of the density of a substance relative to the density of water. A specific

gravity of 2.43 indicates that the density of the river sand is 2.43 times that of water as per IS 2386 (Part 3): 2016.

Water Absorption:

- The water absorption of the river sand was determined to be 1.8%. Water absorption refers to the amount of water absorbed by the aggregate particles when immersed in water. Water absorption of 1.8% means that the river sand can absorb 1.8% of its weight in water as per IS 2386 (Part 3): 2016.

Fineness Modulus:

- The fineness modulus of the river sand was found to be 3.14. The fineness modulus measures the fineness or coarseness of the aggregate. It is calculated by summing up the cumulative percentages by mass retained on each standard sieve (sieve sizes typically range from 150 microns to 4.75 mm) and dividing by 100. The resulting value indicates the grading and particle size distribution of the sand. A fineness modulus of 3.14 suggests moderately fine sand as per IS 2386 (Part 1): 2016.

The specific gravity, water absorption, and fineness modulus of fine aggregates are crucial in the concrete mix design. They help determine the aggregates' relative density, volume, and grading, which influence the workability, strength, and durability of the concrete mixture.

3.2.4 *Sodium chloride (NaCl)*

Analytical-grade salt was procured for the experiment’s purpose. Analytical grade salts are specially manufactured and processed to meet stringent purity requirements for use in analytical chemistry, research, and laboratory experiments. These salts undergo additional purification and quality control measures to ensure a high purity level and minimize impurities that could interfere with analytical measurements or experiments. It was procured from a reputable chemical supplier from the market.

3.2.5 *Water*

Potable tap water mixed with 1% and 3% NaCl (by weight of cement) was used for casting and curing specimens. Curing in NaCl water was necessary because in normal

water, chloride from the concrete specimens will move out through osmosis and de-ionized water was used for all the testing purposes so that the ions like Ca^{+}, Al^{3+}, Na^{+}, and K^{+} cannot influence further testing.

3.3 Corrosion Inhibitor

In this thesis work, organic chemicals were employed as corrosion inhibitors. The specific inhibitor used in this research was 2-Aminopyridine (2AP). Its IUPAC name is Amino-2-Pyridine. The properties of 2-AP are shown in Table 3.2. Previous literature by Tiwari et al. (2021), has indicated the effectiveness of this organic inhibitor in corrosion prevention without BIEM. 2AP is characterized by an amino group located at the ortho position and replacing one carbon atom with a nitrogen atom in the benzene ring. The presence of hetero-atoms, ringed structure and functional groups makes it a potential corrosion inhibitor for rebar protection in chloride-affected concrete. (Tiwari et. al. 2023). 2-AP is moderately soluble in water. Its solubility in water at room temperature (around 25 degrees Celsius) is approximately 37 grams per liter (g/L). This means that 37 grams of 2-Aminopyridine can dissolve at that temperature in one liter of water. The solubility of 2-Aminopyridine can be affected by factors such as temperature, pH, and the presence of other solutes. As the temperature increases, the solubility of 2-Aminopyridine in water also increases.

Table 3.2 Properties of 2AP

Inhibitor's Name	Molecular wt. (g/mol)	Molecular formula	Chemical structure	Physical appearance
2- Amino Pyridine	94.12	C5H6N2	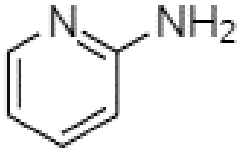	

3.4 Steel

HYSD steel bars (made) with a diameter of 12mm and a length of 360 mm were employed for experimental purposes complying with code IS 1786:2008. Table 3.3 provides detailed information about the diverse physical and chemical properties of the steel bars, as obtained from the manufacturer.

Table 3.3 Properties of steel bars used (*www.tatatiscon.co.in*)

Property	**Constituents**	**HYSD (Fe 550)**
Chemical Properties	Carbon	0.30%
	Sulphur	0.055%
	Phosphorus	0.055%
	Nitrogen	120 ppm
Physical Properties	Minimum yield stress	500 N/mm2
	Minimum ultimate tensile strength	601 N/mm2
	Minimum elongation	12.0 %

3.5 Epoxy

In this case, the epoxy adhesive employed was Fevitite Rapid. It is a versatile epoxy adhesive with two components: Resin and Hardener. The mixing ratio for these components was 1:1, ensuring equal proportions of each. To apply the adhesive, a thin plate was utilized to coat the steel specimens. Subsequently, the specimens were allowed to dry for 24 hours. Additionally, the same epoxy adhesive was applied to the sides of the concrete specimens while preparing for the BIEM experiment.

3.6 Mix design of concrete

The mix design for M25 concrete was carried out following the guidelines specified in IS 10262-2019, which is the Indian Standard code for concrete mix design. The target strength and water-cement (w/c) ratio were determined, and the specific gravity of the materials was taken into account. The mix proportions for the different components were then calculated.

1. Target Strength: The target strength refers to the desired compressive strength of the concrete after 28 days of curing. It is typically determined based on the

project's structural requirements and design considerations, which came out to be 31.6 MPa.

2. Water-Cement (w/c) Ratio: The water-cement ratio is an essential parameter in mix design as it affects the workability, strength, and durability of the concrete. A w/c ratio of 0.44 was used in the study indicating that for every unit weight of cement, 0.44 units of water will be used in the mix.

3. Cement Content: The cement content is determined based on the w/c ratio. By knowing the water-cement ratio and the desired target strength, the amount of cement required in the mix was 436 kg/m^3. The specific gravity of cement (given as 3.16) is used to convert the volume of cement to its weight.

4. Specific Gravity: The specific gravity of materials is a measure of their density compared to the density of water. In the mix design process, the specific gravity of cement, coarse aggregates, and fine aggregates are considered. The specific gravity values provided (3.16 for cement, 2.7 for coarse aggregates, and 2.43 for fine aggregates) were used in calculating the proportions of the materials.

5. Mix Proportions: The mix proportions for M25 concrete, as determined in the mix design process, is presented in Table-3.4.

Table 3.4 Different proportions of mixed concrete

Mix	Max. Size of aggregate (mm)	Water (kg/m3)	Cement (kg/m3)	Fine aggregate (kg/m3)	Coarse aggregate (kg/m3)	Sodium Chloride by weight of cement (kg/m3)
1	20	191.85	436	635	1103.50	4.36
2	20	191.85	436	635	1103.50	13.08

CHAPTER 4. EXPERIMENTAL PROGRAMME AND METHODS

4.1 Experimental Programme

In this section, the research methodology employed in the thesis is presented. The main focus of the study is to assess the effectiveness of the BIEM technique for repairing corrosion in reinforced concrete structures. The methodology encompasses the principles of the tests conducted, the quality and guidelines adhered to, and the various experimental setup employed. The experimental setup employed for conducting the tests is described. This includes the configuration of the specimens, the procedures for sample preparation, the application of the BIEM technique, and any specific equipment or instrumentation used for data collection.

4.2 Specimen Preparation

Concrete specimens were cast using Ordinary Portland Cement (OPC) of grade 43, verifying IS 8112-1989. The mix proportions for the different concrete mixes can be found in table above. In order to corrode the sample at different levels in the concrete, NaCl (sodium chloride) was added at concentrations of 1% and 3% by weight of cement to the concrete mix.

The concrete specimens were cast with dimensions of 300x300x80 mm two HYSD (High Yield Strength Deformed) of 12mm were embedded in each specimen at a, spacing of 200 mm and with a 25 mm cover from the bottom face, as depicted in Figure 4.1. After 24 hours of casting, the specimens were demoulded and subsequently cured for a period of 28 days in the respective NaCl solutions. This curing process ensured the development of the desired corrosion conditions within the concrete.

To protect the exposed steel bars from corrosion, the ends of the bars were masked with epoxy and covered with a heat shrink sleeve, as shown in Figure 4.2. These measures aimed to isolate the exposed steel surfaces and prevent direct contact with the corrosive environment, allowing for targeted evaluation of corrosion effects within the concrete specimens. Controlled conditions were established by combining specific concrete mix proportions, NaCl concentrations, steel bar arrangement, and corrosion protection

measures. These conditions were utilized for studying the corrosion behavior and evaluating the performance of the concrete specimens.

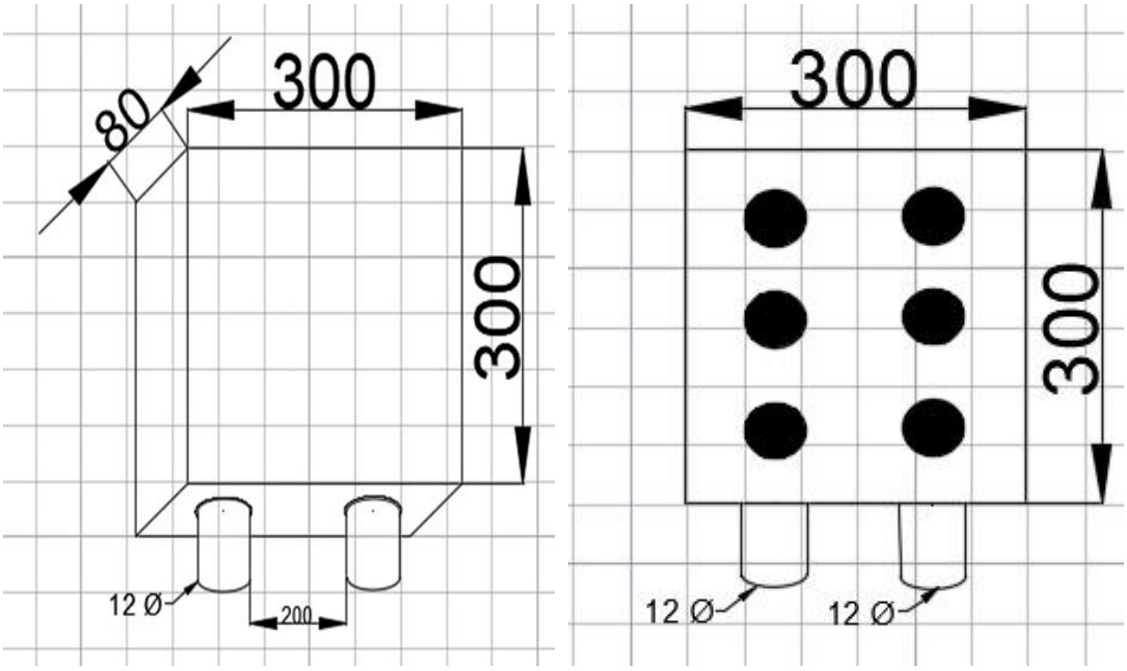

Figure 4-1 Schematic of Specimens

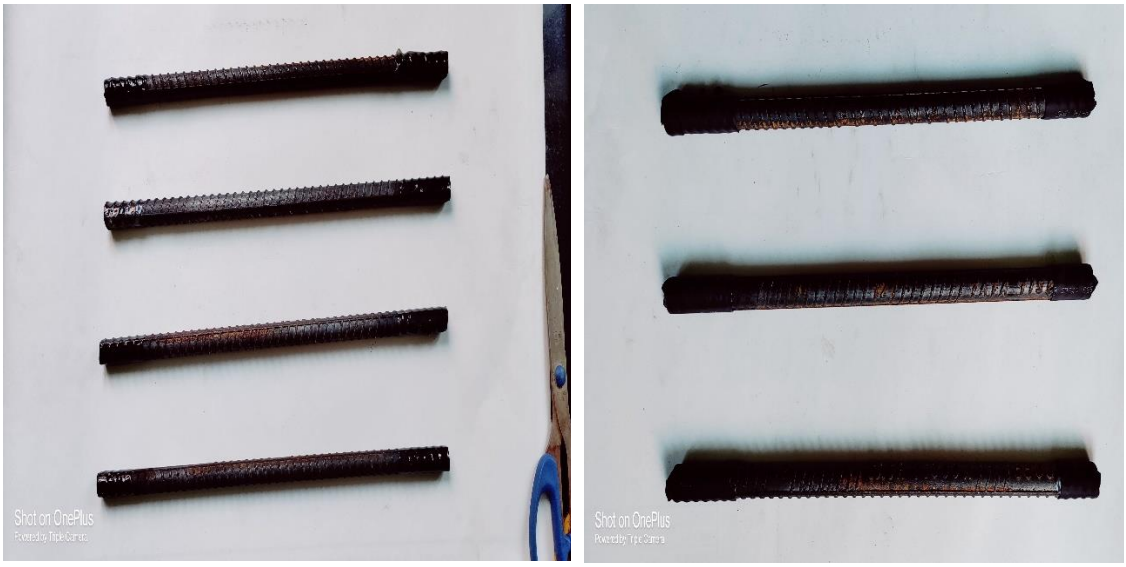

Figure 4-2 Prepared bars before casting

The following procedure was adopted for casting the specimens:

1. Preparation: The necessary materials and equipment, such as cement, sand, coarse aggregates, water, mould forms, reinforcement, mixing equipment (such as a concrete mixer or mixing tray), trowels, and a level were collected.
2. Mould setup: Mould forms were placed on a casting bed. Moulds were cleaned from any debris or dirt. Moulds were then coated with a thin layer of oil to facilitate easy demolding (Figure 4.3).

Figure 4-3 Moulds prepared for casting.

3. Reinforcement placement: The steel bars were placed within the mould forms according to the design specifications. Proper spacing of 200 mm and cover of 25 mm from the bottom were provided.
4. Mixing: The correct proportions of cement, sand, and coarse aggregates to achieve the desired M25 concrete mix design was prepared in the mixer as mentioned in the Table 3.4. Firstly dry materials were thoroughly mixed (Figure 4.4). Then water was gradually added while mixing until a uniform consistency was achieved. Concrete mixer was used to ensure proper blending of the ingredients.

Figure 4-4 Dry mixing of Concrete.

5. Pouring: The concrete mix was then transferred to the oiled mould and compacted in 3 layers. Shovel and scoop were used to distribute the concrete evenly within the moulds (Figure 4.5).
6. Compaction: Mix was compacted within the moulds by using a vibrating table. This helped in eliminating air voids and ensured proper compaction. The specimens were vibrated until air bubbles stop rising to the surface of moulds.
7. Finishing: After compaction, smoothing of the surface of the concrete was done using a trowel and a screed board.

Figure 4-5 Casting of Specimens.

8. Demolding: After 24 hours specimens were carefully removed from the moulds (Figure 4.6). Firstly the sides of the moulds were gently taped using a pry bar to release the concrete slabs and loosen the nuts to open the mould properly.

Figure 4-6 Prepared specimens after demoulding.

9. Curing: Curing of the casted specimens was done for 28 days while maintaining a moist environment (Figure 4.7). The curing was done in the NaCl water with concentration as in mixed concrete.

Figure 4-7 Curing of Specimens in NaCl water.

4.3 Treatment of Specimen

The experimental setup, as depicted in Figure 4.8, consisted of concrete specimens that underwent repair to facilitate the study.

To prevent ion exchange, the side surfaces of the prepared concrete specimens were sealed with epoxy. Subsequently, the specimens were placed in a container with a 304 stainless steel mesh positioned at the bottom, serving as the anode. The embedded steel within the specimens acted as the cathode.

For the treatment process, the bottom surface of the specimens was immersed in an electrolyte solution containing 2AP, reaching a depth of 1mm. To facilitate the desired treatment, a constant current density was applied between the anode and the cathode.

The study investigated the influence of various parameters, including the inhibitor concentration, applied current density, treatment duration, and initial chloride content. Specific details regarding these parameters is shown in Table 4.1.

To maintain consistent conditions throughout the test, the pH of the electrolyte solution was carefully maintained at a level of 10.

By employing this experimental setup, the effects of different variables on the performance and effectiveness of the treatment process were examined.

Table 4.1: Specimen Details

Nomenclature of specimens	**Admixed sodium chloride %**	**Inhibitor Concentration mol/L**	**BIEM Treatment Duration, days**	**Current Density, A/m^2**
C0-1-I0	1	-	0	0
C0-3-I0	3	-	0	0
C0.3-1-B7-I1	1	0.30	7	1
C0.3-1-B15-I1	1		15	
C0.3-3-B7-I1	3		7	
C0.3-3-B15-I1	3		15	
C0.3-1-B7-I0.5	1		7	0.5
C0.3-1-B15-I0.5	1		15	
C0.3-3-B7-I0.5	3		7	
C0.3-3-B15-I0.5	3		15	
C0.15-1-B7-I1	1	0.15	7	1
C0.15-1-B15-I1	1		15	
C0.15-3-B7-I1	3		7	
C0.15-3-B15-I1	3		15	
C0.15-1-B7-I0.5	1		7	0.5
C0.15-1-B15-I0.5	1		15	
C0.15-3-B7-I0.5	3		7	
C0.15-3-B15-I0.5	3		15	

Figure 4-8 Experimental Setup of BIEM

4.4 Experimental Investigation

4.4.1 *Half Cell Potential (HCP)*

In order to monitor the potential shift before and after the application of the BIEM technique, steel, concrete, and electrode potentials were recorded. The measurements were conducted using a high-impedance voltmeter and a reference electrode of Ag/AgCl/0.5M KCl configuration, with the steel bar serving as the working electrode (WE). The experimental setup adhered to the guidelines outlined in ASTM C666 (as shown in Figure 4.8).

Figure 4-9 Measurement of HCP using WE

To obtain accurate readings, the potentials were measured at specific intervals or time points during the experiment. The voltmeter was employed to measure the potential difference between the steel, concrete, and electrode, providing insights into the electrochemical behaviour and any potential shifts occurring in the system.

To ensure reliable measurements, the readings were taken after completely depolarizing the specimens. This step ensures that any transient or residual effects from the treatment or previous electrochemical processes are eliminated, providing a more accurate assessment of the potential shift.

By monitoring and analyzing the recorded potentials, valuable information about the changes in the electrochemical behaviour of the system after the application of the BIEM technique were determined. This data aids in evaluating the effectiveness of the technique in terms of reducing corrosion, altering the electrochemical environment, or influencing the potential distribution within the steel-concrete interface.

4.4.2 *Linear Polarization Resistance (LPR)/ Corrosion Rate (CR)*

LPR stands for Linear Polarization Resistance, which is a commonly used electrochemical technique for measuring the corrosion rate of metallic materials. It is based on the principle that when a metal is immersed in a corrosive environment, it undergoes electrochemical reactions that result in the flow of electric current as per BS EN ISO 14038-2:2020.

The necessity of LPR lies in its ability to provide a quick, non-destructive, and quantitative assessment of the corrosion rate of metals.

The change in corrosion rate before and after the application of the BIEM technique was measured through LPR analysis as technical report 60. ACM Instruments UK was used to measure the change in current by applying a small perturbation (around ±25 mV) from OCP at a scan rate of 0.167 V/sec. A guard ring was placed on top of the specimens and connections were established using reinforcing steel as a working electrode (Fig 4.9).

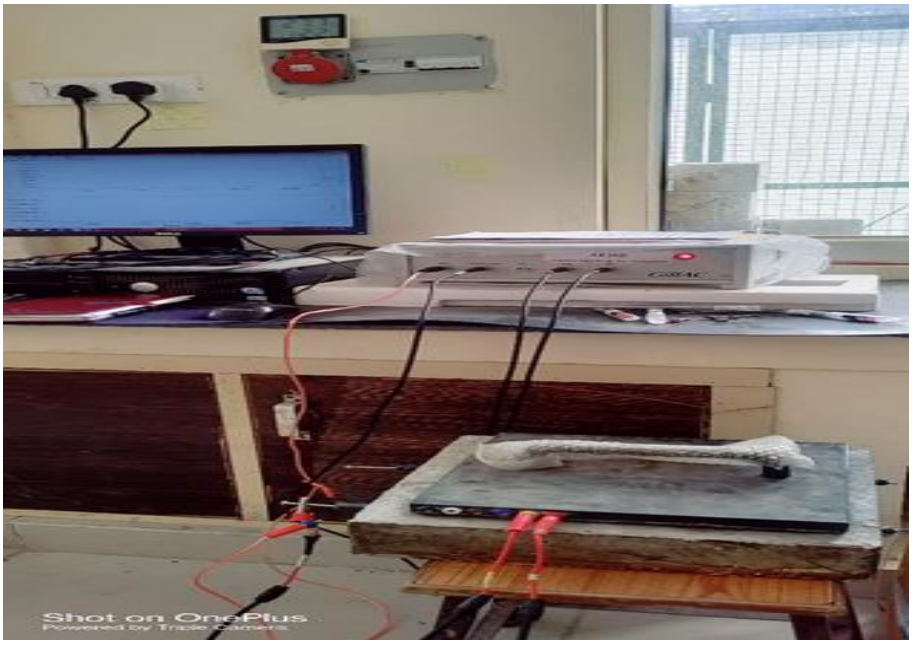

Figure 4-10 LPR Setup.

4.4.3 *Polarization Performance*

To assess the polarization performance of the applied technique, the monitoring followed the guidelines specified in BS EN ISO 14038-2:2020. The 'ON' potentials of steel, concrete, and electrode were continuously recorded throughout the treatment duration, with respect to the reference electrode of Ag/AgCl/0.5M KCl.

During the treatment, the potentials of the steel, concrete, and electrode were measured at regular intervals, providing a continuous record of the electrochemical behaviour of the system. These measurements allow for the evaluation of any shifts or changes in the polarization performance during the treatment process.

Following the completion of the treatment duration, 24-hour decay potentials were recorded. This measurement satisfies the requirement stated in BS EN ISO 14038-2:2020 for the ECE (Electrochemical Chloride Extraction) technique. The decay potentials provide insights into the stability and effectiveness of the treatment over time, indicating the ability of the technique to maintain the desired polarization performance.

By adhering to the standards outlined in BS EN ISO 14038-2:2020 and monitoring the potentials throughout the treatment and decay periods, researchers can assess the efficacy

and durability of the applied technique in terms of achieving the desired polarization performance and fulfilling the requirements of the standard.

4.4.4 *Corrosion Current Density (Icorr)*

These values were further put in equation (1) to calculate the corrosion inhibition efficiency (η%) with 1% and 3% admixed chloride concentrations, with the variation of 7 days and 15 days of BIEM employment.

$$\eta(\%) = \frac{(I0-I1)}{I0} \times 100 \qquad \text{Equation 4.1}$$

4.4.5 *Penetration profile of Corrosion Inhibitor*

After the treatments, the concrete specimens underwent a drying process to remove any excess moisture. Then, a 10 mm diameter drill was used to extract concrete powder at regular intervals of 10 mm along the migration path originating from the treated surface area. This step allowed for the collection of representative samples along the depth of the concrete. The specific drilling positions along the migration path can be observed in Figure 4.11 and 4.12, providing a visual representation of the locations from which the concrete powder was extracted for analysis.

For each specimen, a 25 mg sample of the drilled concrete powder was carefully obtained and securely wrapped. These samples were then stored in a moisture-free environment to prevent any potential degradation or alteration.

To determine the concentration of the corrosion inhibitor, present in the samples, a UV testing machine was employed (Tiwari et al 2023). Initially, a 4gm portion of the sample was used to prepare a solution by mixing it with hot water. After the solution cooled down, it was filtered using filter paper to obtain a clear solution suitable for analysis. The filtered solution was then subjected to UV testing in order to measure the concentration of the corrosion inhibitor present.

The drilled concrete powder was subsequently sieved through a 0.075mm sieve. This sieving process allowed for the separation of fine particles from the larger aggregates, enabling a more accurate calculation of the quantity of the organic corrosion inhibitor that had penetrated into the concrete specimen.

By following these procedures, the depth and concentration of the organic corrosion inhibitor within the concrete specimens were assessed, providing valuable insights into its penetration and distribution characteristics.

Figure 4-11 Drilling positions From Top.

Figure 4-12 Drilling position with depth.

4.4.6 *Penetration Profile of Chloride*

To determine the chloride ion content in concrete specimens, a titration method was employed before and after the implementation of the BIEM technique as per IS code 3025 (Part 32) – 1988.

. The following procedure was followed:

1. A dried sample weighing 4 grams was taken and mixed with 40 ml of hot water (Fig 4.13).
2. After allowing the mixture to cool down, it was filtered using filter paper to obtain a clear solution suitable for titration.
3. For the titration process, a titrant of 0.02 M $AgNO_3$ (silver nitrate) was used.
4. To serve as a color indicator, a makeup solution was prepared by adding 3-4 drops of potassium chromate (Fig 4.14), which imparts a yellow color to the solution (as shown in Fig. 4.15a).

5. The titration was initiated by adding the titrant ($AgNO_3$) to the solution containing the chloride ions.
6. During the titration, a chemical reaction took place between the silver ions (Ag^+) in the titrant and the chloride ions (Cl^-) in the solution.
7. As the reaction progressed, the silver ions combined with the chloride ions, resulting in the formation of silver chloride (AgCl) precipitate.
8. The endpoint of the titration was determined by observing a distinct color change from yellow to red (Fig 4.15b), following the guidelines outlined in the IS 3025-32 (1988) standard.
9. Each titration was repeated three times to ensure accurate and reliable results.

By performing these titrations, the chloride ion content within the concrete specimens were quantitatively analyzed before and after the application of the BIEM technique. The process allowed for the assessment of the effectiveness of the technique in reducing chloride ions in the concrete.

Figure 4-13 Prepared sample for chloride testing.

Figure 4-14 Potassium Chromate as an indicator

(a) (b)

Figure 4-15 (a) Color of makeup solution before titration and (b) Color after titration

4.4.7 pH Testing

In the process of BIEM, maintaining a specific pH level of 10 was a critical factor. The pH level refers to the acidity or alkalinity of a solution and can significantly influence

the outcome of the BIEM process. To ensure that the desired pH level was consistently maintained, regular testing of the pH was done. In between the process of BIEM the sample of inhibitor solution was collected from the setup and tested the pH level as if the pH was decreased more inhibitor solution was added time to time after pH testing to achieve desired level of pH for testing.

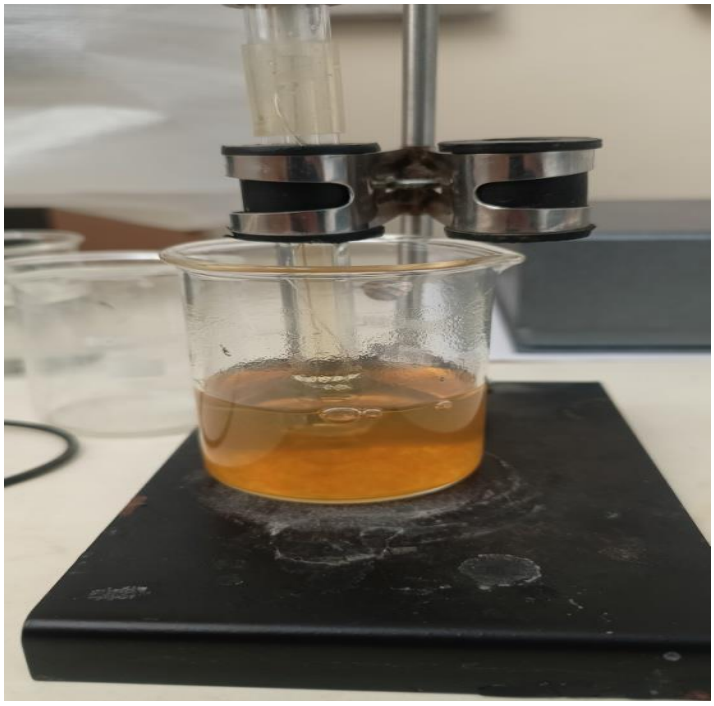

Figure 4-16 Measuring pH of Inhibitor solution during the BIEM process.

4.5 Mechanical Properties

4.5.1 *Compressive Strength*

Compressive strength refers to the maximum compressive stress that a solid material can withstand without fracturing under a gradually applied load. To determine this property, the (IS: 516 2021) standard was followed during testing. The cubes were arranged in such a manner that the load was applied to the opposite side of the cubes from where they were cast, with the casting face and testing face positioned perpendicular to each other. The load was applied axially without any sudden impact and increased steadily at a rate of 2.8 KN/s. The maximum load sustained by the specimen was recorded and then divided by its cross-sectional area to calculate the compressive strength.

In this study, concrete cubes with dimensions of 100 x 100 x 100 mm were cast for testing the compressive strength, following the guidelines specified in is IS 516 (2021).

Figure 4-17 Compressive Testing

The cubes were tested at 7 and 28 days of curing age with an optimal dosage. The process of testing concrete specimens for compression is illustrated in the figure provided. To ensure accuracy, three cubes were tested for each type of concrete mix. The compressive strength of the concrete mix was calculated by taking the average value of the three specimens. The formula for determining compressive strength is given as

$$F_{ck}=P/A$$

Where,

A= Area (100 X 100) mm^2

P = Maximum load applied (N)

F_{ck} = Compressive strength (N/mm^2)

4.5.2 *Split Tensile Test*

Concrete is renowned for its limited tensile strength and brittleness, making it unsuitable for withstanding direct tension. However, assessing the tensile strength of concrete is crucial to identify potential cracks that may occur in concrete structures. To determine

the tensile strength, cylindrical concrete specimens with a diameter of 100mm and height of 200mm are cast and subjected to testing following the guidelines of IS 516 (2021).

Figure 4-18 Split Tensile Testing

During testing, these specimens are carefully positioned in a centering jig, with packing strips and loading pieces strategically placed along the top and bottom of the specimen's plane of loading. The load is then gradually and continuously applied at a controlled rate, ensuring there are no sudden impacts, and the loading rate falls within the range of 0.8 N/(mm^2/min). The maximum load (p) that the specimen can bear before failure occurs is recorded.

To calculate the split tensile strength (Fct) of the concrete cylinder, a specific formula is employed:

$Fct = 2p / (\pi dl)$

Where,

‘p’ represents the maximum load in kn

‘l’ is the length of the cylinder in mm

‘d’ is the depth of the cylinder in mm

The concrete cylinders are tested for optimum dosages at 7 and 28 days of curing age. To ensure accuracy, three cylinders are tested for each type of concrete mix. The split tensile strength of the concrete mix is determined by calculating the average value of the three specimens.

4.5.3 *Flexural Strength*

The flexural test, commonly referred to as the three-point bending test, is a widely employed method to assess the flexural or bending strength of materials, with concrete being a prominent example. For this evaluation, specimens of size 500x100x100 mm are cast. These specimens are subjected to testing on a three-point bending machine after 7 and 28 days from the time of casting. To ensure accuracy, three specimens are tested for each concrete mix as per IS 516 (2021).

Figure 4.19 Flexural Testing

The primary objective of the flexural test is to measure a material's ability to withstand deformation or failure when subjected to a bending load. The test simulates real-world scenarios where materials might experience bending forces, enabling engineers and researchers to understand the material's structural behavior.

The flexural strength of the material is calculated using the formula:

Flexural strength = (3 * load * length) / (2 * width * height^2)

The experiments are summarized in Table 4.1

Table 4. 1 Summary table of tests showing specimen size and standard followed

Test	**Specimen Size**	**Standard Followed**	**No of Specimens**	**Time of Test**
Chloride Titration	Concrete Powder	IS code 3025 (Part 32) – 1988	64	After BIEM
Chloride Titration	Concrete Powder	IS code 3025 (Part 32) – 1988	8	Before BIEM
UV Testing	Concrete Powder	Tiwari et al 2023	64	After BIEM
LPR	300x300x80	BS EN ISO 14038-2:2020	48	After BIEM
LPR	300x300x80	BS EN ISO 14038-2:2020	48	Before BIEM
HCP	300x300x80	ASTM C666	48	During BIEM
Compressive Strength	100x100x100	IS 516:2021	6	After 7 Days of Casting
Compressive Strength	100x100x100	IS 516:2021	6	After 28 Days of Casting
Split Tensile	100x200	IS 516:2021	6	After 7 Days of Casting
Split Tensile	100x200	IS 516:2021	6	After 28 Days of Casting
Flexural Strength	500x100x100	IS 516:2021	6	After 7 Days of Casting
Flexural Strength	500x100x100	IS 516:2021	6	After 28 Days of Casting
PH	-	IS 3025	48	During BIEM Process

CHAPTER 5. RESULTS AND DISCUSSION

In this section, we present the key discoveries of our research. The primary aim of the study was to evaluate how well the BIEM technique repairs corrosion in reinforced concrete structures. We followed all the guidelines given by IS codes, technical reports, and more. We thoroughly discuss the final results of the Chloride test, Inhibitor test, I_{corr}, LPR, and HCP before and after using the BIEM technique.

5.1 Corrosion Current Density (I_{corr})

Corrosion current density refers to the rate at which corrosion occurs on a metal surface. It is a measure of the amount of metal that is being lost due to corrosion per unit area and time. Higher corrosion current density values indicate more rapid corrosion, while lower values suggest slower corrosion rates.

In order to explore the efficiency of 2AP to inhibit the chloride-induced corrosion by employing the BIEM technique, an LPR test was conducted and I_{corr} values were evaluated. Alongside, the concentration of 2AP was also varied i.e., 0.15M and 0.3M. Figure 5.1 and 5.2 shows the LPR curves recorded for 1% admixed chloride and Figure 5.3 and 5.4 shows the LPR curves for 3 % admixed chlorides, treated with the 2AP-BIEM technique. Further, the value of I_{corr} and the corresponding η% for various treatment process is presented in Table 5.1.

From Figures 5.1 and 5.2, it is evident that the untreated sample (C0-1-I0) exhibits the highest I_{corr} value in comparison to the treated samples. Examining Figure 5.1, it can be observed that curves 2, 3, and 4, 5 display similar behavior in terms of potential as they shift toward the positive or anodic side while increasing the current density from 0.5A to 1A. The value of I_{corr} decreases as the current density increases in relation to the untreated samples.

In Figure 5.2, curves 4, 5 show a similar trend as observed in Figure 5.1. However, in the case of curves 2, 3 in Figure 5.2, there is a significant difference in the value of potential shift as the treatment duration increases from 7 to 15 days. Regarding the Icorr values, they exhibit a similar trend to that observed in Figure 5.1.

To summarize, the treated samples consistently show lower I_{corr} values compared to the untreated sample. In terms of potential behaviour, increasing the current density results

in a shift towards more positive potentials. Furthermore, as the treatment duration extends from 7 to 15 days, there is a notable difference in the potential shift for curves 2, 3 in Figure 5.2, while the I_{corr} trend remains consistent with that observed in Figure 5.1.

The factor that determines the presence of corrosion is referred to as I_{corr}. If the value of I_{corr} exceeds 0.1 µA/cm2, it indicates that corrosion is active. Conversely, if the value of I_{corr} is below 0.1 µA/cm2, it signifies that the corrosion is passive or inactive (Fan et. al. 2020 #18).

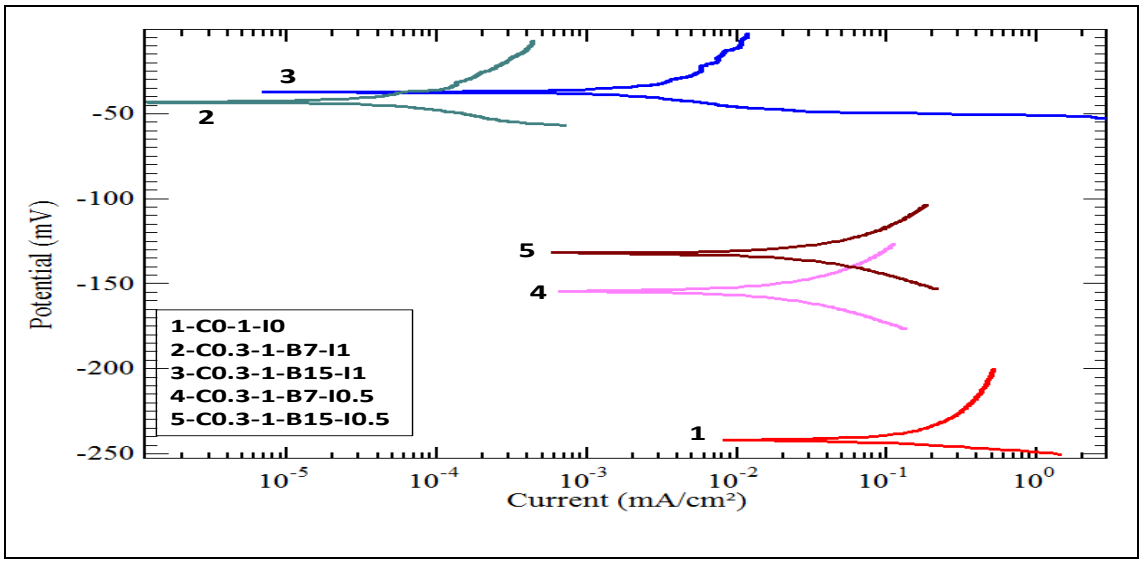

Figure 5.1 LPR curves for different concrete samples with 1% admixed NaCl and 0.3M 2AP concentration.

From Figures 5.3 and 5.4, it is evident that the untreated sample (C0-3-I0) exhibits the highest Icorr value compared to the treated samples. Looking at Figure 5.3, it can be observed that curves 2, 3, and 4, 5 exhibit similar behavior in terms of potential, shifting towards the positive or anodic side as the current density increases from 0.5A to 1A, with significant changes in the potential values. Additionally, the value of Icorr decreases as the current density increases in relation to the untreated samples.

In Figure 5.4, curves 2, 3, and 4, 5 follow a similar trend as observed in Figure 5.3. However, in the case of curves 2, 3 in Figure 5.4, there is a notable difference in the I_{corr} values as the treatment duration increases from 7 to 15 days. Furthermore, the potential values exhibit a similar trend as observed in Figure 5.3.

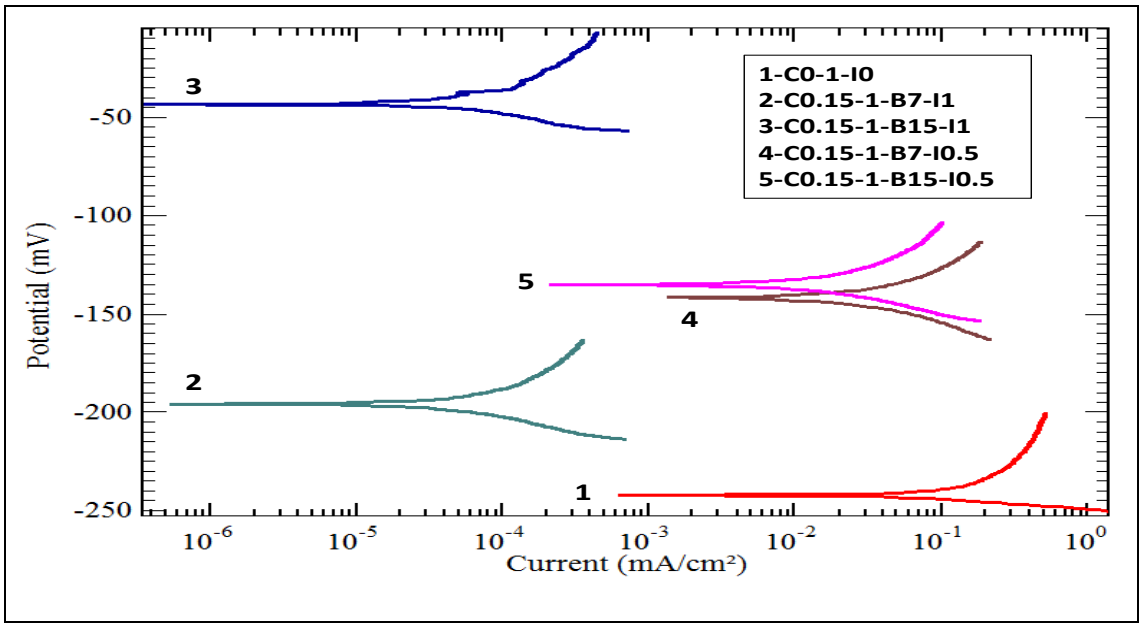

Figure 5.2 LPR curves for different concrete samples with 1% admixed NaCl and 0.15M 2AP concentration.

In summary, the treated samples consistently show lower I_{corr} values compared to the untreated sample. In terms of potential behavior, increasing current density leads to a shift towards more positive potentials. Additionally, as the treatment duration extends from 7 to 15 days, there is a significant difference in the I_{corr} values, while the potential trend remains consistent with that observed in Figure 5.3.

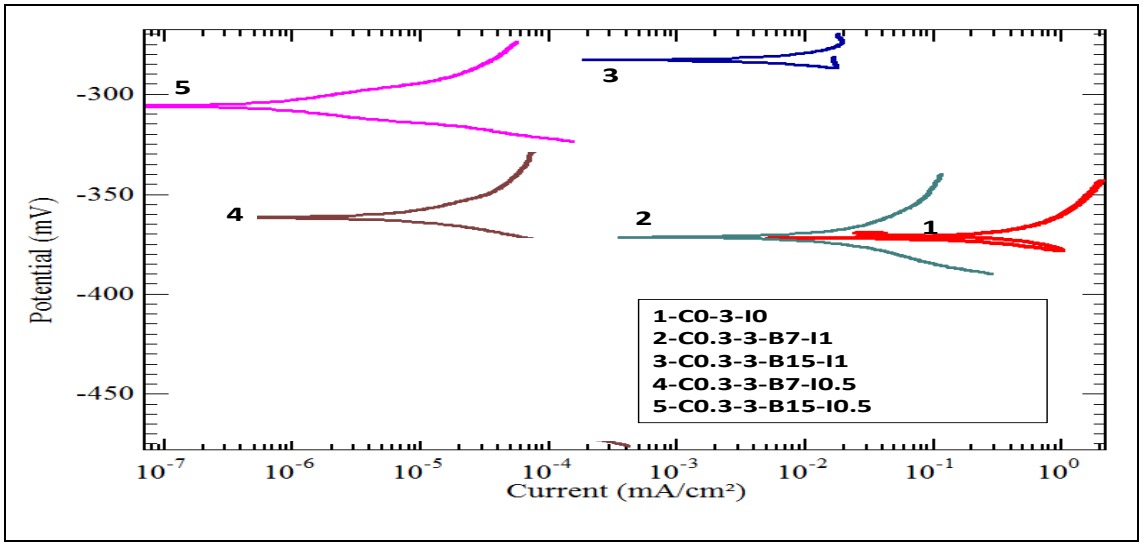

Figure 5.3 LPR curves for different concrete samples with 3% admixed NaCl and 0.3M 2AP concentration.

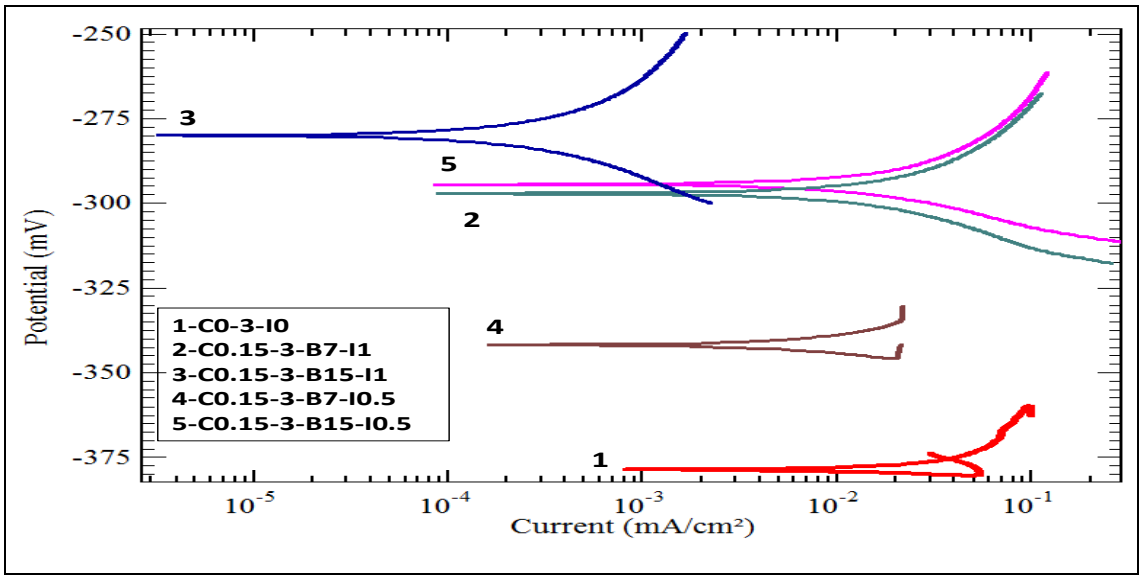

Figure 5.4 LPR curves for different concrete samples with 3% admixed NaCl and 0.15M 2AP concentration.

Table 5.1 Inhibition efficiency (η) of 2AP as corrosion inhibitor for different admixed chloride concentrations.

Admixed Chloride	Sample Description	I_{corr} (μA/m^2)	η (%)
1 % (by weight of cement)	C0-1-I0	0.232	-
	C0.3-1-B7-I1	1.30E-05	99.99
	C0.3-1-B15-I1	5.39E-08	99.99
	C0.3-1-B7-I0.5	4.65E-04	99.79
	C0.3-1-B15-I0.5	9.10E-05	99.96
	C0.15-1-B7-I1	2.10E-04	99.90
	C0.15-1-B15-I1	5.60E-06	99.99
	C0.15-1-B7-I0.5	3.20E-04	99.86
	C0.15-1-B15-I0.5	5.80E-06	99.99
3 %	C0-3-I0	1.94	-
	C0.3-3-B7-I1	6.80E-05	99.99

(by weight of cement)	C0.3-3-B15-I1	9.15E-09	99.99
	C0.3-3-B7-I0.5	1.90E-04	99.99
	C0.3-3-B15-I0.5	5.70E-06	99.99
	C0.15-3-B7-I1	6.52E-03	99.66
	C0.15-3-B15-I1	6.68E-05	99.99
	C0.15-3-B7-I0.5	7.79E-03	99.59
	C0.15-3-B15-I0.5	8.10E-04	99.95

5.2 Chloride Profile

5.2.1 *Influence of Admixed Chloride Content*

Upon evaluating the outcomes of our comprehensive observations, it has been revealed that the presence of chloride ions in the concrete specimens exhibits a noteworthy reduction after the implementation of the BIEM technique. Subsequent analysis of the titration results has confirmed a decline in Cl- concentration in the proximity of the steel bar, while an increase in Cl- concentration has been detected around the concrete surface. These findings suggest a migration of Cl- ions away from the steel bar towards the external anode, namely the 304 steel mesh.

The profiles depicting the concentration of Cl- and 2-aminopyridine following BIEM are displayed for specimens mixed with different initial quantities of sodium chloride. These specimens were formulated using M25 concrete, which additionally incorporated sodium chloride at two distinct levels, namely 1% and 3%.

Figure 5.5 (a) and Table 5.2 illustrates the influence of the initial chloride concentration on the efficiency of chloride extraction from concrete in the cases of C0.3-1-B7-I1 and C0.3-3-B7-I1. In specimens with a sodium chloride mixed ratio of 1%, approximately 19% of the chlorides were extracted in the vicinity of the steel bars. However, in the 3% sodium chloride groups, only 33% of the chlorides were extracted.

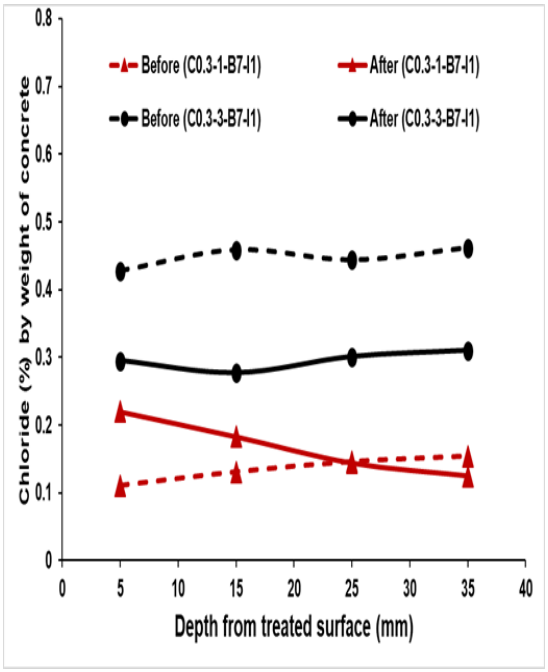

(a)

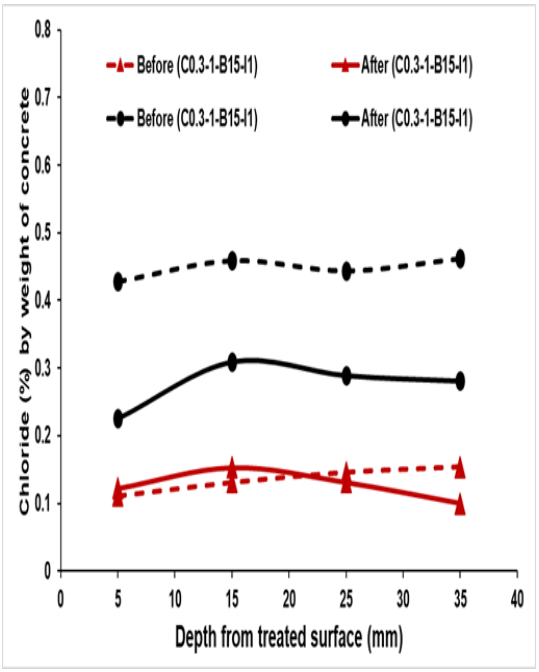

(b)

Figure 5.5 Concentration profile of Chloride in specimens before and after BIEM of different admixed chloride (1A 0.3M) (a) 7 Days (b) 15 Days

Table 5.2 Concentration of Chloride in specimens before and after BIEM (1A 0.3M) for 7 and 15 Days.

Depth	Before (C0.3-1-B7-I1)	After (C0.3-1-B7-I1)	Δ (%)
5	0.111	0.22	-98.1981982
15	0.131	0.183	-39.69465649
25	0.146	0.144	+1.369863014
35	0.154	0.125	+18.83116883
Depth	Before (C0.3-3-B7-I1)	After (C0.3-3-B7-I1)	Δ (%)
5	0.428	0.295	+31.07476636
15	0.459	0.277	+39.65141612

25	0.444	0.301	+32.20720721
35	0.462	0.31	+32.9004329
Depth	Before (C0.3-1-B15-I1)	After (C0.3-1-B15-I1)	Δ (%)
5	0.111	0.122	-9.90990991
15	0.131	0.153	-16.79389313
25	0.146	0.131	+10.2739726
35	0.154	0.1	+35.06493506
Depth	Before (C0.3-1-B15-I1)	After (C0.3-1-B15-I1)	Δ (%)
5	0.428	0.226	+47.19626168
15	0.459	0.309	+32.67973856
25	0.444	0.289	+34.90990991
35	0.462	0.281	+39.17748918

*- implies an increase in concentration. *+ implies a decrease in concentration.

Simultaneously, as Cl- ions migrated from the cathode (internal steel bar) to the anode (externally provided SS 304 steel mesh), the concentration of Cl- ions experienced a significant increase. At a distance of 5mm from the outer surface, the concentration increased by 98%. At 15mm from the outer surface, it reached a 39% increase. For specimens with an initial chloride content of 1%, the chloride concentration decreased by 13% at a distance of 25mm from the outer surface. On the other hand, in specimens with an initial chloride content of 3%, the concentration of Cl- ions decreased consistently across all depths. At 5mm from the outer surface, it decreased by 32%, at 15mm it decreased by 40%, and at 25mm it decreased by 33%.

In Figure 5.5 (b) and Table 5.2, we can observe the impact of the initial chloride concentration on the efficacy of chloride extraction from concrete in the cases of C0.3-1-

B15-I1 and C0.3-3-B15-I1. In specimens with a sodium chloride mixed ratio of 1%, approximately 35% of the chlorides were extracted in the proximity of the steel bars. Conversely, in the 3% sodium chloride groups, only 40% of the chlorides were extracted.

Additionally, for specimens with an initial chloride concentration of 1%, the concentration of chloride ions experienced an increase. At a distance of 5mm from the outer surface, the concentration increased by 9%. At 15mm from the outer surface, it exhibited a 17% increase. However, at 25mm from the outer surface, the concentration of chloride decreased by 10%.

For specimens with an initial chloride content of 3%, the concentration of Cl- ions decreased notably. At a distance of 5mm from the outer surface, there was a 47% decrease. At 15mm from the outer surface, the decrease was around 33%. Finally, at 25mm from the outer surface, the concentration decreased by 35%.

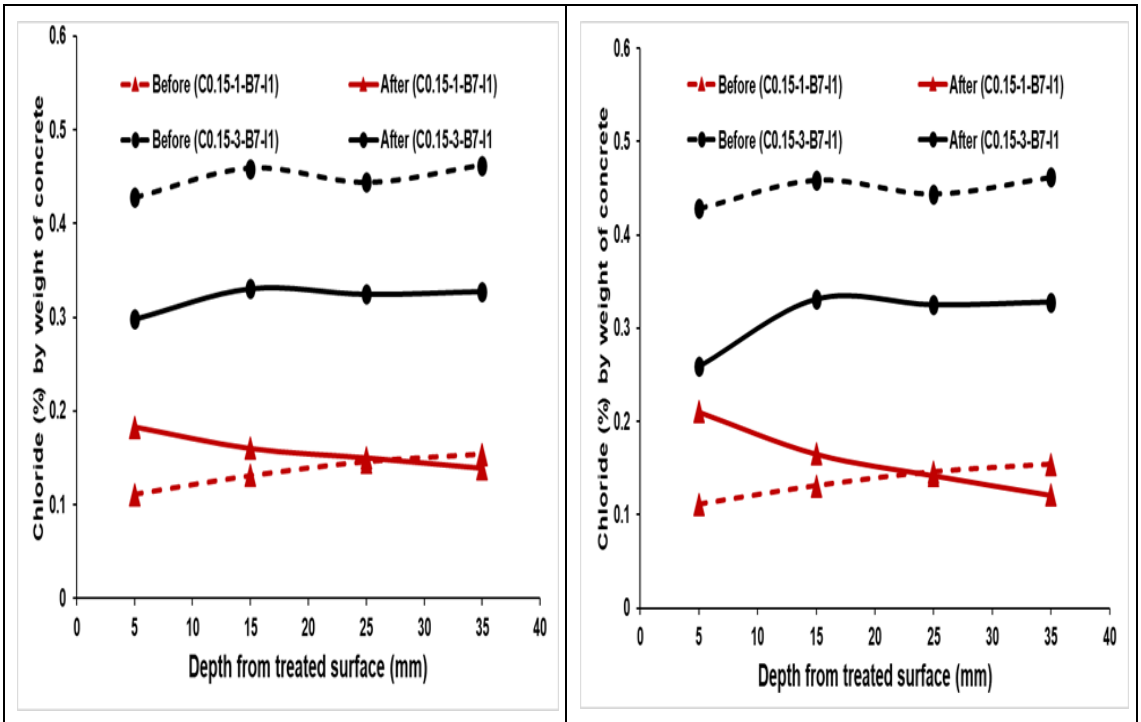

(a) (b)

Figure 5.6 Concentration profile of Chloride in specimens before and after BIEM of different admixed chloride (1A 0.15M) (a) 7 Days (b) 15 Days

Table 5.3 Concentration of Chloride in specimens before and after BIEM (1A 0.15M) for 7 and 15 Days.

Depth	Before (C0.15-1-B7-I1)	After (C0.15-1-B7-I1)	Δ (%)
5	0.111	0.183	-64.86486486
15	0.131	0.16	-22.13740458
25	0.146	0.15	-2.739726027
35	0.154	0.139	9.74025974
Depth	Before (C0.15-3-B7-I1)	After (C0.15-3-B7-I1	Δ (%)
5	0.428	0.298	30.37383178
15	0.459	0.331	27.88671024
25	0.444	0.325	26.8018018
35	0.462	0.328	29.004329
Depth	Before (C0.15-1-B15-I1)	After (C0.15-1-B15-I1)	Δ (%)
5	0.111	0.21	-89.18918919
15	0.131	0.165	-25.95419847
25	0.146	0.142	2.739726027
35	0.154	0.121	21.42857143
Depth	Before (C0.15-3-B15-I1)	After (C0.15-3-B15-I1)	Δ (%)
5	0.428	0.259	39.48598131

15	0.459	0.331	27.88671024
25	0.444	0.325	26.8018018
35	0.462	0.328	29.004329

Figure 5.6 (a) and Table 5.3 illustrates the influence of the initial chloride concentration on the efficiency of chloride extraction from concrete for specimens labeled as C0.15-1-B7-I1 and C0.15-3-B7-I1. In the case of specimens with a 1% sodium chloride mixed ratio, approximately 9% of the chlorides were extracted in front of the steel bars, while only 29% were extracted in the 3% sodium chloride groups.

Regarding the concentration of Cl- ions, at a distance of 5mm from the outer surface, there was a 65% increase in chloride concentration for specimens containing 1% initial chloride content. At a distance of 15mm from the outer surface, the concentration increased by 2%, and at 25mm from the outer surface, it increased by 2.7%.

However, for specimens with 3% initial chloride content, the concentration of Cl- ions decreased by 30% at a distance of 5mm from the outer surface. Similarly, it decreased by 28% at a distance of 15mm from the outer surface, and at 25mm from the outer surface, it decreased by 27%.

Figure 5.6 (b) and Table 5.3 demonstrates the impact of the initial chloride concentration on the efficacy of chloride extraction from concrete for specimens labeled as C0.15-1-B15-I1 and C0.15-3-B15-I1. In the case of specimens with a 1% sodium chloride mixed ratio, approximately 21% of the chlorides were extracted in front of the steel bars, while only 29% were extracted in the 3% sodium chloride groups.

Regarding the concentration of Cl- ions, for specimens containing 1% initial chloride content, there was an 89% increase in chloride concentration at a distance of 5mm from the outer surface. At a distance of 15mm from the outer surface, the concentration increased by 26%, and at 25mm from the outer surface, there was a 2.7% decrease in chloride concentration.

However, for specimens with 3% initial chloride content, the concentration of Cl- ions decreased by 39.5% at a distance of 5mm from the outer surface. Similarly, it decreased

by 28% at a distance of 15mm from the outer surface, and at 25mm from the outer surface, it decreased by 26.8%.

Figure 5.7 (a) and Table 5.4 demonstrates the influence of the initial chloride concentration on the effectiveness of chloride extraction from concrete for specimens labeled as C0.3-1-B7-I0.5 and C0.3-3-B7-I0.5. In the case of specimens with a 1% sodium chloride mixed ratio, approximately 8.4% of the chlorides were extracted in front of the steel bars, while only 20.5% were extracted in the 3% sodium chloride groups.

Regarding the concentration of Cl- ions, for specimens containing 1% initial chloride content, there was a 62% increase in chloride concentration at a distance of 5mm from the outer surface. At a distance of 15mm from the outer surface, the concentration increased to 18%, and at 25mm from the outer surface, there was a 2% increase in chloride concentration.However, for specimens with 3% initial chloride content, the concentration of Cl- ions decreased by 30% at a distance of 5mm from the outer surface. Similarly, it decreased by 40% at a distance of 15mm from the outer surface, and at 25mm from the outer surface, it decreased by 26.4%.

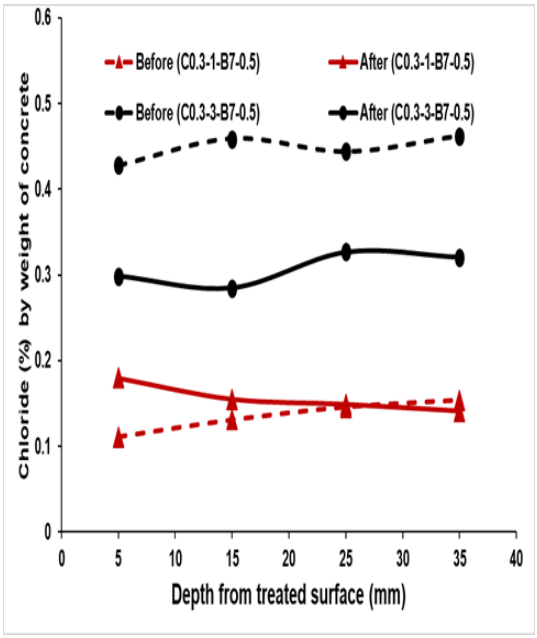

(a)

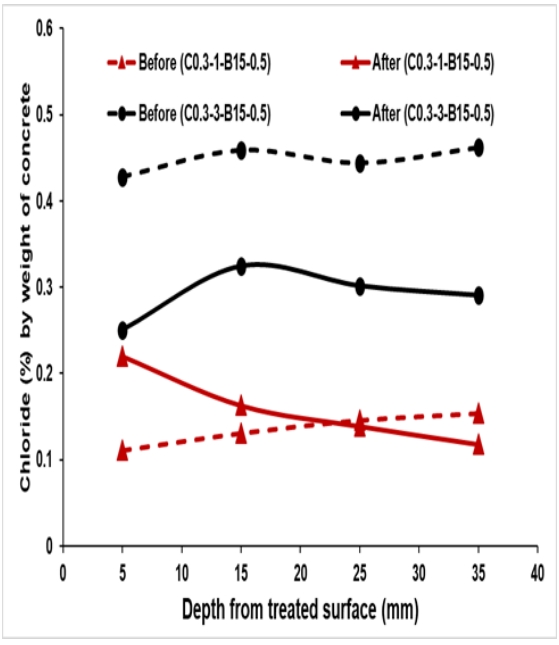

(b)

Figure 5.7 Concentration profile of Chloride in specimens before and after BIEM of different admixed chloride (0.5A 0.3M) (a) 7 Days (b) 15 Days

Table 5.4 Concentration of Chloride in specimens before and after BIEM (0.5A 0.3M) for 7 and 15 Days.

Depth	Before (C0.3-1-B7-0.5)	After (C0.3-1-B7-0.5)	Δ (%)
5	0.111	0.18	-62.16216216
15	0.131	0.155	-18.32061069
25	0.146	0.149	-2.054794521
35	0.154	0.141	8.441558442
Depth	Before (C0.3-3-B7-0.5)	After (C0.3-3-B7-0.5)	Δ (%)
5	0.428	0.299	30.14018692
15	0.459	0.285	37.90849673
25	0.444	0.327	26.35135135
35	0.462	0.321	30.51948052
Depth	Before (C0.3-1-B15-0.5)	After (C0.3-1-B15-0.5)	Δ (%)
5	0.111	0.22	-98.1981982
15	0.131	0.163	-24.42748092
25	0.146	0.139	4.794520548
35	0.154	0.118	23.37662338
Depth	Before (C0.3-3-B15-0.5)	After (C0.3-3-B15-0.5)	Δ (%)
5	0.428	0.251	41.35514019

15	0.459	0.325	29.19389978
25	0.444	0.302	31.98198198
35	0.462	0.291	37.01298701

Figure 5.7 (b) and Table 5.4 showcases the impact of the initial chloride concentration on the efficiency of extracting chlorides from concrete for specimens labeled as C0.3-1-B15-I0.5 and C0.3-3-B15-I0.5. In the case of specimens with a 1% sodium chloride mixed ratio, approximately 23% of the chlorides were extracted in front of the steel bars, while only 37% were extracted in the 3% sodium chloride groups.

Regarding the concentration of Cl- ions, for specimens containing 1% initial chloride content, there was a 98% increase in chloride concentration at a distance of 5mm from the outer surface. At a distance of 15mm from the outer surface, the concentration increased by 24%, and at 25mm from the outer surface, there was a 4.7% decrease in chloride concentration.

However, for specimens with 3% initial chloride content, the concentration of Cl- ions decreased by 41% at a distance of 5mm from the outer surface. Similarly, it decreased by 29% at a distance of 15mm from the outer surface, and at 25mm from the outer surface, it decreased by 32%.

Figure 5.8 (a) and Table 5 demonstrates the impact of the initial chloride concentration on the effectiveness of extracting chlorides from concrete for specimens labeled as C0.15-1-B7-I0.5 and C0.15-3-B7-I0.5. In the case of specimens with a 1% sodium chloride mixed ratio, approximately 9% of the chlorides were extracted in front of the steel bars, while only 24.7% were extracted in the 3% sodium chloride groups.

Regarding the concentration of Cl- ions, for specimens containing 1% initial chloride content, there was a 61% increase in chloride concentration at a distance of 5mm from the outer surface. At a distance of 15mm from the outer surface, the concentration increased to 11.77%, and at 25mm from the outer surface, there was a 2.7% decrease in chloride concentration.

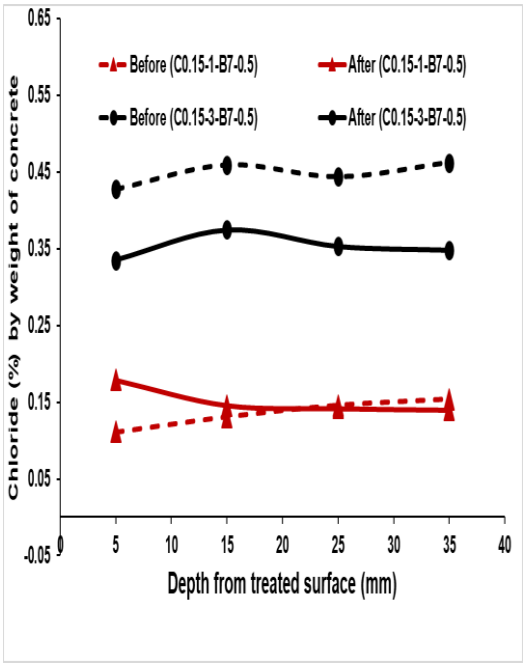

(a)

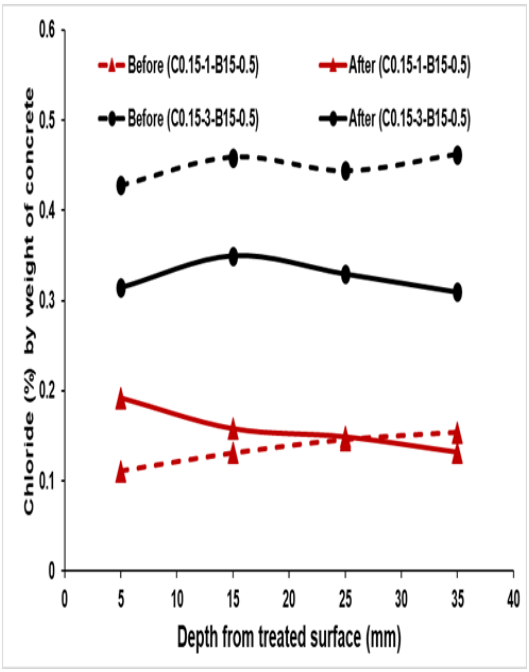

(b)

Figure 5.8 Concentration profile of Chloride in specimens before and after BIEM of different admixed chloride (0.5A 0.15M) (a) 7 Days (b) 15 Days

Table 5.5 Concentration of Chloride in specimens before and after BIEM (1A 0.15M) for 7 and 15 Days.

Depth	Before (C0.15-1-B7-0.5)	After (C0.15-1-B7-0.5)	Δ (%)
5	0.111	0.179	-61.26126126
15	0.131	0.146	-11.45038168
25	0.146	0.142	2.739726027
35	0.154	0.14	9.090909091
Depth	Before (C0.15-3-B7-0.5)	After (C0.15-3-B7-0.5)	Δ (%)

5	0.428	0.335	21.72897196
15	0.459	0.375	18.30065359
25	0.444	0.353	20.4954955
35	0.462	0.348	24.67532468
Depth	Before (C0.15-1-B15-0.5)	After (C0.15-1-B15-0.5)	Δ (%)
5	0.111	0.192	-72.97297297
15	0.131	0.158	-20.61068702
25	0.146	0.149	-2.054794521
35	0.154	0.132	14.28571429
Depth	Before (C0.15-3-B15-0.5)	After (C0.15-3-B15-0.5)	Δ (%)
5	0.428	0.315	26.40186916
15	0.459	0.35	23.74727669
25	0.444	0.33	25.67567568
35	0.462	0.31	32.9004329

However, for specimens with 3% initial chloride content, the concentration of Cl- ions decreased by 21.7% at a distance of 5mm from the outer surface. Similarly, it decreased by 18.3% at a distance of 15mm from the outer surface, and at 25mm from the outer surface, it decreased by 20.5%.

Figure 5.8 (b) and Table 5.5 showcases the influence of the initial chloride concentration on the efficacy of extracting chlorides from concrete for specimens labeled as C0.15-1-

B15-I0.5 and C0.15-3-B15-I0.5. In the case of specimens with a 1% sodium chloride mixed ratio, approximately 14% of the chlorides were extracted in front of the steel bars, while only 33% were extracted in the 3% sodium chloride groups.

Regarding the concentration of Cl- ions, for specimens containing 1% initial chloride content, there was a 72.6% increase in chloride concentration at a distance of 5mm from the outer surface. At a distance of 15mm from the outer surface, the concentration increased by 20.9%, and at 25mm from the outer surface, there was a 2% increase in chloride concentration.

However, for specimens with 3% initial chloride content, the concentration of Cl- ions decreased by 26.4% at a distance of 5mm from the outer surface. Similarly, it decreased by 23.7% at a distance of 15mm from the outer surface, and at 25mm from the outer surface, it decreased by 25.7%.

5.2.2 *Influence of Current Density*

The profiles of Cl- and 2-aminopyridine concentrations change as different current densities are applied, as depicted in the figures. As the current density increases, the remaining Cl- content in the specimens decreases. It is natural that with an increase in circuit charge, higher current density can improve the efficiency of chlorine extraction. However, when the current density is less than 3 A/m2, the residual Cl- concentration in the outermost layer is even higher than in the untreated specimens. This suggests that the applied electric field is insufficient to completely remove Cl-, resulting in the accumulation of Cl- in the outer layer of the specimens.

Figure 5.9 and Table 5.6 illustrates the impact of current density on the efficiency of chloride extraction from concrete for specimens labeled as C0.3-1-B7-I0.5 and C0.3-1-B7-I1. At the end of 7 days, the percentage of extracted chlorides in front of the steel bars was approximately 8.4% for specimens under 0.5A current density, while only 18.8% was found for specimens under 1A current density. As chloride ions migrate from the cathode to the anode, they tend to accumulate more near the outer surface, increasing Cl- ion concentration near the outer surface and a decrease near the steel bar.

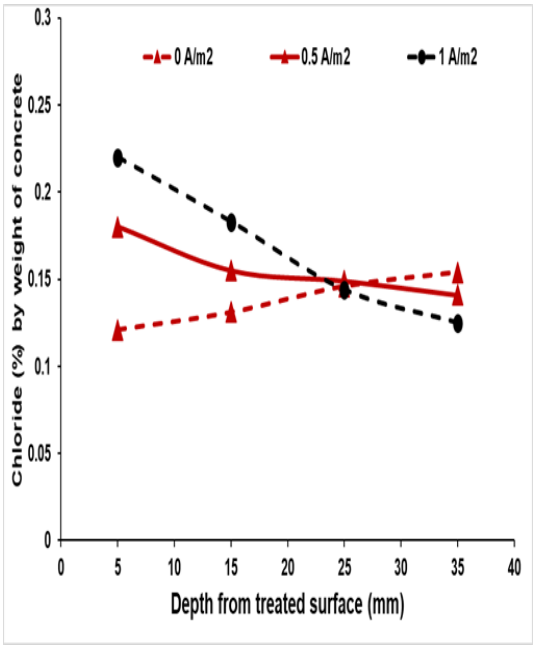

(a)

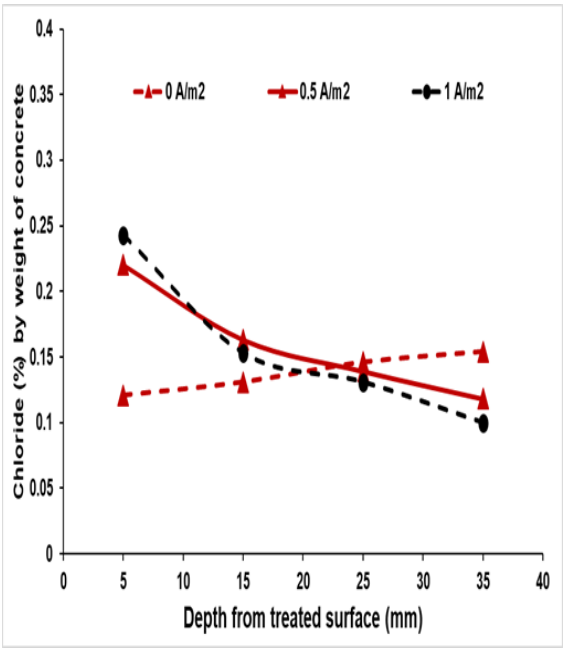

(b)

Figure 5.9 Concentration profile of Chloride in specimens before and after BIEM at different Current Densities (1% NaCl 0.3 M) (a) 7 Days (b) 15 Days

Table 5.6 Concentration of Chloride in specimens before and after BIEM (1% NaCl 0.3 M) for 7 and 15 Days.

		C0.3-1-B7-I0.5		C0.3-1-B7-I1	
Depth	0 A/m2	0.5 A/m2	Δ (%)	1 A/m2	Δ (%)
5	0.121	0.18	-48.760330	0.22	-81.81818
15	0.131	0.155	-18.320610	0.183	-39.69465
25	0.146	0.149	-2.0547945	0.144	1.3698630
35	0.154	0.141	8.44155844	0.125	18.831168
		C0.3-1-B15-I0.5		C0.3-1-B15-I1	
Depth	0 A/m2	0.5 A/m2	Δ (%)	1 A/m2	Δ (%)

5	0.121	0.22	-81.818181	0.243	-100.8264
15	0.131	0.163	-24.427480	0.153	-16.79389
25	0.146	0.139	4.7945205	0.131	10.2739
35	0.154	0.118	23.3766233	0.1	35.064935

Specifically, at a distance of 5mm from the outer surface, the concentration of Cl- ions increased by 48.7% and 81.8% for current densities of 0.5A and 1A, respectively. At a distance of 15mm from the outer surface, the concentration increased by 18.3% and 39.6% for 0.5A and 1A current densities, respectively. At a distance of 25mm from the outer surface, the concentration increased by 2% for 0.5A current density, while it decreased by 1.36% for 1A current density.

Similarly, Figure 5.9 and Table 5.6 demonstrates the influence of current density on the efficiency of chloride extraction from concrete for specimens labeled as C0.3-1-B15-I0.5 and C0.3-1-B15-I1. After 15 days, the percentage of extracted chlorides in front of the steel bars was approximately 23.3% for specimens under 0.5A current density and 35% for specimens under 1A current density.

At a distance of 5mm from the outer surface, the concentration of Cl- ions increased by 81.8% and 100.8% for 0.5A and 1A current densities, respectively. At a distance of 15mm from the outer surface, the concentration increased by 24.4% for 0.5A current density and decreased by 16.7% for 1A current density. At a distance of 25mm from the outer surface, the concentration decreased by 4.7% for 0.5A current density and 10.2% for 1A current density.

Figure 5.10 (a) and Table 5.7 illustrates the influence of current density on the effectiveness of extracting chlorides from concrete for specimens labeled as C0.3-3-B7-I0.5 and C0.3-3-B7-I1. After 15 days, the percentage of extracted chlorides in front of the steel bars was approximately 27.4% for specimens under 0.5A current density, while only 32.2% was found for specimens under 1A current density.

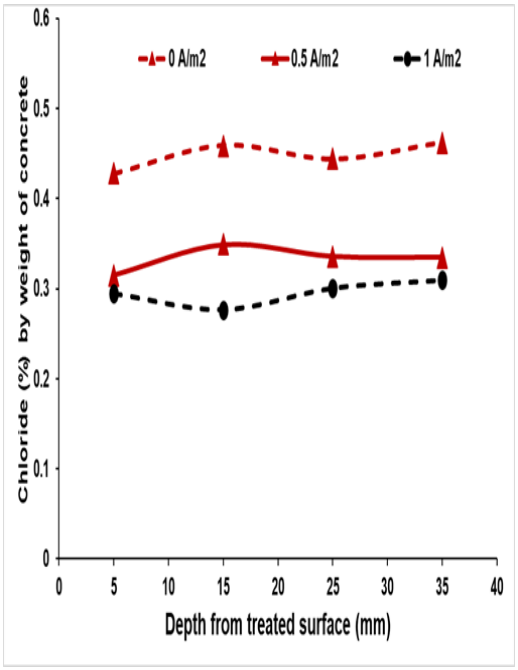

(a)

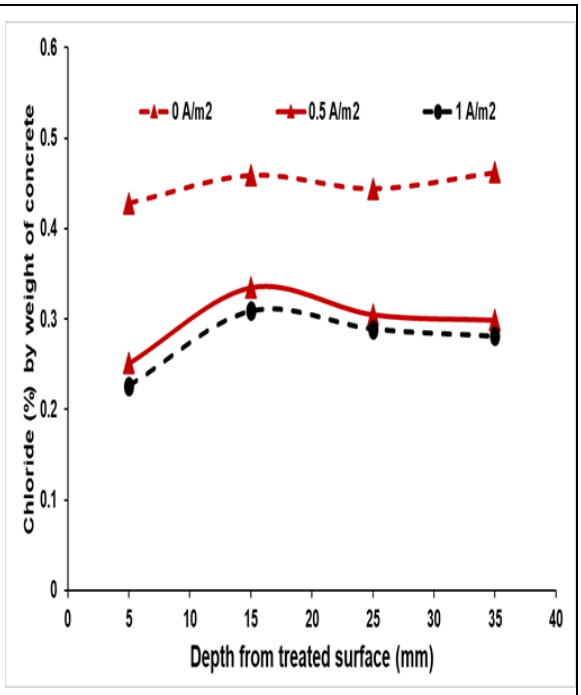

(b)

Figure 5.10 Concentration profile of Chloride in specimens before and after BIEM at different Current Densities (3% NaCl 0.3 M) (a) 7 Days (b) 15 Days

Table 5.7 Concentration of Chloride in specimens before and after BIEM (1% NaCl 0.3 M) for 7 and 15 Days.

		C0.3-3-B7-I0.5		C0.3-3-B7-I1	
Depth	0 A/m2	0.5 A/m2	Δ (%)	1 A/m2	Δ (%)
5	0.428	0.315	26.40186916	0.295	31.074766
15	0.459	0.349	23.96514161	0.277	39.651416
25	0.444	0.336	24.32432432	0.301	32.207207
35	0.462	0.335	27.48917749	0.31	32.900432
		C0.3-3-B15-I0.5		C0.3-3-B15-I1	
Depth	0 A/m2	0.5 A/m2	Δ (%)	1 A/m2	Δ (%)

5	0.428	0.251	41.35514019	0.226	47.196261
15	0.459	0.335	27.01525054	0.309	32.679738
25	0.444	0.305	31.30630631	0.289	34.909909
35	0.462	0.299	35.28138528	0.281	39.177489

At a distance of 5mm from the outer surface, the concentration of Cl- ions decreased by 26.4% and 31.7% for current densities of 0.5A and 1A, respectively. At a distance of 15mm from the outer surface, the concentration decreased by 23.9% for 0.5A current density and 39.4% for 1A current density. At a distance of 25mm from the outer surface, the concentration decreased by 24.3% for 0.5A current density and 32.2% for 1A current density.

Figure 5.10 (b) and Table 5.7 showcases the impact of current density on the effectiveness of extracting chlorides from concrete for specimens labeled as C0.3-3-B15-I0.5 and C0.3-3-B15-I1. After 15 days, the percentage of extracted chlorides in front of the steel bars was approximately 35.2% for specimens under 0.5A current density, while only 39.1% was found for specimens under 1A current density.

At a distance of 5mm from the outer surface, the concentration of Cl- ions increased by 41.3% and 47.1% for current densities of 0.5A and 1A, respectively. At a distance of 15mm from the outer surface, the concentration increased by 27% for 0.5A current density and 32.6% for 1A current density. At a distance of 25mm from the outer surface, the concentration decreased by 31.3% for 0.5A current density and 34.9% for 1A current density.

Figure 5.11(a) and Table 5.8 demonstrates the impact of current density on the effectiveness of extracting chlorides from concrete for specimens labeled as C0.15-1-B7-I0.5 and C0.15-1-B7-I1. After 15 days, the percentage of extracted chlorides in front of the steel bars was approximately 14.2% for specimens under 0.5A current density, while only 21.4% was found for specimens under 1A current density.

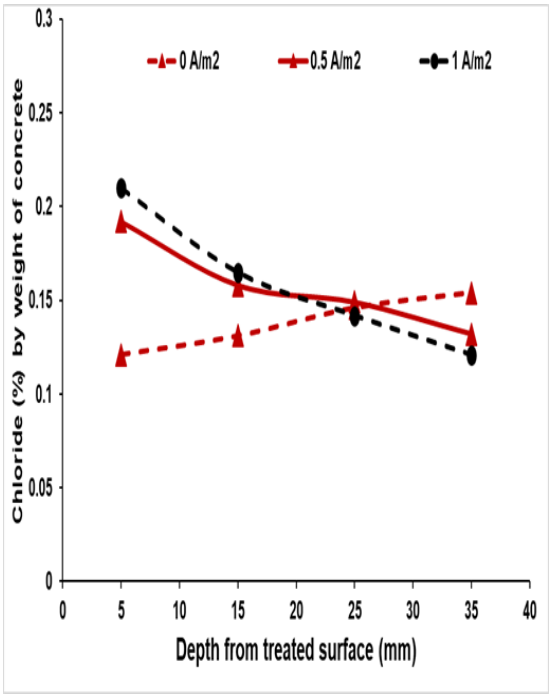

(a)

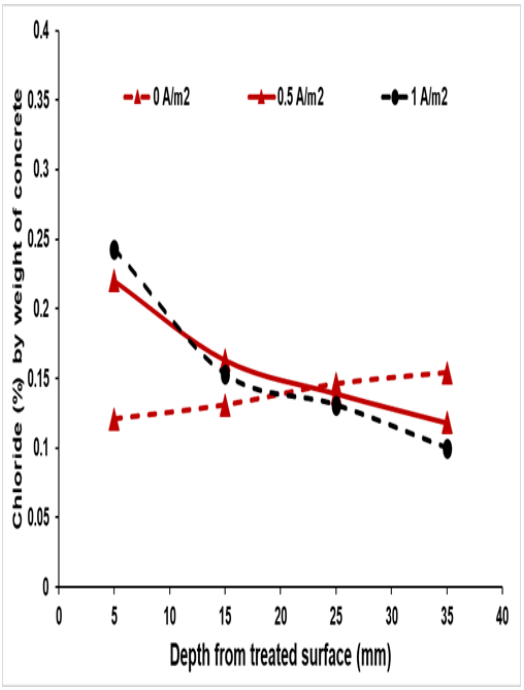

(b)

Figure 5.11 Concentration profile of Chloride in specimens before and after BIEM at different Current Densities (1% NaCl 0.15 M) (a) 7 Days (b) 15 Days

Table 5.8 Concentration of Chloride in specimens before and after BIEM (1% NaCl 0.15 M) for 7 and 15 Days.

		C0.15-1-B7-I0.5		C0.15-1-B7-I0.5	
Depth	0 A/m2	0.5 A/m2	Δ (%)	1 A/m2	Δ (%)
5	0.121	0.192	-58.67768595	0.21	-73.5537190
15	0.131	0.158	-20.61068702	0.165	-25.9541984
25	0.146	0.149	-2.054794521	0.142	2.739726027
35	0.154	0.132	14.28571429	0.121	21.42857143
		C0.15-1-B15-I0.5		C0.15-1-B15-I1	

Depth	0 A/m2	0.5 A/m2	Δ (%)	1 A/m2	Δ (%)
5	0.121	0.22	-81.81818182	0.243	-100.826
15	0.131	0.163	-24.42748092	0.153	-16.794
25	0.146	0.139	4.794520548	0.131	10.274
35	0.154	0.118	23.37662338	0.1	35.065

At a distance of 5mm from the outer surface, the concentration of Cl- ions increased by 58.6% and 73.5% for current densities of 0.5A and 1A, respectively. At a distance of 15mm from the outer surface, the concentration increased by 20.6% for 0.5A current density and 25.9% for 1A current density. At a distance of 25mm from the outer surface, the concentration increased by 2% for 0.5A current density, while it decreased by 2.7% for 1A current density.

Figure 5.11(b) and Table 5.8 showcases the influence of current density on the effectiveness of extracting chlorides from concrete for specimens labeled as C0.15-1-B15-I0.5 and C0.15-1-B15-I1. After 15 days, the percentage of extracted chlorides in front of the steel bars was approximately 23.3% for specimens under 0.5A current density, while only 35% was found for specimens under 1A current density.

At a distance of 5mm from the outer surface, the concentration of Cl- ions increased by 81.8% and 100.8% for current densities of 0.5A and 1A, respectively. At a distance of 15mm from the outer surface, the concentration increased by 24.4% for 0.5A current density and decreased by 16.7% for 1A current density. At a distance of 25mm from the outer surface, the concentration decreased by 4.7% for 0.5A current density and 10.2% for 1A current density.

Figure 5.12(a) and Table 5.9 showcases the influence of current density on the effectiveness of extracting chlorides from concrete for specimens labeled as C0.15-3-B7-I0.5 and C0.15-3-B7-I1. After 15 days, the percentage of extracted chlorides in front of the steel bars was approximately 24.6% for specimens under 0.5A current density, while only 31.8% was found for specimens under 1A current density.

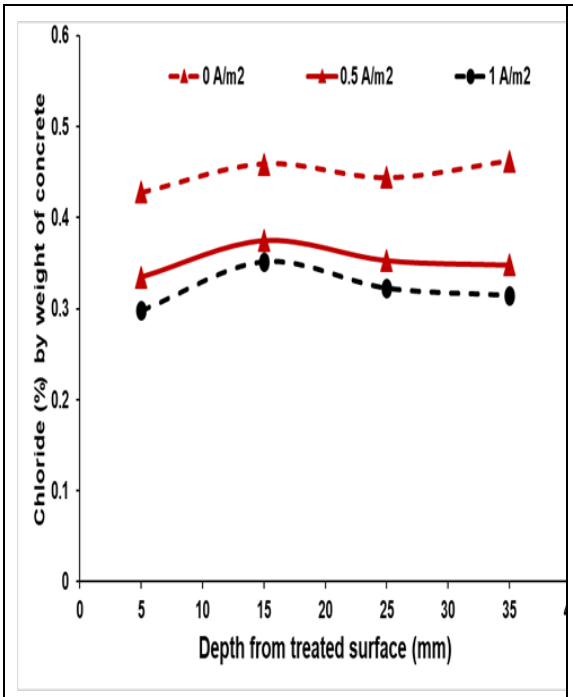

(a)

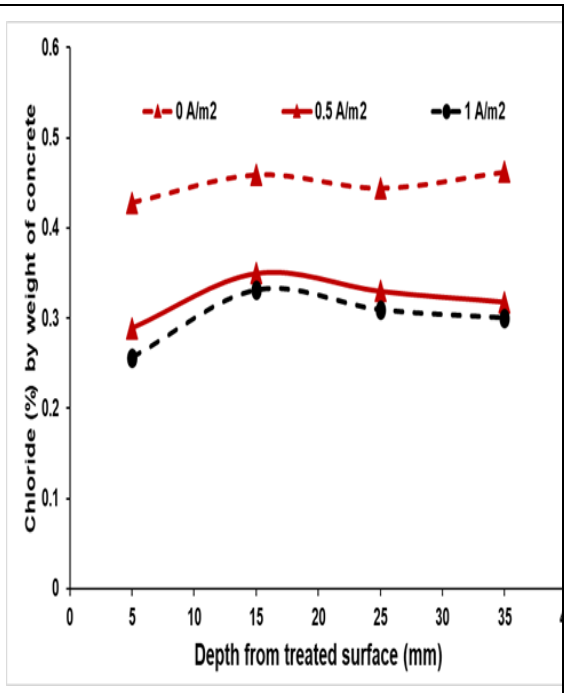

(b)

Figure 5.12 Concentration profile of Chloride in specimens before and after BIEM at different Current Densities (3% NaCl 0.15 M) (a) 7 Days (b) 15 Days

Table 5.9 Concentration of Chloride in specimens before and after BIEM (3% NaCl 0.15 M) for 7 and 15 Days.

		C0.15-3-B7-I0.5		C0.15-3-B7-I0.5	
Depth	0 A/m2	0.5 A/m2	Δ (%)	1 A/m2	Δ (%)
5	0.428	0.335	21.72897196	0.298	30.37383178
15	0.459	0.375	18.30065359	0.352	23.31154684
25	0.444	0.353	20.4954955	0.323	27.25225225
35	0.462	0.348	24.67532468	0.315	31.81818182
		C0.15-3-B15-I0.5		C0.15-3-B15-I1	
Depth	0 A/m2	0.5 A/m2	Δ (%)	1 A/m2	Δ (%)

5	0.428	0.289	32.47663551	0.256	40.186
15	0.459	0.35	23.74727669	0.331	27.886
25	0.444	0.33	25.67567568	0.309	30.405
35	0.462	0.318	31.16883117	0.3	35.064

At a distance of 5mm from the outer surface, the concentration of Cl- ions decreased by 21.7% and 30.3% for current densities of 0.5A and 1A, respectively. At a distance of 15mm from the outer surface, the concentration decreased by 18.3% for 0.5A current density and 23.3% for 1A current density. At a distance of 25mm from the outer surface, the concentration decreased by 20.4% for 0.5A current density and 37.2% for 1A current density.

Figure 5.12(b) and Table 5.9 demonstrates the impact of current density on the effectiveness of extracting chlorides from concrete for specimens labeled as C0.15-3-B15-I0.5 and C0.15-3-B15-I1. After 15 days, the percentage of extracted chlorides in front of the steel bars was approximately 31.1% for specimens under 0.5A current density, while only 35% was found for specimens under 1A current density.

At a distance of 5mm from the outer surface, the concentration of Cl- ions increased by 32.1% and 40.4% for current densities of 0.5A and 1A, respectively. At a distance of 15mm from the outer surface, the concentration increased by 23.7% for 0.5A current density and 27.8% for 1A current density. At a distance of 25mm from the outer surface, the concentration decreased by 25.6% for 0.5A current density and 30.4% for 1A current density.

5.2.3 *Influence of Treatment Duration*

The concentration profile and the relationship between the concentrations of Cl- and 2-aminopyridine are depicted, illustrating the variation in treatment time. The current density was held at 1 A/m2 and 3 A/m2, while M25 concrete with 1% and 3% sodium chloride content was utilized in the experiments.

Figure 5.13(a) and Table 10 depicts the influence of time duration on the effectiveness of extracting chlorides from concrete for specimens labeled as C0.3-1-B7-I1 and C0.3-1-

B15-I1. Under a constant current density of 1 A/m2, after 7 days of treatment, the percentage of extracted chlorides in front of the steel bars was approximately 18.8%, which increased to 35.06% after 15 days of treatment. As chloride ions migrate from the cathode to the anode, they tend to accumulate more near the outer surface, increasing Cl- ion concentration near the outer surface and a decrease near the steel bar.

Specifically, at a distance of 5mm from the outer surface, the concentration of Cl- ions increased by 98.1% after 7 days and by 9.9% after 15 days. At a distance of 15mm from the outer surface, the concentration increased by 39.6% after 7 days and by 16.7% after 15 days. At a distance of 25mm from the outer surface, the concentration decreased by 1.36% after 7 days and by 10.27% after 15 days.

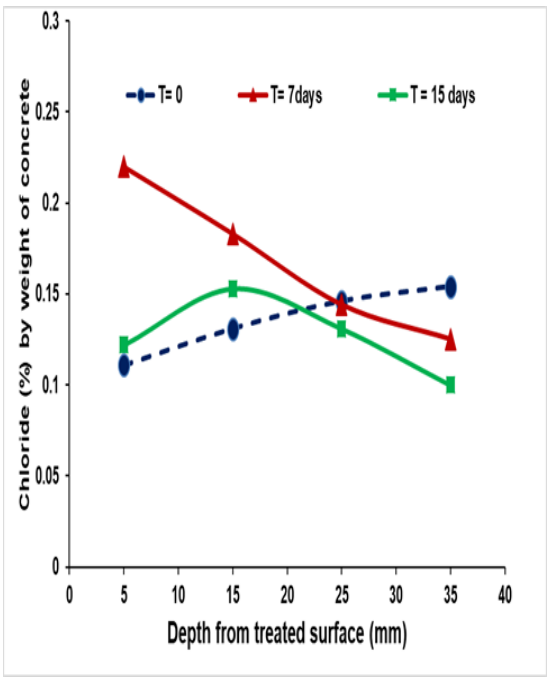

(a)

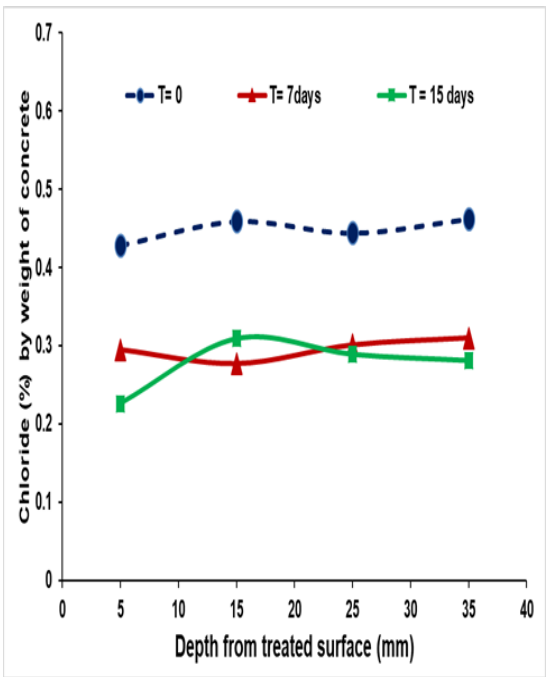

(b)

Figure 5.13 Concentration profile of Chloride in specimens before and after BIEM at different Treatment Duration (1A 0.3M) (a) 1% NaCl (b) 3% NaCl

Table 5.10 Concentration of Chloride in specimens before and after BIEM (1%, 3% NaCl 0.3M) for 7 and 15 Days.

		C0.3-1-B7-I1		C0.3-1-B15-I1	
Depth	T= 0	T= 7days	Δ (%)	T = 15 days	Δ (%)
5	0.111	0.22	-98.1981982	0.122	-9.90990991
15	0.131	0.183	-39.6946564	0.153	-16.793893
25	0.146	0.144	1.36986301	0.131	10.2739726
35	0.154	0.125	18.8311688	0.1	35.0649350
		C0.3-3-B7-I1		C0.3-3-B15-I1	
Depth	T= 0	T= 7days	Δ (%)	T = 15 days	Δ (%)
5	0.428	0.295	31.0747663	0.226	47.196261
15	0.459	0.277	39.6514161	0.309	32.6797385
25	0.444	0.301	32.2072072	0.289	34.9099099
35	0.462	0.31	32.9004329	0.281	39.1774891

Figure 5.13(b) and Table 10 demonstrates the impact of current density on the effectiveness of extracting chlorides from concrete for specimens labeled as C0.3-3-B7-I1 and C0.3-3-B15-I1. Under a constant current density of 1 A/m2, after 7 days of treatment, the percentage of extracted chlorides in front of the steel bars was approximately 32.9%, which increased to 39.1% after 15 days of treatment.

At a distance of 5mm from the outer surface, the concentration of Cl- ions decreased by 31% after 7 days and by 47.19% after 15 days. At a distance of 15mm from the outer surface, the concentration decreased by 39.65% after 7 days and by 32.67% after 15 days. At a distance of 25mm from the outer surface, the concentration decreased by 32.2% after 7 days and by 34.9% after 15 days.

Figure 5.14(a) and Table 11 showcases the effect of time duration on the effectiveness of extracting chlorides from concrete for specimens labeled as C0.15-1-B7-I1 and C0.15-1-B15-I1. Under a constant current density of 1 A/m2, after 7 days of treatment, the percentage of extracted chlorides in front of the steel bars was approximately 9.7%, which increased to 21.4% after 15 days of treatment.

At a distance of 5mm from the outer surface, the concentration of Cl- ions increased by 64.8% after 7 days and by 89.18% after 15 days. At a distance of 15mm from the outer surface, the concentration increased by 22.1% after 7 days and by 25.9% after 15 days. At a distance of 25mm from the outer surface, the concentration increased by 2.7% after 7 days but then decreased by 2.73% after 15 days.

Figure 5.14(b) and Table 11 demonstrates the impact of current density on the effectiveness of extracting chlorides from concrete for specimens labeled as C0.15-3-B7-I1 and C0.15-3-B15-I1.

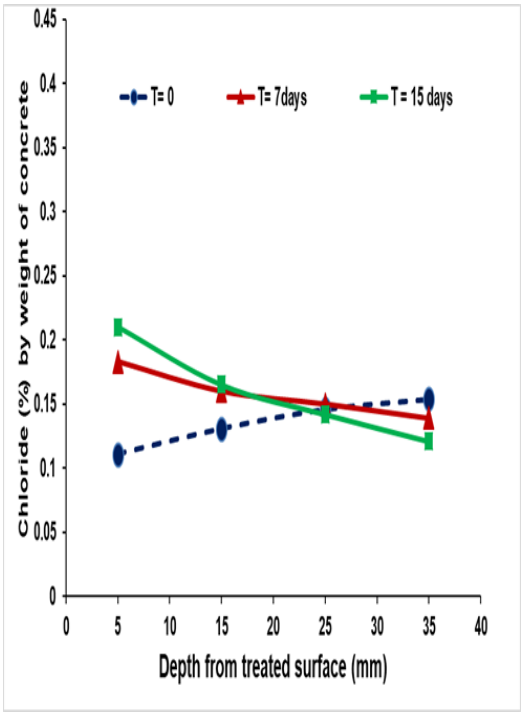

(a)

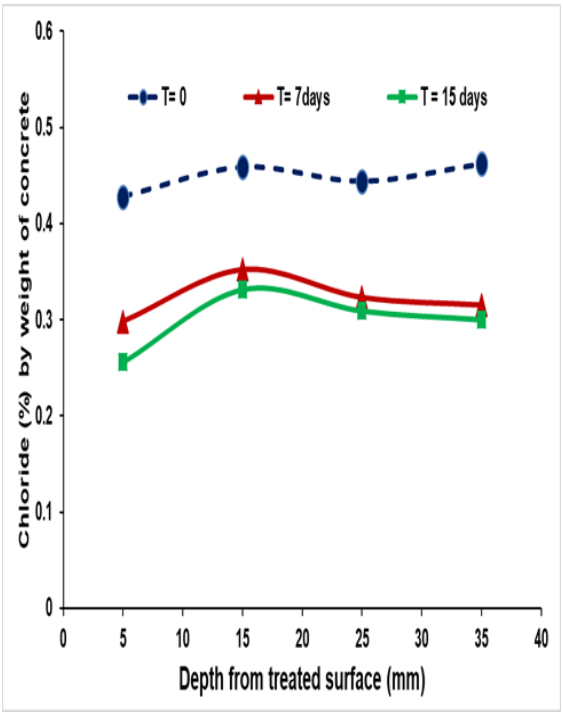

(b)

Figure 5.14 Concentration profile of Chloride in specimens before and after BIEM at different Treatment Duration (1A 0.15M) (a) 1% NaCl (b) 3% NaCl

Table 5.11 Concentration of Chloride in specimens before and after BIEM (1%, 3% NaCl 0.3M) for 7 and 15 Days.

		C0.15-1-B7-I1		C0.15-1-B15-I1	
Depth	T= 0	T= 7days	Δ (%)	T = 15 days	Δ (%)
5	0.111	0.183	-64.86486486	0.21	-89.1891891
15	0.131	0.16	-22.13740458	0.165	-25.9541984
25	0.146	0.15	-2.739726027	0.142	2.739726027
35	0.154	0.139	9.74025974	0.121	21.42857143
		C0.15-3-B7-I1		C0.15-3-B15-I1	
Depth	T= 0	T= 7days	Δ (%)	T = 15 days	Δ (%)
5	0.428	0.298	30.37383178	0.256	40.18691589
15	0.459	0.352	23.31154684	0.331	27.88671024
25	0.444	0.323	27.25225225	0.309	30.40540541
35	0.462	0.315	31.81818182	0.3	35.06493506

Under a constant current density of 1 A/m2, after 7 days of treatment, the percentage of extracted chlorides in front of the steel bars was approximately 31.8%, which increased slightly to 35.06% after 15 days of treatment.

At a distance of 5mm from the outer surface, the concentration of Cl- ions decreased by 30.3% after 7 days and by 40.1% after 15 days. At a distance of 15mm from the outer surface, the concentration decreased by 23.3% after 7 days and by 27.8% after 15 days. At a distance of 25mm from the outer surface, the concentration decreased by 27.2% after 7 days and by 30.4% after 15 days.

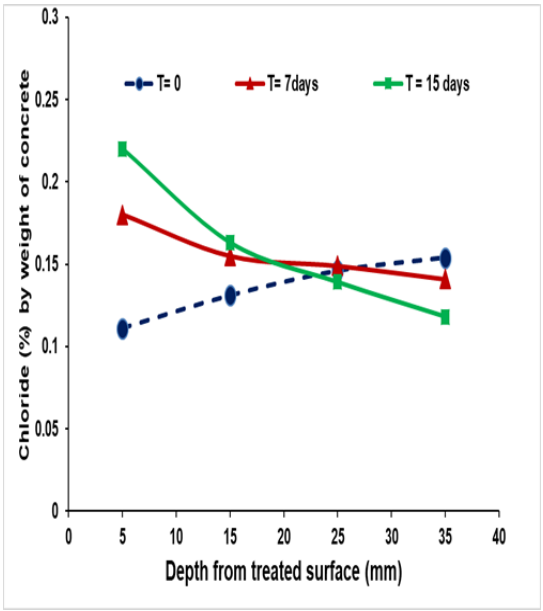

(a)

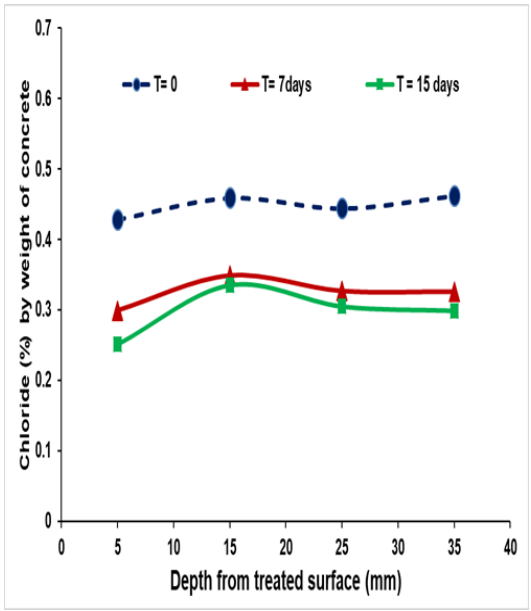

(b)

Figure 5.15 Concentration profile of Chloride in specimens before and after BIEM at different Treatment Duration (0.5A 0.5M) (a) 1% NaCl (b) 3% NaCl

Table 5.12 Concentration of Chloride in specimens before and after BIEM (1%, 3% NaCl 0.3M) for 7 and 15 Days.

		C0.3-1-B7-I0.5		C0.3-1-B15-I0.5	
Depth	T= 0	T= 7days	Δ (%)	T = 15 days	Δ (%)
5	0.111	0.18	-62.1621621	0.22	-98.1981982
15	0.131	0.155	-18.3206106	0.163	-24.4274809
25	0.146	0.149	-2.05479452	0.139	4.794520548
35	0.154	0.141	8.441558442	0.118	23.37662338
		C0.3-3-B7-I0.5		C0.3-3-B15-I0.5	
Depth	T= 0	T= 7days	Δ (%)	T = 15 days	Δ (%)

5	0.428	0.299	30.14018692	0.251	41.35514019
15	0.459	0.349	23.96514161	0.335	27.01525054
25	0.444	0.327	26.35135135	0.305	31.30630631
35	0.462	0.326	29.43722944	0.299	35.28138528

Figure 5.15(a) and Table 5.12 illustrates the impact of time duration on the effectiveness of extracting chlorides from concrete for specimens labeled as C0.3-1-B7-I0.5 and C0.3-1-B15-I0.5. Under a constant current density of 0.5 A/m2, after 7 days of treatment, the percentage of extracted chlorides in front of the steel bars was approximately 8.4%, which increased to 23.3% after 15 days of treatment.

At a distance of 5mm from the outer surface, the concentration of Cl- ions increased by 62.1% after 7 days and by 98.1% after 15 days. At a distance of 15mm from the outer surface, the concentration increased by 18.3% after 7 days and by 24.4% after 15 days. At a distance of 25mm from the outer surface, the concentration increased by 2.05% after 7 days but then decreased by 4.79% after 15 days.

Figure 5.15(b) and Table 5.12 demonstrates the effect of current density on the effectiveness of extracting chlorides from concrete for specimens labeled as C0.3-3-B7-I0.5 and C0.3-3-B15-I0.5. Under a constant current density of 0.5 A/m2, after 7 days of treatment, the percentage of extracted chlorides in front of the steel bars was approximately 29.4%, which increased slightly to 35.28% after 15 days of treatment.

At a distance of 5mm from the outer surface, the concentration of Cl- ions decreased by 30.1% after 7 days and by 41.35% after 15 days. At a distance of 15mm from the outer surface, the concentration decreased by 23.96% after 7 days and by 27.01% after 15 days. At a distance of 25mm from the outer surface, the concentration decreased by 26.35% after 7 days and by 31.3% after 15 days.

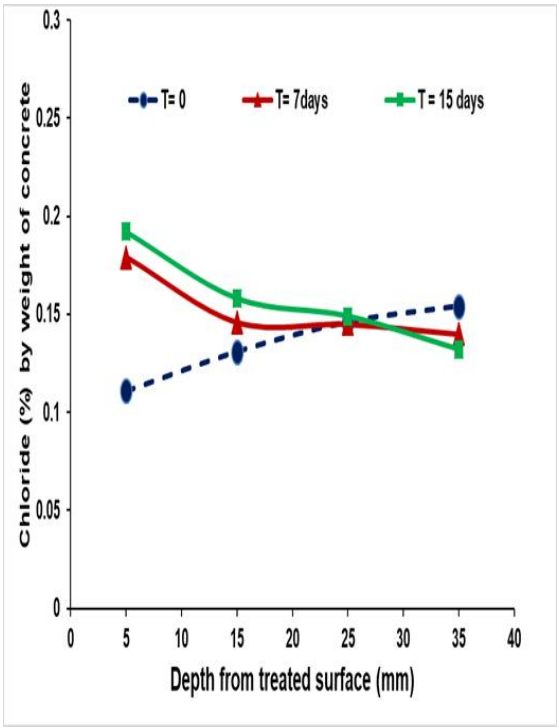

(a)

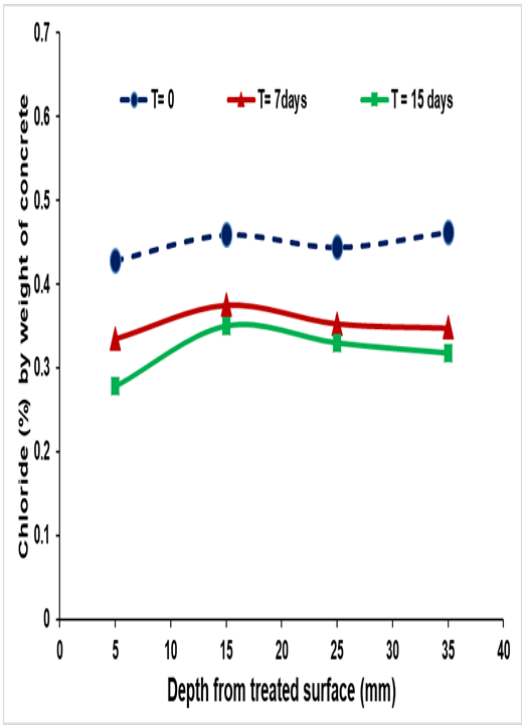

(b)

Figure 5.16 Concentration profile of Chloride in specimens before and after BIEM at different Treatment Duration (0.5A 0.15M) (a) 1% NaCl (b) 3% NaCl

Table 5.13 Concentration of Chloride in specimens before and after BIEM (1%, 3% NaCl 0.5A 0.15M) for 7 and 15 Days.

		C0.15-1-B7-I0.5		C0.15-1-B15-I0.5	
Depth	T= 0	T= 7days	Δ (%)	T = 15 days	Δ (%)
5	0.111	0.179	-61.26126126	0.192	-72.9729729
15	0.131	0.146	-11.45038168	0.158	-20.6106870
25	0.146	0.145	0.684931507	0.149	-2.05479452
35	0.154	0.14	9.090909091	0.132	14.28571429
		C0.15-3-B7-I0.5		C0.15-3-B15-I0.5	

Depth	T= 0	T= 7days	Δ (%)	T = 15 days	Δ (%)
5	0.428	0.335	21.72897196	0.278	35.04672897
15	0.459	0.375	18.30065359	0.35	23.74727669
25	0.444	0.353	20.4954955	0.33	25.67567568
35	0.462	0.348	24.67532468	0.318	31.16883117

Figure 5.16(a) and Table 13 illustrates the effect of time duration on the effectiveness of extracting chlorides from concrete for specimens labeled as C0.15-1-B7-I0.5 and C0.15-1-B15-I0.5. Under a constant current density of 0.5 A/m2, after 7 days of treatment, the percentage of extracted chlorides in front of the steel bars was approximately 9.09%, which increased to 14.28% after 15 days of treatment.

At a distance of 5mm from the outer surface, the concentration of Cl- ions increased by 61.2% after 7 days and by 72.9% after 15 days. At a distance of 15mm from the outer surface, the concentration increased by 11.4% after 7 days and by 20.6% after 15 days. At a distance of 25mm from the outer surface, the concentration decreased by 0.68% after 7 days but then increased by 2% after 15 days.

Figure 5.16(b) and Table 13 demonstrates the impact of current density on the effectiveness of extracting chlorides from concrete for specimens labeled as C0.15-3-B7-I0.5 and C0.15-3-B15-I0.5. Under a constant current density of 0.5 A/m2, after 7 days of treatment, the percentage of extracted chlorides in front of the steel bars was approximately 24.6%, which increased slightly to 31.1% after 15 days of treatment.

At a distance of 5mm from the outer surface, the concentration of Cl- ions decreased by 21.7% after 7 days and by 35% after 15 days. At a distance of 15mm from the outer surface, the concentration decreased by 18.3% after 7 days and by 23.7% after 15 days. At a distance of 25mm from the outer surface, the concentration decreased by 20.4% after 7 days and by 25.6% after 15 days.

5.3 Half Cell Potential

Steel/concrete/electrode potentials were recorded to monitor the shift in potential before and after the application of the BIEM technique. The readings were measured using a

high-impedance voltmeter and an Ag/AgCl/0.5M KCl reference electrode with a steel bar as a working electrode (WE).

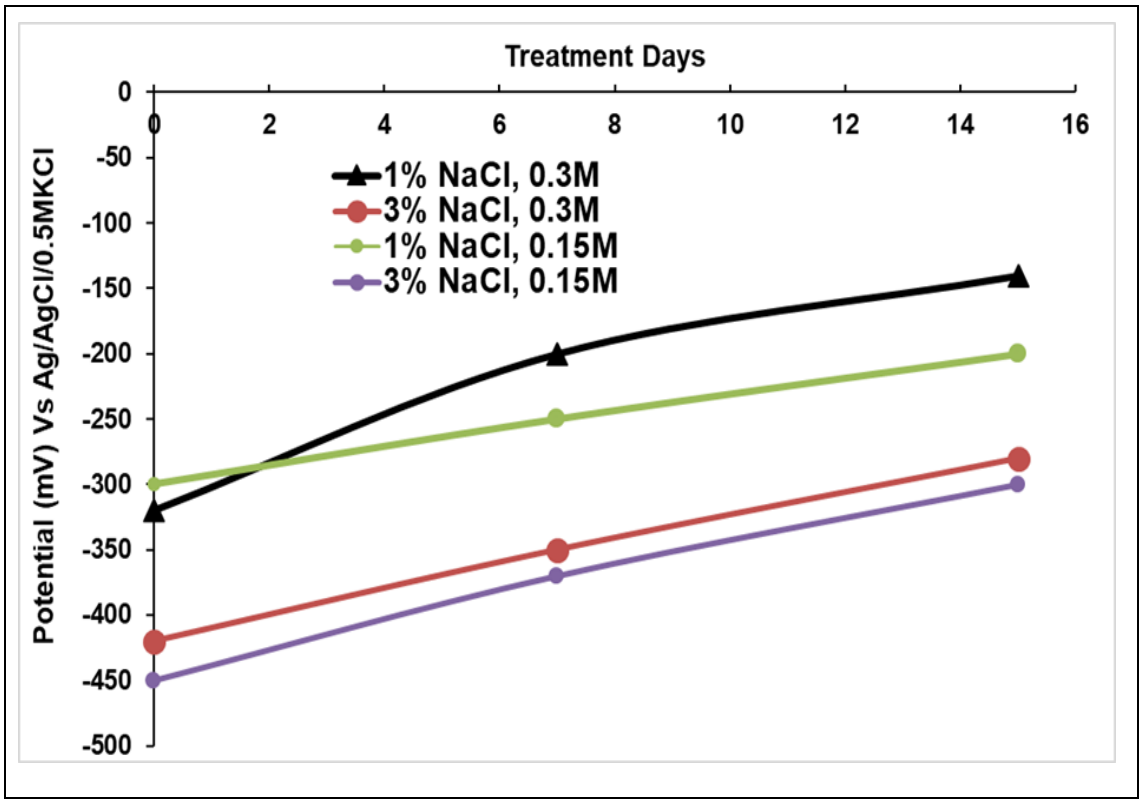

Figure 5.17 HCP after 1A/m^2 current density

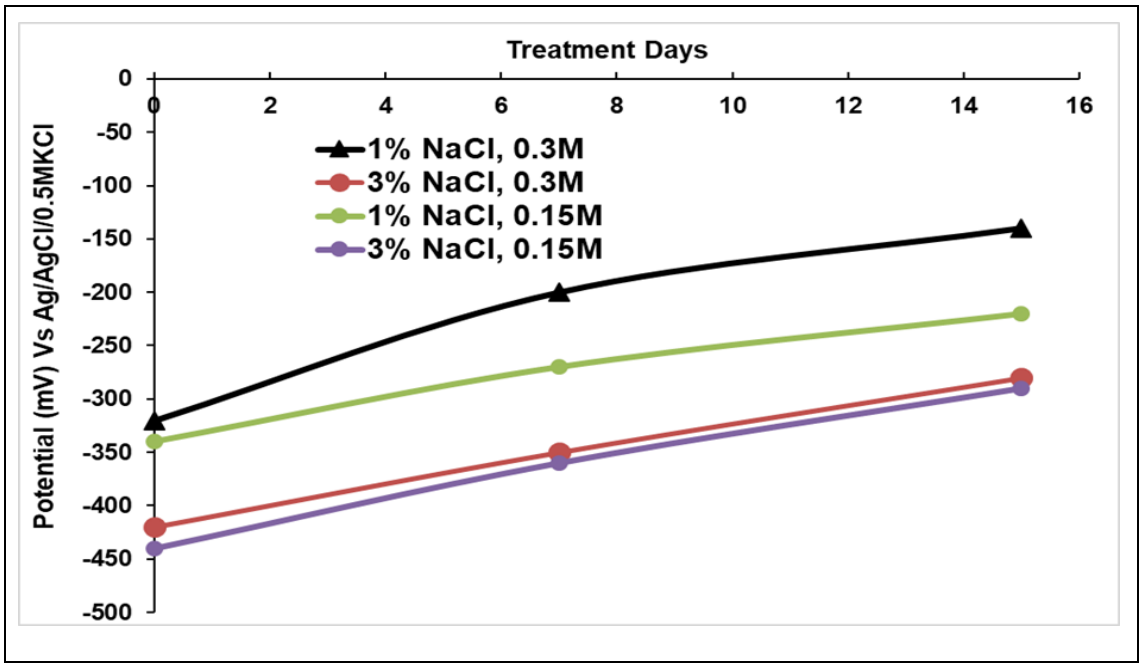

Figure 5.18 HCP after 0.5A/m^2 current density

Figure 5.17 provides valuable insights into the behaviour of specimens under different conditions. Specifically, when specimens are exposed to a treatment involving 1% NaCl (admixed chloride) and a 0.3 M inhibitor concentration, the graph reveals a distinctive parabolic reduction in the values of half-cell potential. This parabolic trend suggests a non-linear relationship between the treatment conditions and the resulting potential values.

On the other hand, when specimens are subjected to alternative variations of the treatment, such as different concentrations of NaCl or inhibitor, the graph demonstrates a linear reduction in the half-cell potential values. In these cases, the potential values decrease steadily in a straight-line fashion.

Similarly, Figure 5.18 corroborates these observations by exhibiting similar trends. The parabolic reduction in half-cell potential values for the specific treatment conditions remains consistent, while the other variations continue to display a linear decline. By analyzing these figures we can gain a deeper understanding of the relationship between the treatment conditions, specifically the concentration of NaCl and inhibitor, and the resulting half-cell potential values.

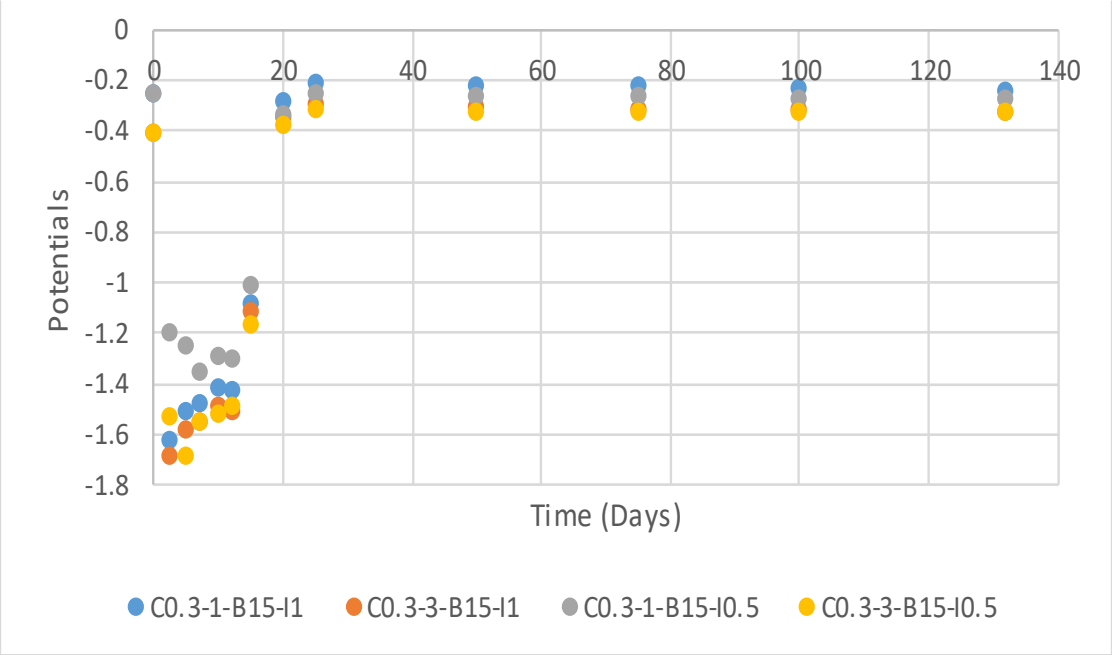

Figure 5.19 Potentials before, during and after the BIEM process.

The data presented in Figure 5.19 clearly indicates a reduction in corrosion potentials after the BIEM (Bacterial-Induced Electrochemical Method) process compared to before

the process. This reduction suggests that the inhibitor used in the BIEM process has formed a protective passivation layer on the surface of the steel bars, preventing further corrosion propagation.

Remarkably, even after a prolonged period of 130 days, the corrosion potentials remained lower than the initial corrosion potentials. This demonstrates the efficacy of the BIEM technique in providing substantial protection to the steel bars. The results indicate that the BIEM process was successful in repairing and controlling corrosion within the specimens across all the variations mentioned in Table 4.1.

In summary, the BIEM technique has proven to be effective in mitigating corrosion and preserving the integrity of the steel bars by forming a protective passivation layer. The long-term corrosion potentials remained lower than the initial values, indicating its potential for long-lasting corrosion control and repair.

5.4 Inhibitor Content

As time advanced during the treatment process, the concentration of the corrosion inhibitor in the concrete cover zone showed a gradual increase, as illustrated in the Figure. In parallel, the concentration of 2-AP in the layer near the surface continued to rise consistently as the treatment proceeded. However, an interesting contrast emerged when examining the area surrounding the embedded steel bars. The concentration improvement in this region followed a different pattern, deviating from the trend observed in the concrete cover zone.

From the Figure 5.19, it is evident that the migration of the inhibitor remained relatively uniform across all variations while keeping the treatment duration and inhibitor concentration constant at 7 days and 0.3 M, respectively. At a distance of 5mm from the outer surface, the inhibitor migration reached its maximum level, ranging between 8.2-8.9 mM. In the vicinity of the embedded steel bars, the inhibitor migration was observed between 7.8-8.4 mM, while in the region between 5-35 mm from the surface, the migration ranged from 7.8-8.8 mM. These findings suggest a consistent and controlled migration of the inhibitor throughout the different zones within the specimen.

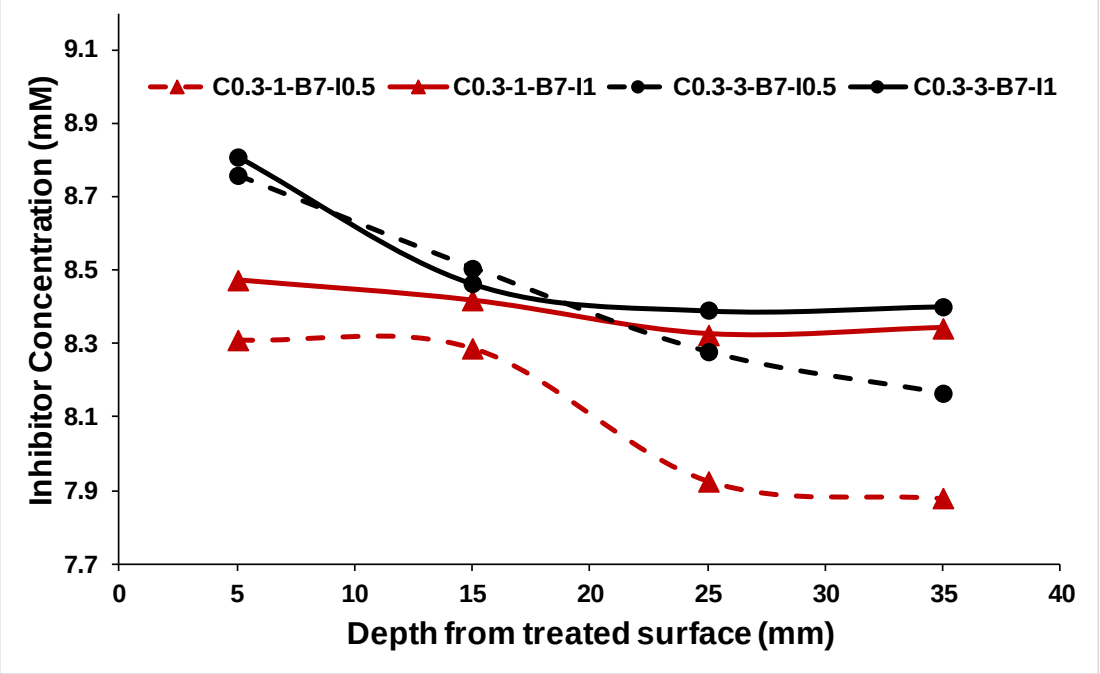

Figure 5.19 Concentration profile of Inhibitor in specimen after BIEM for different admixed chloride and different densities (0.3M 7Days)

Based on Figure 5.20, it is evident that the migration of the inhibitor remained relatively consistent among all variations while maintaining a constant treatment duration of 15 days and an inhibitor concentration of 0.3 M. Notably, each specimen exhibited a similar trend in the migration of the inhibitor. However, it is notable that the migration of the inhibitor in the C0.3-1-B15-I1 specimen was significantly lower compared to the other specimens. This indicates that the particular combination of factors in C0.3-1-B15-I1 led to reduced migration of the inhibitor compared to the rest of the specimens.

Based on the observations from Figures 5.19 and 5.20, it can be concluded that for samples C0.3-3-B7-I1 and C0.3-3-B15-I1, the migration of inhibitors after 15 days of treatment was 2.4% higher compared to the migration after 7 days of treatment in the vicinity of the steel bars. Furthermore, when considering all distances from the outer surface, the migration of the inhibitor between 7 and 15 days, with an initial content of 3% NaCl, fell within the range of 2.4% to 4%. A similar trend was also observed in the specimens with an initial content of 1% NaCl.

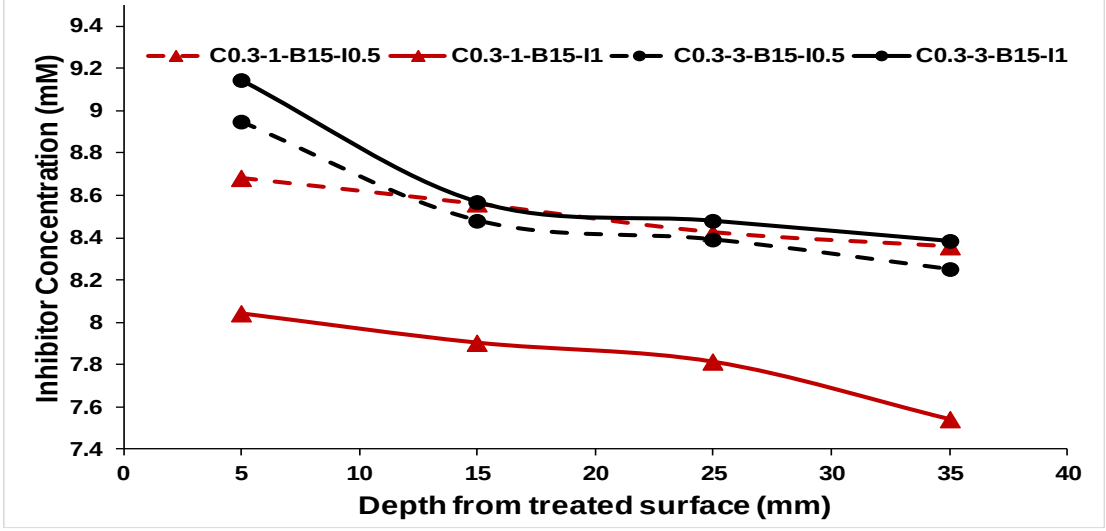

15 Days 0.3 M

Figure 5.20 Concentration profile of Inhibitor in the specimen after BIEM for different admixed chloride and different densities (0.3M 15Days)

The data presented in the Figure 5.21 suggests that the migration of the inhibitor exhibited a consistent pattern across various scenarios with a fixed treatment duration of 7 days and an inhibitor concentration of 0.15 M. specifically, the migration of the inhibitor within the range of 5-15 mm from the outer surface appeared to be similar among all cases. This indicates that regardless of the specific conditions, the inhibitor migrated to a similar extent within this region.

However, it is worth noting that in the case of C0.15-1-B7-I0.5, there was a slightly lower migration of the inhibitor between 15-35 mm from the outer surface compared to the other cases.

This observation suggests that the combination of factors in C0.15-1-B7-I0.5 led to a relatively reduced migration of the inhibitor within that particular region. In other words, the specific parameters involved in C0.15-1-B7-I0.5 contributed to a localized effect, resulting in a decreased movement of the inhibitor in the 15-35 mm region from the outer surface.

From the Figure 5.22, it is evident that the migration of the inhibitor remained relatively consistent across all variations with a constant treatment duration of 15 days and an

inhibitor concentration of 0.15 M. Specifically, the migration of inhibitors in the cases of C0.15-3-B15-I0.5 and C0.15-3-B15-I1 appeared to be similar or comparable at all depths, regardless of the variations in current density.

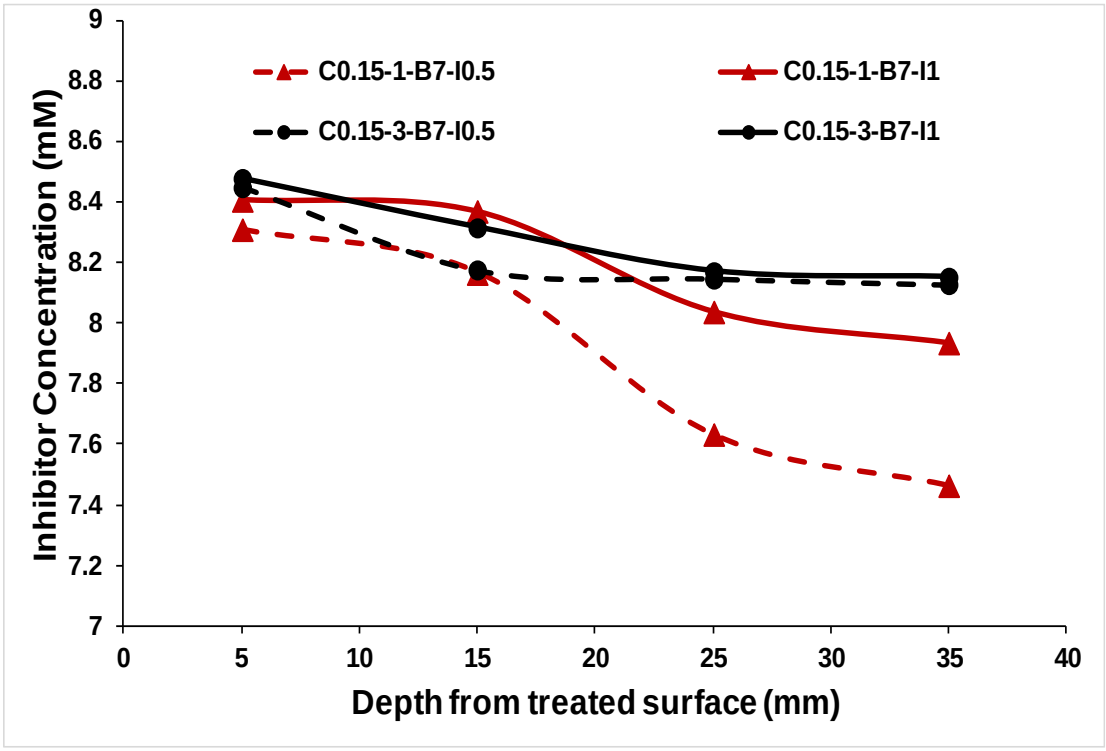

7 Days 0.15M

Figure 5.21 Concentration profile of Inhibitor in specimen after BIEM for different admixed chloride and different densities (0.15M 7Days)

However, in the cases of C0.15-1-B15-I0.5 and C0.15-1-B15-I1, it is clearly observed from the figure that there is a significant difference in the migration of the inhibitor at all depths. This discrepancy suggests that the specific combination of factors, such as current density and inhibitor concentration, in C0.15-1-B15-I0.5 and C0.15-1-B15-I1 has a pronounced impact on the migration of the inhibitor throughout the tested depths.

Based on the observations from Figures 5.21 and 5.22, it can be concluded that for samples C0.15-3-B7-I1 and C0.15-3-B15-I1, the migration of inhibitors after 15 days of treatment was 1.21% higher compared to the migration after 7 days of treatment in the vicinity of the steel bars. Furthermore, when considering all distances from the outer

surface, the migration of the inhibitor between 7 and 15 days, with an initial content of 3% NaCl, fell within the range of 1.21% to 4.11%. A similar trend was also observed in the specimens with an initial content of 1% NaCl.

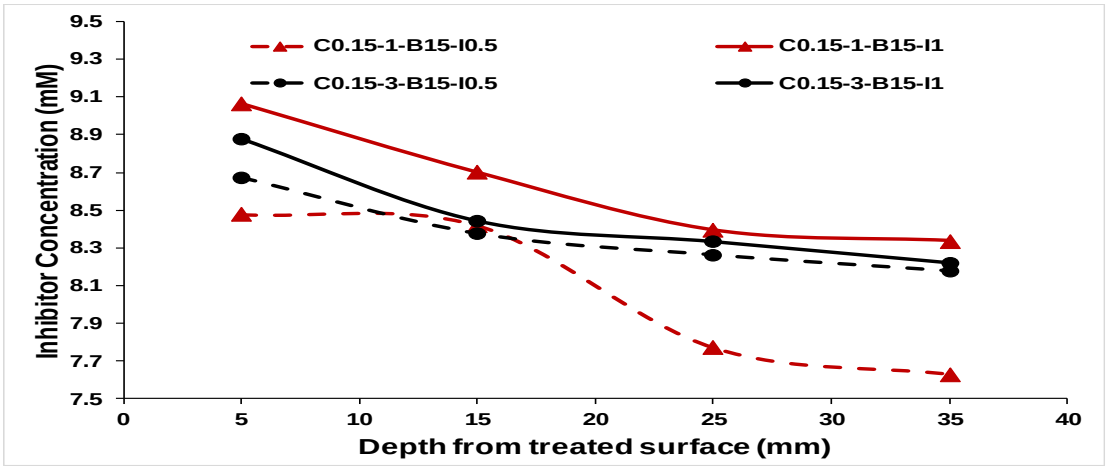

15 Days 0.15M

Figure 5.22 Concentration profile of Inhibitor in specimen after BIEM for different admixed chloride and different densities (0.15M 15Days)

Based on the provided information, it appears that there are four figures, namely Figures 5.19, 5.20, 5.21, and 5.22, which are related to the migration of an inhibitor. The inhibitor migration was studied with respect to its concentration in the electrolyte, specifically at two different concentrations, 0.15 M and 0.3 M. The data analysis from these figures led to the identification of the range of inhibitor migration, which was found to be between 7.9 mM and 9.12 mM, it means that when the inhibitor was present in the electrolyte at concentrations of 0.15 M and 0.3 M.

5.5 Compressive Strength

The compressive strength of the cube casted of size 100x100x100 mm after 7 and 15 days with 1% and 3% NaCl content are presented in the Table 5.12. Here it can be clearly observed the after 7 and28 days of curing the specimens attains the desired strength.

Table 5.12 Compressive Strength

Compressive Strength		
	7 Days (MPa)	28 Days (MPa)
1% NaCl	25.8	35
3% NaCl	25.1	31.8

5.6 Split Tensile Strength

The split tensile strength of the cylinder casted of size 200x100 mm after 7 and 15 days with 1% and 3% NaCl content are presented in the Table 5.13. Here it can be clearly observed the after 7 and 28 days of curing the specimens attains the desired strength.

Table 5.13 Split Tensile Test

Split Tensile Strength		
	7 Days (MPa)	28 Days (MPa)
1% NaCl	1.86	3.1
3% NaCl	1.94	3.09

5.7 Flexural Strength Test

The flexural strength of the beam casted of size 500x100x100 mm after 7 and 15 days with 1% and 3% NaCl content are presented in the Table 5.14. Here it can be clearly observed the after 7 and 28 days of curing the specimens attains the desired strength.

Table 5.14 Flexural Strength Test

Flexural Strength		
	7 Days (MPa)	28 Days (MPa)
1% NaCl	4.35	7.47
3% NaCl	4.69	7.69

CHAPTER 6. CONCLUSION AND FUTURE RECOMMENDATIONS

This research project has worked to analyse the efficiency of Amino-2-Pyridine Inhibitor on the Rehabilitation of Chloride Contaminated Reinforced Concrete with Bidirectional Electro-migration Method for reinforced concrete structures. A summary of the research conclusions and recommendations for the future are given in this chapter.

1. All the specimens treated with BIEM showed the reduced corrosion as compared to the controlled specimens where corrosion increased with time, indicating effectiveness of the applied system.
2. On application of the BIEM technique results indicated migration of indicator towards the steel bars and chloride migrating away from the steel bars towards external anode.
3. The application of BIEM technique was able to protect steel in both low (1% NaCl) and high (3% NaCl) chloride environment.
4. As observed from the results the effectiveness of BIEM technique is influenced by treatment duration, initial chloride content, concentration of inhibitors and current density. On increasing the treatment duration and current density the efficiencies of chloride extraction and inhibitor migration increased.
5. The migration of chloride ions from the vicinity of steel bars to the external anode (304 stainless steel mesh) was maximum observed after 15 days of BIEM treatment at 1 A/cm2 current density for 0.3 M concentration of inhibitor.
6. The migration of chloride ions was observed to be much more in the case of 3% initial chloride content as compared to 1% initial chloride content in all the variations.
7. In the case of 1% initial chloride content specimen's maximum chloride content migrated from the steel bars was 35% and in the case of 1% initial chloride content specimen's maximum chloride content migrated from the steel bars was 48%. The residual concentration of chloride ions in the outer layer of the specimens was higher than in the inner layer of the specimens.

8. The migration of inhibitor (2AP) was almost similar in all the variations with a maximum inhibitor concentration of 9.16 mM in the vicinity of steel bars. This indicates the presence of initial chloride content in the specimens does not influence the migration of inhibitor.
9. The migration of 2AP was not greatly affected by the initial chloride concentration in the specimens. Irrespective of the concentration of inhibitor in the solution the migration achieved was similar. This indicates a lower inhibitor concentration is sufficient to achieve the required protection.
10. As observed from the results of the I_{corr} and potentials, the inhibitor has formed a passivation layer around the steel bars hence the corrosion is not propagating even after 130 days of treatment.
11. After exposing the treating samples to wet and dry cycles the samples continued protection of the steel bars due to formation of inhibitor layer on the steel surface. In comparison the steel bars in the controlled specimen showed continuous corrosion.

FUTURE RECOMMANDATIONS

1. The practical application of BIEM technique on big structures needs to be explored so that the application of this process becomes more convenient.
2. This technique can be explored more by using different organic inhibitors in place of 2AP.
3. The BIEM technique can be explored more by increasing the concentration of inhibitor more.

CHAPTER 7. REFERENCES

1. Ahmad, S. (2003) '*Reinforcement Corrosion in Concrete Structures, Its Monitoring and Service Life Prediction - A Review'. Cement and Concrete Composites* 25 (4–5), 459–471

2. Apostolopoulos, C.A. and Papadakis, V.G. (2008) '*Consequences of Steel Corrosion on the Ductility Properties of Reinforcement Bar*'. *Construction and Building Materials* 22 (12), 2316–2324

3. Das, S.C. (2012) *Zinc Rich Paint as Anode System for Cathodic Protection (CP) of Reinforced Concrete Structures and Development of Corrosion / CP Monitoring Probes*. Coventry: Coventry University

4. Davis, J.R. (2000) 'The Effects and Economic Impact of Corrosion'. in *Corrosion Understanding the Basics*. United States of America: ASM International, 1–21

5. Glass, G.K. and Buenfeld, N.R. (2000) 'Chloride-Induced Corrosion of Steel in Concrete'. *Progress in Structural Engineering and Materials* 2 (4), 448–458

6. Hansson, C.M. (2016) 'An Introduction to Corrosion of Engineering Materials'. in *Corrosion of Steel in Concrete Structures*. ed. by Poursaee, A. vol. 1. Woodhead Publishing, 3–18

7. Hays, G.F. (2010) *World Corrosion Organization* [online] available from <http://events.nace.org/euro/corrodia/Fall_2010/wco.asp>

8. India, P.T. of (2015) 'India Loses Rs 2 Trillion Annually to Corrosion of Infrastructure: Government'. *The Economic Times* [online] available from <http://economictimes.indiatimes.com/news/economy/finance/india-loses-rs-2-trillion-annually-to-corrosion-of-infrastructure-government/articleshow/48792499.cms?intenttarget=no>

9. Javaherdashti, R. (2000) 'How Corrosion Affects Industry and Life'. *Anti-Corrosion Methods and Materials* 47 (1), 30–34

10. Koch, G., Varney, J., Thompson, N., Moghissi, O., Gould, M., and Payer, J. (2016) *International Measures of Prevention , Application , and Economics of Corrosion Technologies Study* [online] Houston. available from

<http://impact.nace.org/documents/Nace-International-Report.pdf>

11. Lambert, P. (2014) 'Economic Aspects'. in *Cathodic Protection of Steel in Concrete and Masonry*. ed. by Chess, M., P. and Broomfield, P., J.B.R. CRC Press, 227–237

12. Popov, B.N. (2015) *Corrosion Engineering: Principles and Solved Problems* [online] 1st edn. Oxford: Elservier. available from <https://ebookcentral.proquest.com/lib/coventry/reader.action?docID=1977749&ppg=20>

13. Service, E.N. (2015) 'Soon , Bureau for Control of Corrosion'. *The New Indian Express* [online] available from <http://www.newindianexpress.com/states/tamil_nadu/Soon-Bureau-for-Control-of-Corrosion/2015/11/20/article3137266.ece>

14. A Tiwari, S. Goyal, V. Luxami 2020 *Assessment of corrosion inhibition efficiency of generic compounds having different functional groups in carbonated pore solution with chlorides and migration ability in concrete*.

15. A. Tiwari, S. Goyal, V. Luxami 2021 *Evaluation of inhibition efficiency of generic compounds with additional heteroatom in simulated concretepore solution and migration potential in concrete.*

16. Khaled A. Alawi Al-Sodani, Mohammed Maslehuddin, Omar S. Baghabra Al-Amoudi 2017 *Efficiency of generic andnproprietary inhibitors in mitigating Corrosion of Carbon Steel in Chloride-Sulfate Environments.*

17. Arpit Goyal, Homayoon Sadeghi Pouya, Eshmaiel Ganjian, Peter Claisse 2018*A Review of Corrosion and Protection of Steel in Concrete*.

18. Arpit Goyal, Homayoon Sadeghi Pouya and Eshmaiel Ganjian 2022 *Field Application of a New Conductive Coating Impressed Current Anode for Performance Assessment on Reinforced Concrete Structures***.**

19. Arpit Goyal, Eshmaiel Ganjian, Homayoon Sadeghi Pouya, Mark Tyrer 2021 *Inhibitor efficiency of migratory corrosion inhibitors to reduce corrosion in reinforced concrete exposed to high chloride environment.*

20. Ryan Cobbs, Rene Brueckner, Chris Atkins, Arpit Goyal 2022 *A Rapid Test to Screen the Functionality of Galvanic Anodes for Cathodic Protection of Reinforced Concrete*.

20. Rene Brueckner, Ryan Cobbs, and Chris Atkins 2022 *A review of developments in cathodic protection systems for reinforced concrete structures.*

21. Arpit Goyal, Homayoon Sadeghi Pouya , Eshmaiel Ganjian *2019 Performance assessment of specialist conductive paint for cathodic protection of steel in reinforced concrete structures.*

22. Arpit Goyal , Ezekiel Kehinde Olorunnipa , Homayoon Sadeghi Pouya, Eshmaiel Ganjian , Adegoke Omotayo Olubanwo 2019 *Potential and current distribution across different layers of reinforcement in reinforced concrete cathodic protection system- A numerical study.*

23. Arpit Goyal, Homayoon Sadeghi Pouya, Eshmaiel Ganjian, Adegoke Omotayo Olubanwo, Morteza Khorami 2018 *Predicting the corrosion rate of steel in cathodically protected concrete using potential shift.*

24. Xu, Jin and Huang 2015 *Bidirectional electro-migration of a corrosion inhibitor in chloride contaminated concrete.*

25. Weijie Fan, Jianghong Mao, Weiliang Jin, Jin Xia, Jun Zhang, Qiang Li 2019 *Repair effect of bidirectional electro-migration rehabilitation on concrete structures at different durability deterioration stages.*

25. Weijie Fan, Jianghong Mao, Weiliang Jin , Jun Zhang, Xiaoping Zhong 2020 *Study on the durability improvement of cracked concrete based on bidirectional electro-migration rehabilitation.*

26. Xiao-Yong Wang, Seokhee Lee, Hyeongkyu Cho 2021 *Penetration properties and injecting conditions of corrosion inhibitor for concrete.*

27. Chonggen Pan, Jianghong Mao and Weiliang Jin 2020 *Effect of Imidazoline Inhibitor on the Rehabilitation of Reinforced Concrete with Electro-migration Method.*

28. Chonggen Pan, Jianghong Mao, Weiliang Jin, Weijie Fan, Dayong Zhu 2020 *Effects of environmental Water-Level changes and bidirectional electro-migration rehabilitation on durability of concrete.*

28. Khaled A. Alawi Al-Sodani, Mohammed Maslehuddin, Omar S. Baghabra Al-Amoudi, Tawfik A. Saleh & Mohammed Shameem 2018 *Efficiency of generic and proprietary inhibitors in mitigating Corrosion of Carbon Steel in Chloride-Sulfate Environments.*

29. R. Heiyantuduwa, M.G. Alexander, J.R. Mackechnie, *Performance of a penetrating corrosion inhibitor in concrete affected by carbonation-induced corrosion*, J. Mater. Civ. Eng.

30. D. Zhang, Y. Shao, *Effect of early carbonation curing on chloride penetration and weathering carbonation in concrete*, Constr. Build. Mater. 123 (2016)

31. F. Cao, J. Wei, J. Dong, W. Ke, *The corrosion inhibition effect of phytic acid on 20 SiMn steel in simulated carbonated concrete pore solution*, Corros. Sci. 100 (2015)

32. S.P. Karthick, A. Madhavamayandi, S. Muralidharan, V. Saraswathy, *Electrochemical process to improve the durability of concrete structures,* J. Build. Eng. 7 (2016)

33. K. Kaur, S. Goyal, B. Bhattacharjee, M. Kumar, *Efficiency of migratory-type organic corrosion inhibitors in carbonated environment*, J. Adv. Concr. Technol. 14 (9) (2016)

M. Osial, *Organic substances as corrosion inhibitors for steel in concrete – an overview*, J. Build. Chem. 1 (2016)

34. H. Lee, H. Yang, J. Kumar, S. Kumar, B. Yoo, *Corrosion mitigation of steel rebars in chloride contaminated concrete pore solution using inhibitor: an electrochemical investigation, Constr. Build. Mater*. 173 (2018)

35. M. Yadav, L. Gope, T.K. Sarkar, *Synthesized amino acid compounds as eco-friendly corrosion inhibitors for mild steel in hydrochloric acid solution: electrochemical and quantum studies,* Res. Chem. Intermed. 42 (3) (2016)

36. H. Verbruggen, H. Terryn, I. De Graeve, *Inhibitor evaluation in different simulated concrete pore solution for the protection of steel rebars,* Constr. Build. Mater. 124 (2016)

L. Yohai, M.B. Valcarce1, M. Vázquez 2015 *Testing phosphate ions as corrosion inhibitors for construction steel in mortars.*

37. Diana Martín and Engin Seyhan 2022 *Protection of Reinforced Concrete Steel Exposed to a Marine Environment: A Preliminary Onsite Study of the Performance of a New Generation of Surface-Applied Corrosion Inhibitors.*

38. Ashish Kumar Tiwari, Purnima, Shweta Goyal, Vijay Luxami 2022 *Influence of corrosion inhibitors on two different concrete systems under combined chloride and carbonated environment.*

39. Guleria H, Purnima, Tiwari AK, Goyal S. *Performance of organic and inorganic functional groups as corrosion inhibitors in concrete experiencing extreme corrosive environment*. Indian Concr J 2021

40. Jin Z, Xiong C, Zhao T, Du Y, Zhang X, Li N, *Passivation and depassivation properties of Cr–Mo alloyed corrosion-resistant steel in simulated concrete pore solution.* Cem Concr Compos 2022

41. Yang H, Li W, Liu X, Liu A, Hang P, Ding R, et al. *Preparation of corrosion inhibitor loaded zeolites and corrosion resistance of carbon steel in simulated concrete pore solution*. Constr Build Mater 2019

42. Lee HS, Yang HM, Singh JK, Prasad SK, Yoo B. *Corrosion mitigation of steel rebars in chloride contaminated concrete pore solution using inhibitor: an electrochemical investigation.* Constr Build Mater 2018

43. Magdalena Osial DW. *Organic substances as corrosion inhibitors for steel in concrete – an overview*. J Build Chem 2016

44. Bolzoni F, Brenna A, Ormellese M. *Recent advances in the use of inhibitors to prevent chloride-induced corrosion in reinforced concrete*. Cem Concr Res 2022

Goni LKMO, Mazumder MAJ. *Green Corrosion Inhibitors.* Corros Inhib 2019.

45. Tiwari A, Goyal S, Luxami V, Chakraborty MK, Gundlapalli P. *Evaluation of inhibition efficiency of generic compounds with additional heteroatom in simulated concrete pore solution and migration potential in concrete.* J Build Eng 2021

46. Tiwari A, Goyal S, Luxami V, Chakraborty MK, Prabhakar G. *Assessment of corrosion inhibition efficiency of generic compounds having different functional groups in carbonated pore solution with chlorides and migration ability in concrete.* Constr Build Mater 2021

47. Quraishi MA, Nayak DK, Kumar R, Kumar V (2017) *Corrosion of Reinforced Steel in Concrete and Its Control: An overview.* J Steel Struct Constr 2: 124.